DNA barcoding and phylogeny based comparative evaluation of anti-cancer properties of *Caulerpa* (J V Lamouroux) spp. from Indian coasts

Thesis submitted to the Central University of Punjab

For the award of
Doctorate of Philosophy

In
Biosciences

By
Richa Mehra

Supervisor: Dr. Felix Bast
Co-Supervsior: Dr. Sandeep Singh

Centre for Biosciences
School of Basic and Applied Sciences
Central University of Punjab, Bathinda

August, 2019

CERTIFICATE

I declare that the thesis entitled "**DNA barcoding and phylogeny based comparative evaluation of anti-cancer properties of *Caulerpa* (J V Lamouroux) spp. from Indian coasts**" has been prepared by me under the guidance of Dr. Felix Bast (Assistant Professor), Department of Plant Sciences, School of Basic and Applied Sciences and Dr. Sandeep Singh (Assistant Professor), Department of Human Genetics and Molecular Medicine, School of Health Sciences, Central University of Punjab. No part of this thesis has formed the basis for the award of any degree or fellowship previously.

Richa Mehra
Reg. No: CUPB/MPH-PHD/SBAS/BIO/2012-13/05
Centre for Biosciences
School of Basic and Applied Sciences
Central University of Punjab
Bathinda

DATE:

CERTIFICATE

We certify that 'Mrs. Richa Mehra" has prepared her thesis entitled "**DNA barcoding and phylogeny based comparative evaluation of anti-cancer properties of *Caulerpa* (J V Lamouroux) spp. from Indian coasts**" for the award of the Ph.D. degree of the Central University of Punjab, under our guidance. She has carried out this work at the Centre for Biosciences and Department of Pharmaceutical Sciences and Natural Products, School of Basic and Applied Sciences; and Department of Human Genetics and Molecular Medicine, School of Health Sciences, Central University of Punjab.

Dr. Felix Bast (Assistant Professor)
Department of Plant Sciences
School of Basic and Applied Sciences
Central University of Punjab
Bathinda

Dr. Sandeep Singh (Assistant Professor)
Department of Human Genetics and Molecular Medicine
School of Health Sciences
Central University of Punjab
Bathinda

DATE:

ABSTRACT

DNA barcoding and phylogeny based comparative evaluation of anti-cancer properties of *Caulerpa* (J V Lamouroux) spp. from Indian coasts

Name of Student	Richa Mehra
Registration Number	CUPB/MPHIL-PHD/SBAS/BIO/2012-13/05
Degree for which submitted	Doctorate of Philosophy
Name of Supervisor	Dr. Felix Bast
Name of Co-Supervisor	Dr. Sandeep Singh
Department	Centre for Biosciences
School of Studies	School of Basic and Applied Sciences
Keywords	*Caulerpa*, barcoding, cancer, phylogeny, anti-cancer

A total of 15 *Caulerpa* samples were collected from Indian coasts and identified based on morphological and molecular data inferred from ITS, 18S, t*ufA* and *rbc*L. Seven different species viz. *C. scalpelliformis*, *C. racemosa*, *C. sertularioides*, *C. verticillata*, *C. taxifolia*, and *C. corynephora*; and their geographical isolates were identified. Barcode data for these species was generated using aforementioned molecular markers and used for phylogenetic assessment. Phylogenetic trees using Bayesian inference (BI) and Maximum Likelihood (ML) function were generated for each molecular marker. *tufA* was found to be most suitable marker for the genus *Caulerpa,* resolving the species into 17 different lineages, with 15 corresponding to already known sections and 2 new lineages. Besides, a database named *DbIndAlgae* of Indian algae was generated and all the morphological as well as molecular data generated in this study is uploaded on the database. In addition, the phycochemical analysis revealed the presence of alkaloids, terpenoids, steroids, tannins, saponins, flavonoids, and phenols in different *Caulerpa* species. The selective cytotoxicity of methanolic extracts of *Caulerpa* (CMEs) was evaluated on MDA-MB-231, T47-D and H1299 cells, and the results revealed significant cytotoxicity of all species. *C. racemosa* KNY-254 and *C. taxifolia* TEN-158 were found to be most potent on MDA-MB-231 cells with IC_{50} value of 0.226 ± 0.004 and 0.246 ± 0.009 µg/µL. The mitochondrial membrane perturbation was revealed by JC-1 and apoptotic cell death was confirmed by Annexin V/FITC staining. CMEs also induced ROS in MDA-MB-231 cells as depicted by DHE, and increased activity of SOD, decreased activity of gluthatione reductase. The CMEs also exhibit anti-invasion activity and inhibited up to 71% migration across the artificially scratched wound in MDA-MB-231, w.r.t. untreated control cells. Moreover, chemical probing of *C. racemosa* KNY-254 by LC-MS analysis revealed six previously reported and six unreported molecules. The molecular docking analysis revealed weak to moderate interactions with all of the protein targets viz. Bcl2, AMPK, mTOR, BID, PERK, IGF-1R, PI3K, PTP1B and Akt2, known to play important role in cancer cell signaling. Additionally, a moderately positive correlation amongst the phylogeny and anti-cancer activity was observed suggesting that phylogeny might provide cues for anti-cancer activity, subject to further validations.

Richa Mehra Dr. Felix Bast Dr. Sandeep Singh

ACKNOWLEDGEMENTS

"Roots of all goodness lies in the soil of appreciation for goodness" Dalai Lama.

My belief in god can be classified as 'meagre', as I only beleive in what I see, however, I have witnessed the 'goodness of god' in many people surrounding me. Here I am expressing my deepest gratitude to all those who have knowingly or unknowingly given me the strength to complete *The Doctoral Journey*.

Firstly, I wish to acknowledge *Mother Nature* for providing the mankind with abundant resources for research and a lap of peace for refereshment.

I am very thankful to my supervisor Dr. Felix Bast who has provided me consistent guidance, support and freedom for carrying out my research work. I would really like to acknowledge his calm and cooperative attitude that has alleviated my research journey in a true sense. His time-management and productivity has always inspired me to become 'one-man-army' like him.

Worlds only can't describe the sense of gratitude and regards I have for my co-supervisor Dr. Sandeep Singh. He is the man I can think of whenever I am in trouble, be it relevant to research, health, or personal life. His relentless guidance and suggestions have helped me in improving my research skills and personality. I am forever indebted to him for all the help and advises I have received from him.

I would like to acknowledge Dr. Pankaj Bhardwaj, who has inculcated initial research elements in me, during my M.Phil dissertation. I wholeheartedly thank him for making me expert in DNA sequencing, which has turned out to be very fruitful for me.

I express my heartfelt thanks to Dr. Raj Kumar, Mr. Gaurav Joshi, Dr. Saurav Kalra and Ms. Neha Pathak, for their profound help with the chemistry work. I am also extremely thankful to Ms. Praveen Sharma for her support in cell-cultre work.

A sincere thanks is due to Dr. Sanjeev Thakur, Head of Department, Department of Plant Sciences and Coordinator of Centre, Centre for Biosciences, for all the encouragement, official and moral support. I am also very grateful to all the faculty members of Department for Plant Sciences and erstwhile Centre for Biosciences for their precious guidance and support.

I would also like to acknowledge Dr. Sumeer Razdan, Technical Officer, CIL, for the technical support in DNA sequencing and confocal microscopy and Mr. Ashish Pandey, former Resident Engineer, DSS Imagetech Pvt. Ltd., for the intial optimization study on confcal microscopy. I am also thankful to Mr. Ashwani Kumar (TA), Mr. Ravi Dutt (LA), Mr. Pawan Poonia (LA) for their help and assistance during experimental and offical work.

I am also very grateful to Prof. R. K. Kohli, Vice Chancellor and Prof. Jai Rup Singh, former and founder Vice Chancellor, Central University of Punjab, Bathinda for creating and providing world class research facilities. I am extremely thankful to Prof. R. K. Kohli, for being so accessible and hearing me out so patiently and helping me for all the issues that I have ever brought to his office. I am also extremely grateful to Prof. P. Rama Rao, Dean Academic

Affairs, Central University of Punjab, for his valuable suggestions and guidance for making this thesis worthwhile.

I would also like to extend my sincere gratitude to all my seniors, lab-mates and juniors for their cooperation, support and help. Special mention is due to Mr. Digvijay Singh Yadav and Mr. Wahid Ul Rehman for making the lab environment amicable.

I owe an extra-special thank to some of the wonderful people who accidently crossed my path during my M.Phil.-Ph.D. journey. A special thanks to my loving husband Dr. Satej Bhushan for his abundant love, support, constant encouragement, bearing my emotional break-downs and being there by my side always, come what may. This journey would not have been possible without the love and support of my dearest friends Mr. Vicky Kumar, Dr. Shruti Choudhary, Ms. Sapna Thakur, Dr. Balraj Singh Gill, Dr. Raman Preet Kaur, Mr. Abhilash Ludhiadch, Mr. Shishir Upadhyay, Dr. Ramit Singla, and Mr. Ashishranjan Dwivedi. Thanks and love is also due for baby Krisha and Advik for bringing in the much needed refreshing moments. A special mention to my girls' gang and partners-in-crime including Ms. Gursharan Kaur, Ms. Sheetal Dubey, Ms. Ritu, and Ms. Igona. Much love to all of you!

My heartfelt regards and gratitude for my Parents, Bhai and Bhabhi, for showing faith in me and giving me liberty to choose the things that I have always desired. I owe you a lot for your selfless love, encouragement and care that helped me shape my life my way.

I would also like to acknowledge Indian Council of Medical Research (ICMR), for the Junior Research Fellowship (JRF) and Senior Research Fellowship (SRF), that has helped me carry out my research smoothly.

Richa Mehra

TABLE OF CONTENTS

LIST OF TABLES

LIST OF FIGURES

LIST OF ABBREVIATIONS

Abbreviation	Full Form
°C	Degree Celsius
bp	Base Pairs
BLAST	Basic Local Alignment Search Tool
BI	Bayesian Inference
cm	Centimetre
CMEs	Caulerpa Methanolic Extracts
COI	Cytochrome oxidase 1
DNA	Deoxyribonucleic Acid
dNTPs	Deoxyribonucleotide triphosphates
DHE	Dihydroethidium
EMA	European Medicines Agency
GR	Glutathione Reductase
GSH	Reduced Glutathione
h	Hour
IC_{50}	Half maximal inhibitory concentration
ITS	Internal Transcribed Spacer
JC-1	5,5',6,6'-tetraethylbenzimidazolylcarbocyanine iodide
L	Litre
LC-MS	Liquid Chromatography-Mass Spectrometry
min	Minute
mg	Milligram
mL	Maximum Likelihood
µL	Microlitre
mM	Millimolar
MNP	Marine Natural Products
MMP	Mitochondrial Membrane Potential
MTT	3-(4,5-dimethylthiazol-2-yl)-2,5-diphenyltetrazolium bromide
MUSCLE	Multiple Sequence Comparison by Log-Expectation
NCBI	National Centre for Biotechnology Information
hPBMCs	Human Peripheral Blood Mononuclear Cells
PBS	Phosphate Buffer Saline
PCR	Polymerase Chain Reaction
PI	Propidium Iodide
R^2	Coefficient of Determination
*rbc*L	Ribulose bisphosphate carboxylase large subunit

RNA	Ribonucleic acid
ROS	Reactive Oxygen Species
SOD	Superoxide Dismutase
tufA	Elongation Factor Tu-1 (EF-Tu-1)
TLC	Thin Layer Chromatography
U	Unit
US-FDA	United States-Food and Drug Administration

LIST OF APPENDICES

INTRODUCTION

Marine organisms have undergone a longer evolutionary period than terrestrial organisms, resulting in an enormous genetic diversity amongst them (Vermeij and Grosberg, 2010). This genetic diversity and their widely adaptable nature makes marine life an exciting field of research, especially for the search of novel bioactive natural compounds. These marine organisms are known to possess bioactive secondary metabolites with unique structural features, thereby, gaining attention from the pharmaceutical industry. A fair number of marine-derived drugs have been approved and entered clinical trials e.g. Trabectedin (Yondelis®), Eribulin (Halaven®), and Brentuximab Vedotin (Adcetris®) (Kiuru *et al.,* 2014). Among marine organisms, macro-algae or seaweeds are one of the most promising source of bioactive metabolites (O'Sullivan *et al.,* 2010; Zhao *et al.,* 2018). Seaweeds have been used as traditional medicine from thousands of years (Chengkui *et al.,* 1984). Earliest records suggest the use of *Chondrus crispus* and *Mastocarpus stellatus* in beverages, as a remedy for various ailments like cold, sore throat, chest infections, kidney disorders and burn injuries. The juice of another seaweed, *Porphyra umbilicalis* Kützing, is reported to be effective against breast cancer (Korzeniowska *et al.,* 2018).

Many seaweeds are edible and consumed in various countries worldwide viz. Japan, China, Korea, Ireland, Coastal areas of USA and Canada. Seaweeds are known for high nutrional value and are also included in the diets of Asian countries since ancient times (Chapman and Chapman, 1980). Scientists have documented an interesting correlation between seaweeds consumption and a lower prevalence of diet-related cancer, breast cancer, coronary heart diseases, and inhibitory effects on benign and tumour neoplasia (Teas *et al.,* 2013; Jiang and Shi, 2018). Extracts from a various algae like *Gracilaria corticata* (red alga)*, Capsosiphon fulvescens* (green alga), *Laminaria japonica* and *Sargassum oligocystum* (brown algae) have displayed anti-cancer and anti-metastatic properties on different cancer cells (Patel, 2012). Seaweeds have also been shown to modulate ROS (reactive oxygen species) generation which in turn plays an essential role in carcinogenesis (Gerasimenko *et al.,* 2016; Lopes-Costa *et al.,* 2017). Macroalgal secondary metabolites like fucoidans, lectins, aplysiatoxins, and kainoids have secured their place in biomedical research while many others are under clinical trials for lung, breast, colon and prostate cancers (Russo *et al.,* 2015; Ruiz-Torres *et al.,* 2017).

Seaweeds are fetching enormous attention from pharmaceutical industries and researchers for novel anti-cancer compounds.

This study is focused on one such green macroalgae genus *Caulerpa* (J V Lamouroux 1809), which belongs to family Caulerpaceae. The genus *Caulerpa* contains 97 species, over 100 different varieties and is distributed in the intertidal and sub-tidal tropical and semitropical marine waters (Guiry and Guiry, 2018). This genus is mainly known for its aesthetic value and invasive potential as some of its species are widely used in aquaria while *C. taxifolia* is listed in world's worst invasive algal species as a federal noxious weed (Talha*,* 2018). Besides, species like *C. lentillifera* and *C. racemosa* are known for their nutritional value and consumed in Japan, Thailand, Philippines and Fiji (De Gaillande *et al.,* 2017). However, little is known about the pharmacological worth of these species. *Caulerpa* species produce several secondary molecules like bisindole alkaloids and diterpenoids, of which particular interest lies in diterpenoids and sesquiterpenoids with an aldehyde or/and enol acetate (Pádua *et al.,* 2015). Many of these compounds exhibit diverse range of bioactivities like insecticidal, anti-microbial, anti-fouling, feeding deterrent, ichthyotoxic, anti-inflammatory, plant growth regulatory, cytotoxic, anti-proliferative, and anti-metastatic activities (Wijesekara *et al.,* 2011; Li *et al.,* 2018). Metabolites like caulerpenyne, caulerpin and caulersin obtained from *Caulerpa* have unusual structures and prominent pharmacological properties (Su *et al.,* 1997; Gross *et al.,* 2006). Despite its significance the genus still remains underexplored with around 300 unverified taxonomic entries (Guiry and Guiry, 2018), no phylogeny based assessment of bioactivity and no records of comparative analysis of *in vitro* anti-cancer activity, to the best of my knowledge. Considering that study of this genus may reveal unique evolutionary trends as well as further insights in to its medicinal properties, following objectives were planned–

I. Development of DNA barcodes for inter-specific and intraspecific level taxonomic identification of evaluated *Caulerpa* spp. and designing a database of Indian algae based on morphological and molecular data
II. Comparative evaluation of *in-vitro* anti-cancer and anti-oxidant activities of *Caulerpa* spp.
III. Analysis of putative correlation between anti-cancer activity and phylogeny of *Caulerpa*

REVIEW OF LITERATURE

2.1 Marine Diversity: Richness, Identification and Significance

Life on the planet Earth originated in the primordial sea around 3.6 billion years ago and is constantly evolving enormously in this aquatic milieu (Joyce, 2002). 'Water' is essential for life and scientists are curiously searching for life in outer space, however, limited knowledge is available about the biodiversity on our own planet, particularly marine diversity. Oceans cover around 70% earth's surface, and inhabit a vast diversity of marine organisms. Marine ecosystem generates half of the atmospheric oxygen, plays a critical role in climate regulation and supports an enormously diverse and exquisitely adapted array of living organisms (St John *et al.,* 2016). Systematic paleontologists have documented marine diversity through the Phaenerozoic era during the last 200 years. Of the 34 major phyla of life, 17 occupy land while 32 inhabit sea, with some existing both on land and sea. It is estimated that 3 million to over 10 million marine species may exist in oceans with around 1,50,000 – 2,74,000 extant described species, and 70-80% undiscovered species (Appeltans *et al.,* 2012). Major life forms of marine ecosystem include microorganisms, marine algae, plants, fungi, invertebrates, vertebrates and planktons. Marine macroalgae or seaweeds, benthic animals and protists account for 98% of species diversity and the rest is pelagic. Many of these species are physiologically and economically important to mankind (Cardozo *et al.,* 2007; Song *et al.,* 2015; Shannon and Ghannam, 2016).

As compared to the richness of marine diversity, little is known about the taxonomy of the marine organisms. The ecological changes because of human interventions and constant evolutionary pressure, further complicate the identification process. In addition, morphological plasticity, highly adaptable nature, shorter life span, cryptic species and human error, make it difficult to identify these organisms only on the basis of morphology (Bast *et al.,* 2015; Nauer *et al.,* 2018). Hebert *et al.* proposed a pioneering approach for species identification in 2004, **DNA barcoding** which is based on the identification of taxa by using a small signature DNA sequences e.g. small mitochondrial genome fragment, COI for animal kingdom (Hebert *et al.,* 2003). Barcoding uses a small fraction of genome as an identifying tag or marker, which differentiates one taxon from the others. The basis of species identification is the 'barcoding gap' amongst intra- and interspecific genetic distance

with 2-3% threshold value for species delimitation. Although barcoding was initially proposed for animals, but also turned successful in land plants, algae and fungi with markers of mitochondrial, plastid, or nuclear origin (Schindel and Miller, 2005; Hajibabaei *et al.,* 2007). Barcoding utilizes unique concept unlike prior molecular studies and provides manifold attributes, allowing identification of genetically distinct populations, cryptic species, synonymy and comparison of datasets amongst different researchers (Li *et al.,* 2015).

However, mere documentation of an increasing number of taxa is only a baby step towards understanding the marine biodiversity, as this rise in number of taxa leads to complexity of individual as well as community-level-interactions. Further expansion and diversification of clades may be accounted for the continuous alterations and complexities of community structures underneath sea (Möllmann *et al.,* 2015). Since the origin of life in sea, around 3.6 billion years ago, extensive evolutions and adaptations have equipped marine organisms with the appropriate mechanisms to thrive in a hostile milieu of extreme temperatures, salinity, pressure, predation and competition. Thereby, marine organisms, especially algae, contribute to varied range of commercial products of industrial, nutraceutical, dietary, cosmetic and pharmaceutical worth e.g. agar, carrageenan, salads, shampoos, and medicines (Griffiths *et al.,* 2016). The Marine Board of European Science Foundation provided a road-map and policy agenda for regional research in *Marine Biotechnology*. The priority research includes clinical drug research, health and personal care products, marine food, and other value-added products for life sciences industry sector (Hurst *et al.,* 2016). Similarly, “Drugs from sea” programme of Ministry of Earth Sciences (MoES), India, led by Central Drugs Research Institute (CDRI), Lucknow, is another example of nationwide efforts towards bioprospecting and drug discovery from marine life (DSF-MoES). Such initiatives in several parts of the globe enkindles curiosity of researchers towards the gigantic biodiversity locked in oceans.

2.2 Algae: Macroalgae /Seaweeds

Algae are heterogeneous, undifferentiated plant-like organisms that have photosynthetic ability and are called thallophytes. Most of the algae are capable of autotrophic and generate carbohydrates and oxygen directly from sun-light. However, the nutritional strategies of whole algal taxa vary over a spectrum of

phototrophy to heterotrophy and thus, are considered mixotrophic (Burkholder *et al.,* 2008). Likewise, algae reproduce by asexual or sexual methods. In asexual reproduction, a motile spore grows into multicellular individuals/gametophytes without fertilization. Alternatively, fission, budding or fragmentation is widely observed in many species. In sexual reproduction, union of two gametes, from individual plants, takes place to form a zygote that develops into a new organism (De Wreede *et al.,* 1988). Algae can be aquatic or terrestrial in origin, microscopic (microalgae) or macroscopic (macroalgae) and can be distributed in every environment, ranging from snow, deserts, hot springs, deep sea to bare rocks with lichen association. Of particular interest, here, are marine macro-algae or seaweeds, which, on the basis of pigments, are further grouped in to Chlorophyta (green algae), Rhodophyta (red algae) and Phaeophyta (brown algae). Green algae get their green color from chlorophyll a and b, and the overall color is determined by the amount of accessory pigments like beta-carotene (yellow), and xanthophylls (yellow/brown) (Chapman and Chapman, 2012). These are commonly found in areas with abundant light, shallow water, tide pools and grows well in marine and fresh water and rarely on land. Red algae get its red colour mainly from phycoerythrin and grows deeper than green and brown algae, as it absorbs blue light. Brown algae of the phylum Phaeophyta (dusky plants) is brown due to pigment fucoxanthin. These are large and complex marine algae and often grows attached to stationary structures like rocks (Guiry, 2012).

Caulerpa (J V Lamouroux 1809), is a genus of green macroalga, belonging to family Caulerpaceae, order Bryopsidales, class Ulvophyceae. Currently, the genus contains 97 species, over 100 varieties and several taxonomically unverified entries (Guiry and Guiry, 2018). *Caulerpa* spp. are distributed in the intertidal and sub-tidal tropical and semitropical marine waters. This genus is known for its unusual anatomy, as it consists of only one cell with several nuclei, and bringing them in the list of biggest cells in the world. These coenocytic algae have creeping rhizome with colorless rhizoids and erect fronds. The fronds occur in variable shapes ranging from oval grapes and flat blades to feather like structures (Bhushan *et al.,* 2016). Many species of this genus are widely used in aquaria owing to their aesthetically pleasing phenotype, and other features like adaptability to new environments, fast growth rate, pH stabilization and nutrient export. An aquarium strain of *C. taxifolia* had created havoc in 1984 due to its unrestrained spread in the

Mediterranean Sea and was listed as one of the world's worst invasive species by IUCN-ISSG (International Union for Conservation of Nature-Invasive Species Specialist Group) (Streftaris and Zenetos, 2006). On the contrary, species like *C. lentillifera* and *C. racemosa* have high nutritional value and are consumed as vegetable and salad delicacies in various countries like Indonesia, Japan, Philippines, Fiji and Thailand (Paul *et al.,* 2014). The genus is also known for its bioactive properties like anti-microbial, anti-inflammatory, anti-cancer (Nagappan and Vairappan, 2014)

2.3 Taxonomic Conflicts

There are many reports of taxonomic conflicts amongst seaweeds and *Caulerpa* is no different, with around 300 unverified intraspecific taxonomic entries, as ascribed in AlgaeBase (Guiry and Guiry, 2018). The earliest accounts of *Caulerpa* spp. were recorded on the basis of morphology by Lamouroux, Agardh and Weber-van Bosse. Later, Svedelius explored the diversity of *Caulerpa* from Sri Lanka (Svedelius, 1906). Pioneering work on Indian *Caulerpa* spp. was done by De Toni, who first identified *C. serrulata* (as *C. freycinetii*), *C. lessonii* and *C. racemosa* var*. turbinata* (*C. chemnitzia*). Subsequent studies added more species to the knowledge pool, with significant contributions by Rao, Duraiswamy, Kazi and co-workers (Duraiswamy, 1984; Rao and Rao 1986; Kazi *et al.,* 2013). The key identifying features of the genus, assimilators and ramuli, vary with respect to environmental factors like temperature, water, movement and irradiance (Monro and Poore, 2005), resulting in several varieties and forms, making identification of *Caulerpa* species bewildering. Famá *et al.*, (2000) described high levels of intra- and inter-specific polymorphism in ITS1 region that affects phylogenetic reconstruction, while 5.8-ITS2 region resulted in well resolved phylogenetic reconstruction (Famá *et al.,* 2000). In another study, Famà *et al.,* (2002) investigated the efficacy of *tufA* and revealed conflicts of intraspecific classification based on morphology and molecular phylogeny. In addition, monophyly of *C. mexicana*, *C. taxifolia*, *C. webbiana*, *C. sertularioides*, *and C. prolifera* and paraphyly or polyphyly of other species was reported (Famà *et al.,* 2002). Another study revealed suitability of *tufA* and ITS for species identification and 18S rDNA insertion sequences for character-based identification (Kazi *et al.,* 2013). Topological differences amongst phylogenies inferred by *tufA* and *rbc*L were observed and their incongruity is

possibly attributed to various organism-level causes like hybridization, horizontal gene transfer, incomplete lineage sorting, and gene-level causes like rate heterogeneity, base/codon composition biases and selection (Belton *et al.,* 2014). Further clarification is required about the classification scheme of the genus *Caulerpa*. Initially, Bosse (1898) classified the genus on the basis of morphology into in to 12 sections namely Vaucherioideae, Charoidae, Bryoideae, Zosteroideae, Phyllantoideae, Fillicoideae, Hippuroideae, Lycopodioideae, Thuyoideae, Araucarioideae, Paspaloideae, and Sedoideae (Bosse, 1898). In 1976 Calvert and team investigated the phylogeny of these pre-recognized 12 sections by using chloroplast ultrastructure and proposed an evolution of large, complex chloroplast with amylogenic and photosynthetic efficiency to existing, simple chloroplast with photosynthetic efficiency alone. *Caulerpa* species were, later, categorized in to five sections by Duraiswamy (Calvert *et al.,* 1976). However, subsequent works using molecular data report that *Caulerpa* species do not follow sectional schemes as proposed earlier, and the classification needs appropriate revision and validation (Famà *et al.,* 2002; Draisma *et al.,* 2014). In order to truly identify and understand the phylogenetic position of various *Caulerpa* species a detailed study with different molecular markers is required.

2.4 Marine Natural Products: Hidden Treasures

Nature harbors a vast biodiversity which is an endless source of valuable natural products that human beings have been using as herbs from thousands of years (Newman and Cragg, 2007). It is estimated that only around 10% world's diversity is evaluated for putative biological activity, and innumerable lead compounds still await discovery (Dias *et al.,* 2012). Despite living in an oceanic planet, the 'silent world' remains largely untapped and is believed to possess unique structural moieties of pharmaceutical interests. Since 1970s, technological advancements like snorkeling, SCUBA, manned submersibles and ROVs (remotely operated vehicles), led to progressive advancements towards understanding of marine environment. Marine natural products (MNP) caught preliminary attention since a symposium 'Drugs from Sea' was held in United States and Huge D. Freudenthal portrayed an enriched future in the marine waters. Subsequently, the discovery of prostaglandin A_2 methyl ester (PGE2) provided an additional thrust to incite research in the field of marine pharmacology (Molinski *et al.,* 2009). Over

10,000 novel compounds have been isolated from marine bacteria, fungi, microalgae, seaweeds, sponges, soft corals, bryozoans, and other marine organisms. Apparently, more than 0.1% of them are structurally unique and display significant biological activity; thus, are considered potential drug leads and are of particularly high interest. These unique structural moieties are possibly a result of marine environment and various stresses therein (Stengel *et al.,* 2011). Marine organisms have developed several physiological and biochemical adaptations through evolutionary processes including production of bioactive compounds for protection from predators, communication, reproduction, competition and infection. Owing to their broad range of activities like anti-tumor, anti-inflammatory, anti-microbial, antinociceptive and anti-diabetic activity, these MNP are considered as source of several value-added products in pharmaceuticals, nutraceuticals and cosmeceuticals (Centella *et al.,* 2017; Mehra *et al.,* 2018a; Mehra *et al.,* 2018c). It is estimated that a 10% increase in novel compounds is recorded as the hunt of drugs from sea is progressing. Till date, 7 marine-derived drugs have been approved by FDA, namely, Ziconotide (Prialt®), Trabectedin/ET-743 (Yondelis®), Brentuximab vedotin/SGN-35 (Adcetris®), Eribulin Mesylate/E7389 (Halaven®), Omega-3-acid ethyl esters (Lovaza®), Vidarabine/Ara-A (Ara-A®), Cytarabine/Ara-C (Cytosar-U®), and 22 are in clinical trials while several others are in pre-clinical pipeline (Mayer*,* 2018).

In the last 40 years, marine resources have fetched enormous attention of researchers for the extraction of novel bio-products which can be used against cancer. Statistical models estimate around 2,53,120 – 5,95,232 novel compounds (90.4 – 92.6% undiscovered) and pending discoveries of anti-cancer drugs worth US $563 billion – 5.69 trillion from marine organisms (Erwin *et al.,* 2010). Of the already known drugs, several drugs are often characterized as working on multiple targets and/or different set of diseases, as in case of Bryostatin, and Aplidin® (Sun and Alkon, 2006; Mitsiades *et al.,* 2008; Safaeinejad *et al.,* 2018). Bryostatin-1, initially developed as anti-cancer drug has shown efficacy against other diseases like Alzheimer's disease and HIV (Gutiérrez *et al.,* 2016). There are several marine or marine-derived drugs which have been approved as anti-cancer drugs by FDA (Food and Drug Administration)/EMA (European Agency for the Evaluation of Medicinal Products) or are in clinical trials **(Table 2.1)** and few others have been patented (**Table 2.2)**. These drugs vary in structure from as simple as linear

peptides (dolastatin-10) to complex macrocyclic polyethers (halichondrin B) and act as microtubule targeting agents (MTAs), nucleic acid interfering agents, enzyme inhibitors, membrane depolarizing agents, PKC inhibitors, protein antagonists, or apoptotic agents. Marine drugs have unique structural modifications and intricate C-skeletons associated with specific mechanisms and tolerance of human body, with negligible manipulations, making them suitable target for research (Bai *et al.,* 1990; Altmann, 2017)

Amongst marine organisms, **seaweeds** are of great interest, as these are being used as traditional and folk medicine since ages (Chengkui *et al.,* 1984). Ancient Romans and Egyptians used them to treat wounds, burns and breast cancer, owing to their potential as anti-inflammatory and antimicrobial agents. Reports suggest that during 1977-1987, algae were the source of around 35% newly discovered chemicals, followed by sponges (29%) and cnidarians (22%). Macroalgae are multicellular, undifferentiated plant-like organisms and inhabit the littoral zone in the sea (El Gamal, 2010). Macroalgae, previously serving as gelling agents, have multifaceted use in food, agriculture, chemical and pharmaceutical industry. These versatile marine resources have been widely used as emulsifier in fruit jelly, toothpaste and organic cosmetic products (Bhakuni and Rawat, 2005). These are well documented as a prolific source of bioactive compounds like terpenoids, sterols, amines, phenazine and guanidine derivatives, brominated and oxygen heterocycles (Bhakuni and Rawat, 2005). Many seaweeds are edible and are being consumed in various countries worldwide viz. Japan, China, Korea, Ireland, coastal areas of USA and Canada. Scientists have reported that these seaweeds consuming regions have lower prevalence of diet related cancer, breast cancer and coronary heart diseases with inhibitory effects on benign and tumour neoplasia (Kono *et al.*, 2004). Seaweeds have also been shown to modulate ROS (reactive oxygen species) generation which in turn plays essential role in carcinogenesis (Murugan and Iyer, 2014). Extracts from a broad range of algae like *C. taxifolia* (green alga), *Gracilaria corticata* (red alga), and *Laminaria japonica* and *Sargassum oligocystum* (brown algae) have displayed anti-cancer and anti-metastatic properties on different cancer cell lines (Lee *et al.*, 2013). Macroalgal secondary metabolites like fucoidans, lectins, aplysiatoxins and kainoids have secured their place in biomedical research while many others are under clinical trials for lung, breast, colon and prostate cancers (Mohamed *et al.*, 2012). Seaweeds are

fetching enormous attention from pharmaceutical industries and biomedical researchers for novel anti-oxidant, anti-inflammatory, anti-viral, anti-AIDS and anti-cancer compounds (**Table 2.3)**.

2.5 *Caulerpa* Striking Against Cancer

Cancer arises with the unrestrained growth and proliferation of normal cells that escape apoptosis. The resultant changes in the cancerous cells are predominantly a consequence of alterations in the genetic material that may be credited to unhealthy living, environmental risks and lifestyle (Vineis and Wild, 2014; Ashford *et al.,* 2015). Historical evidence of cancer dates back to 3400 BC in Egyptian bones that were described as 'ulcers' and 'swellings' of skin in *Egyptian papyri*. Similar descriptions can be found in the ancient medical literature of Persia, Mesopotamia and India too but these writings ascribe no cure to the disease (Ackerknecht, 1958). Cancer is posing a great challenge to the pharmaceutical industry from many decades and ranks second after the cardiovascular diseases for the rate of mortality, claiming about 9.5 million deaths globally in 2018. The projected incidence is estimated to reach 29.5 million per year by 2040, in comparison to 18.1 million per year in 2018, representing a 62% hike (Ferlay *et al.,* 2018). As per the 'World Cancer Report' more than 60% diagnosed cases are from underdeveloped or developing countries (Stewart and Wild, 2014). Developing countries are heading towards the development, following rapid societal and economic progresses and are likely to be 'westernized'; so the patterns of cancer incidence is likely to shift from infection-related cancers to dietary, reproductive and hormonal related risk factors. At present, Indians are particularly at higher risk of acquiring cancers owing to their unhygienic living conditions, and unhealthy habits like excessive smoking, tobacco use, occupational risks etc. adversely affecting country's economy (Sinha *et al.,* 2003; Rajanandh *et al.,* 2018).

Finding a novel, efficient and cost effective drug is of primary concern for researchers at present. Despite some of the very promising drugs like Taxol, Mutamycin and Cytoxan, the hunt for new candidate drugs, preferably natural products, is continuing at a greater pace (Harvey *et al.,* 2015). Nature possesses a vast biodiversity possessing valuable natural products that human beings have been using as herbs from thousands of years (Mehra *et al.,* 2018a; Gill *et al.,* 2018). Although no such treatments for cancer were available back then. However, after

the advent of microscopy and autopsy, the famous surgeon John Hunter described that surgeries can cure non-malignant cancers; a Century thereafter, surgeries flourished with the help of anaesthesia and radical mastectomy became popular (Wakeley, 1955). In the 21st Century, developments in cancer research have led to better understanding of mechanisms underlying cancer development. Increasing focus on cancer therapeutics is evident from the considerable increase in the number of new candidate drugs entering clinical studies every year. While conventional drugs don't differentiate between healthy and cancerous cells, the newer ones work on much efficient targeted approach (Weinberg and Chandel 2015; Kim *et al.,* 2016). These targeted therapies work majorly on angiogenesis inhibition, apoptosis induction, signal transduction inhibition, gene therapies and monoclonal antibodies (Asghar *et al.,* 2015; Jones *et al.,* 2016; Sau *et al.,* 2017).

Having grown in the inter-tidal zone, *Caulerpa* species are periodically exposed to various kinds of stresses like UV, salt, nutrient limitation, light, temperature, shear and desiccation stress etc. which leads to production of many stress molecules (Paul and Fenical, 1986). In response to stress, these species produce many secondary metabolites like bisindole alkaloids and diterpenoids of which particular interest lies in diterpenoids and sesquiterpenoids with aldehyde or/and enol acetate. Many of these compounds exhibit diverse range of bioactivities like insecticidal, anti-microbial, antifouling, feeding deterrent, ichthyotoxic, anti-inflammatory, plant growth regulatory, cytotoxic, anti-proliferative, and anti-metastatic activities (Lin *et al.,* 2012; Nagappan and Vairappan, 2014). The uniqueness of secondary metabolites of *Caulerpa* can be attributed to distinct marine environment and physiological adaptations through evolutionary processes. These metabolites include various bioactive compounds for defense, communication, reproduction, competition and infection (Montaser and Luesch, 2011). Initial probing of this genus was because of a peppery taste of edible species and avoidance of *Caulerpa* species by herbivores and, which fascinated researchers for chemical profiling of several species. *Caulerpa* spp. produce several unprecedented secondary metabolites and most of them are linear or monocylic terpenoids possessing aldehydic and enol-acetate functional groups. A terminal bis-enol acetate group is uniquely found in this genus of marine algae. This functional group is represented by an acetylated bis-enol category of 1,4-dialdehyde group imparting biological activity to several species (Gavagnin *et al.*, 1994). Major

metabolites **(Figure 2.1)** documented from genus *Caulerpa* and their bioactivities are listed in **Table 2.4**.

Despite continuous efforts and promising claims of scientists about assured cures of cancer, it is still daunting the clinicians. One major cause for this is notorious survival strategies of cancer cells by modifying multiple signalling pathways (Vogelstein and Kinzler, 2004). Researchers are now attempting to target cancer cells the same way, so that cancer cells don't survive multiple damages (Dreaden *et al.,* 2011; Khan *et al.,* 2015). Secondary metabolites and crude extracts of *Caulerpa* have shown promising results *in vitro* and *in vivo,* and are considered potential candidates against cancer. These species are reported to cause modulations in microtubule dynamics, inhibit PTP1B (protein tyrosine phosphatase-1B), ER stress, AMPK pathway modulations, inhibit HIF-1 (hypoxia inducing factor-1), cell cycle arrest and apoptosis. Caulerpenyne and methanolic extract of *C. racemosa* are reported to interfere with microtubule dynamics, highlighted by abnormal DNA replication, and neurite inhibition, respectively (Barbier *et al.,* 2001; Bourdron *et al.,* 2009). Another study reports, ER stress pathway activation in leukaemia WEHI-3 cells via upregulation of GRP78 (glucose-regulated protein-78) and GADD153 (growth arrest and DNA damage), by caulerpenyne treatment, subsequently leading to apoptosis (Chou *et al.,* 2014). Secondary metabolites isolated from *C. racemosa* viz. 4′,5′-dehydrodiodictyonema A, (23*E*)-3*β*-hydroxystigmasta-5,23-dien-28-one, *α*-tocopherolquinone, *α*-tocospirone, (3*β*,24*R*)-stigmasta-5,28-diene-3,24-diol, racemosin-C and caulersin exhibit PTP1B inhibitory activity with IC_{50} values of 2.30, 3.85, 11.01, 3.80, 10.34, 5.86 and 7.14 μM, respectively (Mao *et al.,* 2006; Yang *et al.,* 2015). Caulerpin also induces mitochondrial dysfunctions, (Ferramosca *et al.,* 2016) and incurs inhibitory effects on complex I of electron transport chain (ETC) and decreases oxygen consumption rate in SW480 and LOVO cells (colorectal cancer) with a concomitant elevation of ROS and decrease in ATP production (Yu *et al.,* 2017). This disrupts the crucial energy balance of cells and leads to cell death. Decreased expression of GLUT1, HKII and PFKB3 suggest an activation of AMPK pathway in a calcium-dependent member, possibly by LKB1 that senses elevated AMP:ATP ratio. Caulerpenyne interrupts DNA replication, causing cell cycle arrest at metaphase-like-stage in sea urchin embryos (Pesando *et al.,* 1996). Likewise, methanolic extracts of *Caulerpa* are reported to supress the expression of cyclin D, cyclin E, CDK6, CDK2 and

elevate the expression of p21, p27, p53 in myelomonocytic leukemia (WEHI-3) cells. These results suggest and *Caulerpa*-induced cell damage which activates p53 protein, p21 and p27, thereby, inhibiting CDK6/cyclin D and CDK2/cyclin E, respectively, causing cell cycle arrest at G_0/G_1 phase (Lin *et al.,* 2012). *C. microphysa* pepsin digested extract (CME) induces apoptotic pathway in WEHI-3 cells. CME disrupts the cellular homeostasis by inducing Ca^{2+} release and decreases mitochondrial membrane potential (MMP), thus, initiating apoptotic events. CME also causes downregulation of protein levels of bcl-2 and upregulation of Bid, Bax, AIF (apoptosis inducing factor), caspase-9 and caspase-3 (Chou *et al.,* 2014). Likewise, PARP-1, caspase-9 and caspase-3 activation is also reported by caulerpin, in LOVO cells (Yu *et al.,* 2017). The proposed mechanism of action is shown in **Figure 2.2** where *Caulerpa* affects multiple signalling pathways in cancer causing metabolic reprogramming, cell cycle arrest and apoptosis (Mehra *et al.,* 2018b).

2.6 Interplay Between Oxidative Stress and Cancer

Oxidative stress refers to the imbalance of homeostasis between generation and body's ability of scavenging ROS. This homeostasis is crucial for the cell survival and perturbed physiological concentrations lead to several diseases like cardiovascular diseases, neurodegenerative diseases and cancer. ROS are believed to play a diphasic role in the development as well as suppression of cancer (Schumacker, 2015). While low levels of ROS are required to maintain cell survival and help in defences against pathogen; high levels of ROS are toxic to cells. Cancer cells are adapted for high ROS level and growing body of evidences suggest that a further increase in ROS level leads to oxidative damage-driven cell death (Gorrini *et al.,* 2013). Piperlogumine, a natural product isolated from *Piper longum* L., has been shown to selectively suppress cancer cells via increased ROS and apoptosis (Raj *et al*., 2011). Likewise, many natural anti-oxidants like flavonoids and phlorotannins are reported from marine algae and are shown to exhibit various bioactivities (Nakai *et al.,* 2006; Shipeng *et al.,* 2015). High SOD (superoxide dismutase), CAT (catalase) and GSH-Px (glutathione peroxidase) activities have been observed in *Caulerpa* species with their possible association with anti-cancer therapy (Cavas and Yurdakoc, 2005a).

2.7 Correlation between Phylogeny and Activity

Evolution plays an important role in the development of chemical defenses in plants and other organisms leading to the production of specialized metabolites which have proven bioactive properties in various organisms. This correlation of phylogeny and biosynthetic pathways has emerged as a new predictive approach enabling more selective targeting of source organisms for the development of traditional as well as novel drugs (Evans-Illidge *et al.,* 2013). Previously, activity profiling of marine sponge-associated bacteria was done using 16S rRNA gene and 16S rRNA-derived bacterial community analysis. It was inferred that sponge-specific bacteria were clustered together in monophyletic groups suggesting similar activity profiles based on genetic distance (Kamke *et al.,* 2010). Similar results were obtained in another study, where an association between phylogenetic positions and anti-fouling activity of bacterial epiphytes from the marine green alga, *Ulva lactuta*, was demonstrated. Likewise, positive correlation was ascribed between nucleotide divergence and pheromone diversity in tephritid fruit fly, *Bactrocera* (Symonds *et al.,* 2009) and diversity of cuticular hydrocarbons in ant species suggesting differences in biosynthetic pathways in different lineages (Wilgenburg *et al.,* 2011). A case study of plant subfamily Amaryllidoideae involving parsimony and Bayesian phylogenetic analysis of nuclear, mitochondrial and plastid DNA sequences of 100 species, revealed significant correlation between phylogenetic signals of alkaloid diversity and *in vitro* bioassays for the same (Rønsted *et al.,* 2012). Positive correlation between evolutionary relatedness and anti-cancer activity was observed in traditional Chinese marine medicines derived from species of super-kingdom bacteria, class Viridiplantae and class Holothuroidea (Fu *et al.,* 2017). Similar correlations are believed to exist amongst all other groups including seaweeds, that may revolutionize the field of bioprospecting.

2.8 Drug Development from Marine Sources: Major Roadblocks

Development of drugs from marine organisms is not that easy as it seemed to be, mainly because of the technical obstacles that prevented their commercial success. The foremost reason is the ‘supply of source’; majority of MNPs have complex structures which require huge amounts of samples for chemical synthesis (Bhatnagar and Kim, 2010). Generally, the yield of MNPs is quite low, up to 10^{-6}% based on fresh weight. The extent of supply issue can be imagined from the fact over 1 ton of *Ectenaiscidia turbinate*, would lead to production of only 1 g of

bryostatin-1 or ecteinascidin. Secondly, accessibility of the marine samples is quite difficult, as some of the organisms are deep-dwelling and some reside in marine mangroves (Proksch *et al.,* 2003). There are also difficulties in harvesting the product, as enough biomass needs to be generated in order to isolate adequate amounts of purified product. Structural complexity is another hindrance which may pose difficulty in the isolation of lead molecule. High quality drug leads which satisfy the criteria of a 'future drug candidate' and ADMET (absorption, distribution, metabolism, excretion and toxicity) properties of disposition within an organism are hard to find. The complex structure of marine drugs makes it difficult to synthesize the related compounds and requires several steps to attain the final structure (Glaser and Mayer, 2009). In addition, lack of ample literature on the culturing and isolation procedures makes the it worse. Besides, lack of enough funds and resources hinders the progress of marine drug discovery. Considering the above-mentioned difficulties, it becomes obligatory to design strategic approach for drug discovery from marine environment. In order to tackle the supply and harvesting issue, one can opt for aquaculture to enhance the production of biomass. Alternatively, strategic selection of species like *C. taxifolia* which are invasive and can be procured easily, can be beneficial in terms of activity, supply and harvesting (Montefalcone *et al.*, 2015; Mehra *et al.,* 2018a). Secondly, it is possible to synthesize the complex lead molecule by a semi-synthetic approach, thereby reducing the number of synthesis steps required to produce the target compound and increase the yield at each step. For example, bryostatin-2 which initially had a 40-step synthesis chemistry can now be synthesized in 20 steps by Keck's pathway (Manaviazar and Hale, 2011). Additionally, novel compounds can also be generated by genetic manipulations in the original biosynthetic pathways of already existing complex MNPs or by genetically engineering biosynthetic genes from two different organisms. Various other techniques and strategies are continuously evolving for disease understanding, probing of new cancer drugs, high throughput screening and several analytical methods for exploring rich marine diversity that derives many researchers to inquisitively look for promising drug leads of commercial value (Nastrucci *et al.,* 2012).

Table 2.1 Clinical status of various anti-cancer drugs from marine organisms.

S. No.	Name	Chemical Class	Organism	Mode of Action	Company	Status	References
1.	Cytarabine, ARA-C	Nucleoside with a modified sugar	Sponge: *Cryptotheca crypta*	DNA Polymerase Inhibitor	Bedford, Enzon, Pfizer	FDA-EMA Approved for childhood. FDA-approved intrate cal in relapsed pediatric leukemia	(Mayer *et al.*, 2010)
2.	Trabectedin (ET-743)/ Yondelis®	Tetrahydroisoqui noline alkaloid	Tunicate: *Ecteinascidia turbinate*	Binding to minor groove DNA alkylating Guanine at N2.	PharmaMar	EMA Approved FDA: Orphan drug status for soft-tissue sarcoma and ovarian cancer	(Kim, 2015)
3.	Brentuximab vedotin/ SGN-35 (Adcetris®)	Antibody drug conjugate (ADC)	Mollusc/ Cyanobacteriu m	CD30 and microtubule interference	Seattle Genetics Inc.	FDA Approved	(Chen *et al.*, 2015)
4.	Eribulin Mesylate (E7389)/ Halaven®	Fully synthetic macrocyclic ketone, Halichondrin B analogue	Sponge: *Halichondria okaday, Axinella carteri* (Halichondrin B)	Microtubule interfering agent	Eisai Inc.	FDA-EMA Approved for metastatic breast cancer	(Gerwick and Moore, 2012)
5.	Plitidepsin (Aplidine®)	Cyclic depsipeptide; didemnin B derivative	*Aplidium albicans* Milne Edwards (Tunicate)	Rac 1 and JNK activation	PharmaMar	Phase III; Orphan Drug for multiple myeloma	(Spicka *et al.,* 2017)
6.	Plinabulin (NPI-2358)	Diketopiperazine	Fungus	Microtubule Interfering agent	Beyond Spring Pharmaceuticals	Phase III	(Mohanlal *et al.,* 2016)
7.	Depatuxizuman mafodotin (ABT-414)	ADC	Mollusk/ cyanobacterium	Modulations of EGFR and microtubules	AbbVie	Phase III	(Mayer, 2018)

8.	Lurbinectedin (PM01183)	Alkaloid	Tunicate	RNA polymerase II inhibition	Pharma Mar	Phase III	(Mayer, 2018)
9.	Polatuzumab vedotin (DCDS-4501A)	Beta-lactone-gamma lactam	Bacterium	CD79b and microtubule modulations	GeneTech/Roche	Phase III	(Mayer, 2018)
10.	Marizomib, Salinosporamide A (PI-0052)	Lactam-lactone bicycle	Marine bacterium: *Salinispora tropica*	20S Proteasome inhibitor	Triphase	Phase III	(Mayer, 2018)
11.	Kahalalide-F	Cyclic depsipeptide	Mollusc *Elysia rufescens*	Lysosomotropic	PharmaMar	Phase II in NSCLC, melanoma, liver carcinoma	(Miguel-Lillo *et al.,* 2015)
12.	Bryostatin-1	Polyketide	Bacterium/ Bryozoa: *Bugala neritina*	PKC activation	National Cancer Institute	Phase II in colon-rectal cancer disease progression.	(Murphy *et al.*, 2014)
13.	Zalypsis®, (PM00104)	Synthetic alkaloid tetra-hydroisoquinoline related to *Jorumycin*	Nudibranch: *Jorunna funebris* (*Jorumycin*)	Double strand DNA breaks triggering a DNA damage response	PharmaMar	Phase II unresectable metastatic Ewing family of tumors (EFT)	(Ocio *et al.,* 2016)
14.	Enfortumab Vedotin (ASG-22ME)	ADC	Mollusk/ cyanobacterium	Nectin-4 and microtubule interferance	Seatle Genetics	Phase II	(Mayer, 2018)
15.	Elisidepsin, (PM02734), Irvalec®	Synthetic cyclic depsipeptide of the kahalalides family. Dehydro amino- butyric acid-containing peptides	Mollusc: *Elysia rufescens*	Necrosis and plasma membrane alterations	PharmaMar	Phase IB/II In pretreated advanced gastroesophageal cancer	(Serova *et al.,* 2013)

16.	Tasidotin*, Synthadotin® (ILX-651)	Third-generation Dolastatin-15 analogue. Seven- subunit depsipeptide	Mollusc: *Aplysidae*	Microtubule interfer- ing agent	Genzyme Corporation	Phase II	(Petit and Biard, 2013)
17.	LAF389	Bengamide B synthetic analogue. Amino acid derivative	Sponge: *Choristida* (Ben- gamide)	Methionine amino-peptidase inhibitor	Novartis	Phase I advanced cancer	(Nastrucci *et al.,* 2012)
18.	ARX-788	ADC	Mollusk/ cyanobacterium	HER2 and Microtubule modulation	Ambrex & Zhediang Medicine	Phase I	(Mayer, 2018)
19.	Taltobulin (HTI-286)	Hemiasterlins analogue. Tripeptide	Sponge: *Siphonochalina* (Hemiasterlins)	Microtubule interfering agent (depolarizing)	Wyeth	Phase I	(Schippers *et al.,* 2012)
20.	Discodermolide	Polyhydroxylate d lactone	Sponge: *Discodermia dissoluta*	Microtubule stabilizing agent.	Novartis Pharma AG	Phase I	(Joseph and Nair, 2013)
21.	Spisulosine (ES-285)	Sphingoid -type base	Mollusc: *Spisula polynyma*	RhoA as target	PharmaMar	Phase I	(Sarfaraj *et al.,* 2012)

Table 2.2 Representative List of Patents related to Marine-derived Drugs

US Number Patent	Description of the Invention	Reference
US7439265B2	Synthesis of anti-tumor agents, Irciniastatins A and B from the Indo-pacific marine sponge *Ircinia ramosa*	(Pettit and Xu, 2008)
US7759345B2	Anti-tumorous derivatives of Ecteinascidin-743	(Martinez *et al.,* 2011)
US7622289B2	Methods to identify inhibitor of Ornithine δ-amino transferase (OAT)- assisted microtubule assembly (target of anti-cancer drugs)	(Harran *et al.,* 2009)
US7947671B2	Synthesis scheme of natural ecteinascidins and related compounds, having anti-tumor property	(Barrasa *et al.,* 2011)
US20090142331	Bio-active compounds from novel actinomycete taxa MAR3A, MAR3B and MAR4 (Family Treptomycetaceae)	(Fenical and Jensen, 2009)
US20110081690	Sustainable method for synthesizing marine natural product– tetrodotoxin (TTX)	(Strand and Sundberg, 2011)
US8450366B2	Novel isobenzofuran analogues of sclerophytin A with anti-tumor activity	(McIntosh, 2013)
CN100509002C	Marine medicine for treating hypertension, preparation process and dispersible tablet thereof	(刘永宏 *et al*., 2007)
JP5107043B2	Novel therapeutic agents from marine organisms	(Foong and Kuwabara, 2009)
US5089481A	Anti-viral agents from seaweeds	(Muto *et al.,* 1992)
US20080145380A1	Cancer treatment by algae	(Teas, 2008)

Table 2.3 Algal metabolites with anti-cancer activity

Chemical Class	Compound	Source	Bioactivity	Reference
Polysaccharide	Alginate	*Sargassum vulgare* C. Agardh (Brown alga)	Inhibition of tumor proliferation and Immunomodulation	(Park, 2015)
Polysaccharide	Laminarin	*Laminaria japonica* (Brown alga)	Induction of apoptosis in HT29 colon cancer cell line	(Park *et al.*, 2013)
Polysaccharide	Ulvan	*Ulva* Linnaeus and *Enteromorpha* Link (Green algae)	Anti-tumour and Immunomodulation	(Qi *et al.*, 2005)
Sulphated Polysaccharide	Κ & λ Carrageenan	*Kappaphycus striatum* Doty and *Chondrus ocellatus* Holmes resp. (Red algae)	Anti-tumor and Immunomodulation	(Luo *et al.*, 2015; Venkatesan *et al.*, 2015)
Sulphated Polysaccharide	Fucoidan	*Fucus vesiculosus* Linnaeus and S*argassum* C. Agardh spp. (Brown algae)	Cytoxic against melanoma cells and lung carcinoma *in vitro* and NK cells activation in mice *in vivo*	(Kwak, 2014)
Sulphated Polysaccharide	Sarg A	*Sargassum stenophyllum* Martius (Brown alga)	Anti-angiogenic, Tumor inhibition, reduced cell viability and migration of cancer cell line B16F10	(Murphy *et al.*, 2014)
Sulphated Polysaccharide	Porphyran	*Porphyra yezoensis* Ueda (Red alga)	Anti-tumor: caspase mediated apoptosis	(Moussavou *et al.*, 2014)
Sulphated Polysaccharide	Translam	*Laminaria* spp. (Brown algae)	Cytotoxic activities	(Taskin *et al.,* 2010)

Depsipeptide	Kahalalide F	*Bryopsis pennata* (Green alga)	Induces oncosis in tumor cells	(Smit, 2004)
Depsipeptide	Coibamide A	*Leptolyngbya* Anagnostidis & Komarek sp. (Cyanobacteria)	Cytotoxicity against human NCIH460 cell line	(Medina *et al.*, 2008)
Cyclic depsipeptide	Largazole	*Symploca* Kützing ex Gromont sp. (Cyanobacteria)	Cytotoxicity against melanoma and renal cell lines	(Cole *et al.*, 2011)
Amino acid derivative	Dimethylsulfonio-propionate (DMSP)	*Polysiphonia fastigata* Greville (Red alga)	Anti-cancerous effects against Ehrich ascites carcinoma in mice *in vivo*	(Lee *et al.*, 2013)
Sterol derivative	β-Sitosterol	*Caulerpa* spp. (Green algae)	Anti-tumor activity, oxidoredutase inhibition	(Azhaguraz *et al.*, 2012)
Polyphenol	Phlorotannins	*Ecklonia kurome* Okamura (Brown alga)	Anti-oxidant activity and Inhibition of cell proliferation	(Li *et al.*, 2011)
Phenol derivative	Phloroglucinol and its polymers (eckol, phlorofucofuroeckol)	*Eisenia bicyclis* Setchell (Brown alga)	Anti-cancerous activity against LI210 leukemia cells	(Lee *et al.*, 2013)
Orthoquinone	Stylopoldione	*Stypodium zonale* Papenfuss (Brown alga)	Inhibits mitotic spindle formation	(Simmons *et al.*, 2005)
Indole-alkaloid	Scytonemin	*Stigonema* C. Agardh ex Bornet & Flahault sp. (Cyanobacteria)	Anti-proliferative	(Stevenson *et al.*, 2002)

Naphthyridine Alkaloids	Lophocladine A and B	*Lophocladia* F. Schmitz sp. (Red alga)	Cytotoxic against lung cancer and neuroblastoma cell lines	(Tohme *et al.*, 2011)
Terpene	Meroterpenes and Usneoidone	*Cystoseira usneoides* Linnaeus (M. Roberts) (Brown alga)	Anti-inflammatory, antioxidant and anti-proliferative activity	(Mhadhebi *et al.*, 2014)
Terpeneoid	β-Carotene	*Porphyra* C. Agardh (Red alga), *Undaria pinnatifida* Surinagar (Green alga)	Anti-mutagenic, prevention of breast cancer	(Yang *et al.*, 2010)
Triterpenoid	Taraxerol	*C. lamourouxii* (Turner) C. Agardh (Green algae)	Anti-tumor activity	(Azhaguraz *et al.*, 2012)
Sesquiterpenoid	Caulerpenyne	*Caulerpa* J. V. Lamouroux sp. (Green algae)	Anti-proliferation in SKN-SH cell lines	(Sithranga and Kathiresan, 2011)
Bis(indole) amide	Chondriamide A	*Chondria atropurpurea* Harvey (Red alga)	Cytotoxic to colorectal and nasopharyngeal cell lines	(Sithranga and Kathiresan, 2011)
Mixed peptide-polyketide	Apratoxin A	*Lyngbya bouilloni* L. Hoffmann & V. Demoulin (Cyanobacteria)	Inhibition of adenocarcinoma: G_1 cell cycle arrest and FGFR inhibition	(Tohme *et al.*, 2011)

Table 2.4 Bioactivity of semi-purified extracts and pure compounds obtained from various species of *Caulerpa*

S.No.	Compound	Activity	References
1.	Caulerpenyne	Anti-bacterial; anti-neoplastic; neurotoxic; allelotoxic; anti-mitotic; phytotoxic; and anti-proliferative activity	(Barbier *et al.,* 2001; Mozzachiodi *et al.,* 2001; Bourdron *et al.,* 2009)
2.	Caulerpin	Anti-tumor; anti-inflammatory; anti-mitotic, anti-microbial; AMPKα modulatory; and antinociceptive activity	(De Souza *et al.,* 2009; Liu *et al.,* 2009; Yu *et al.,* 2017)
3.	Racemosin C	PTP1B inhibitory activity	(Yang *et al.,* 2014)
4.	Caulersin	PTP1B inhibitory activity	(Yang *et al.,* 2014)
5.	10,11-epoxycaulerpenyne	Cytotoxic	(Lemée *et al.,* 1993)
6.	Flexilin	anti-bacterial, anti-fungal	(Paul and Fenical, 1986)
7.	(23E)-3β-hydroxy-stigmasta-5,23-dien-28-one	PTP1B inhibitory; and neuroprotective activity	(Yang *et al.,* 2015)
8.	40 ,50 - dehydrodiodictyonema A	PTP1B inhibitory activity	(Yang *et al.,* 2015)
9.	Trans-phytol	PTP1B inhibitory activity	(Yang *et al.,* 2015)
10.	Trans-phytyl acetate	PTP1B inhibitory activity	(Yang *et al.,* 2015)
11.	α-tocopherol quinone	PTP1B inhibitory activity	(Yang *et al.,* 2015)
12.	α-tocospirone	PTP1B inhibitory; and neuroprotective activity	(Yang *et al.,* 2015)
13.	(3β,24R)-stigmasta-5,28-diene-3,24- diol	PTP1B inhibitory activity	(Yang *et al.,* 2015)
14.	(3β,24S)-stigmasta-5,28-diene-3,24-diol	PTP1B inhibitory activity	(Yang *et al.,* 2015)
15.	(22E)- 3β-hydroxy-cholesta-5,22-dien-24-one	PTP1B inhibitory; and neuroprotective activity	(Yang *et al.,* 2015)
16.	Taraxerol	Anti-viral; phosphatase inhibitory; anti-nephretic; phospholipase-C (PLC) inhibitory activity	(Azhaguraj *et al.,* 2012)
17.	β-sitosterol	PLC inhibitory; nephrotoxic,	(Azhaguraj *et al.,* 2012)

		Transcription factor inhibitory; acylglycerol lipase inhibitory; hepatoprotectant; phosphatase inhibitory activity	
18.	Palmitic acid	Superoxide dismutase (SOD) inhibitory; Catalase inhibitory; NADPH inhibitory; NADH inhibitor; Succinate-CoA ligase inhibitory; apoptosis agonistic activity	(Azhaguraj *et al.,* 2012)
19.	Sulfoquinovosyldiacylglycerol (SQDG)	anti-viral activity, DNA pol inhibitory activity	(Ohta *et al.,* 1998; Wang *et al.,* 2007)
20.	Two unnamed compounds isolated from *C. prolifera* and *C. bikinensis,* respectively	Phospholipase-A_2 inhibitory activity	(Mayer *et al.,* 1993)
21.	Sulphated polysaccharide fractions	Antinociceptive; anti-inflammatory; anti-coagulant activity; anti-herpetic activity	(Ghosh *et al.,* 2004; Rodrigues *et al.,* 2012)

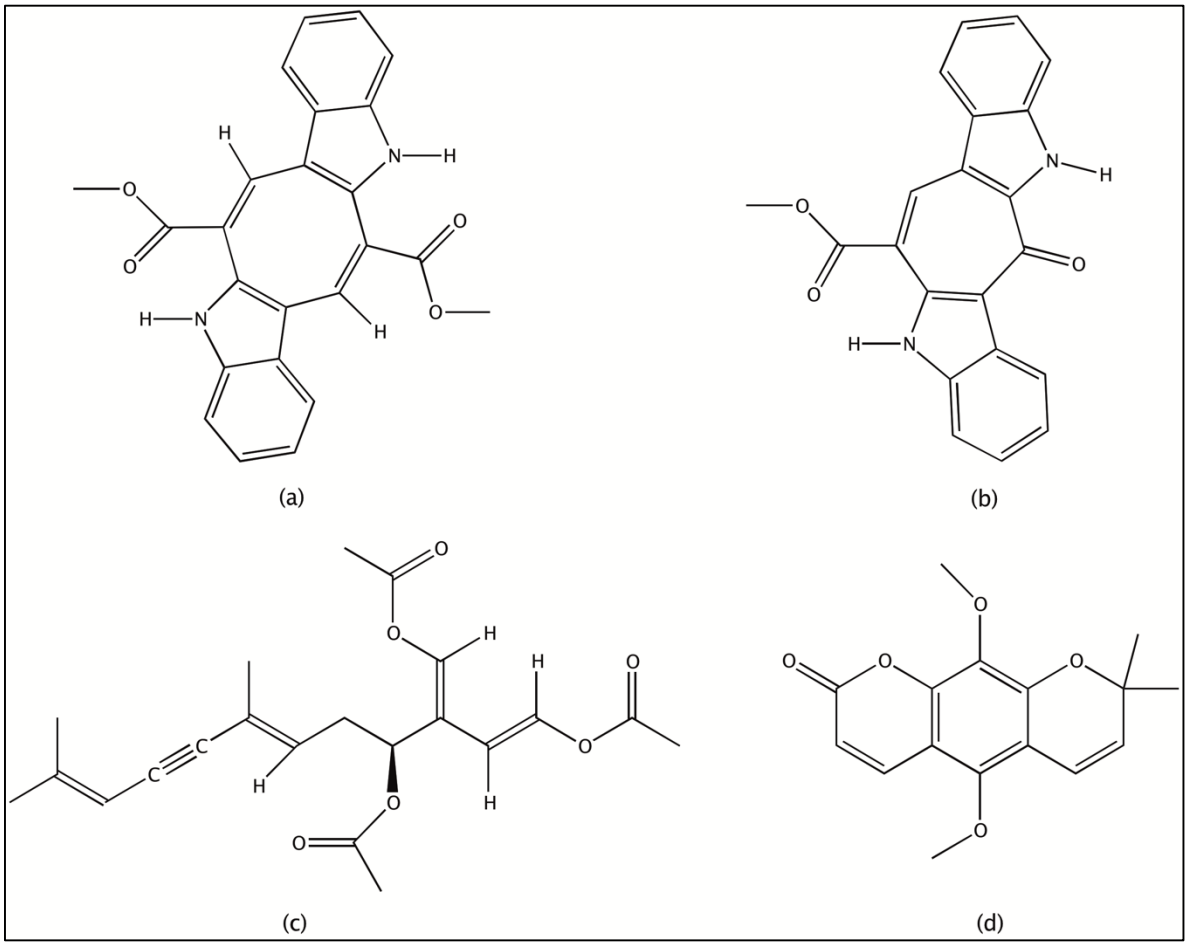

Figure 2.1 Chemical Structures of major secondary metabolites from genus *Caulerpa* : (a) Caulerpin; (b) Caulersin; (c) Caulerpenyne; and (d) Racemosin C. (Kim *et al.,* 2016)

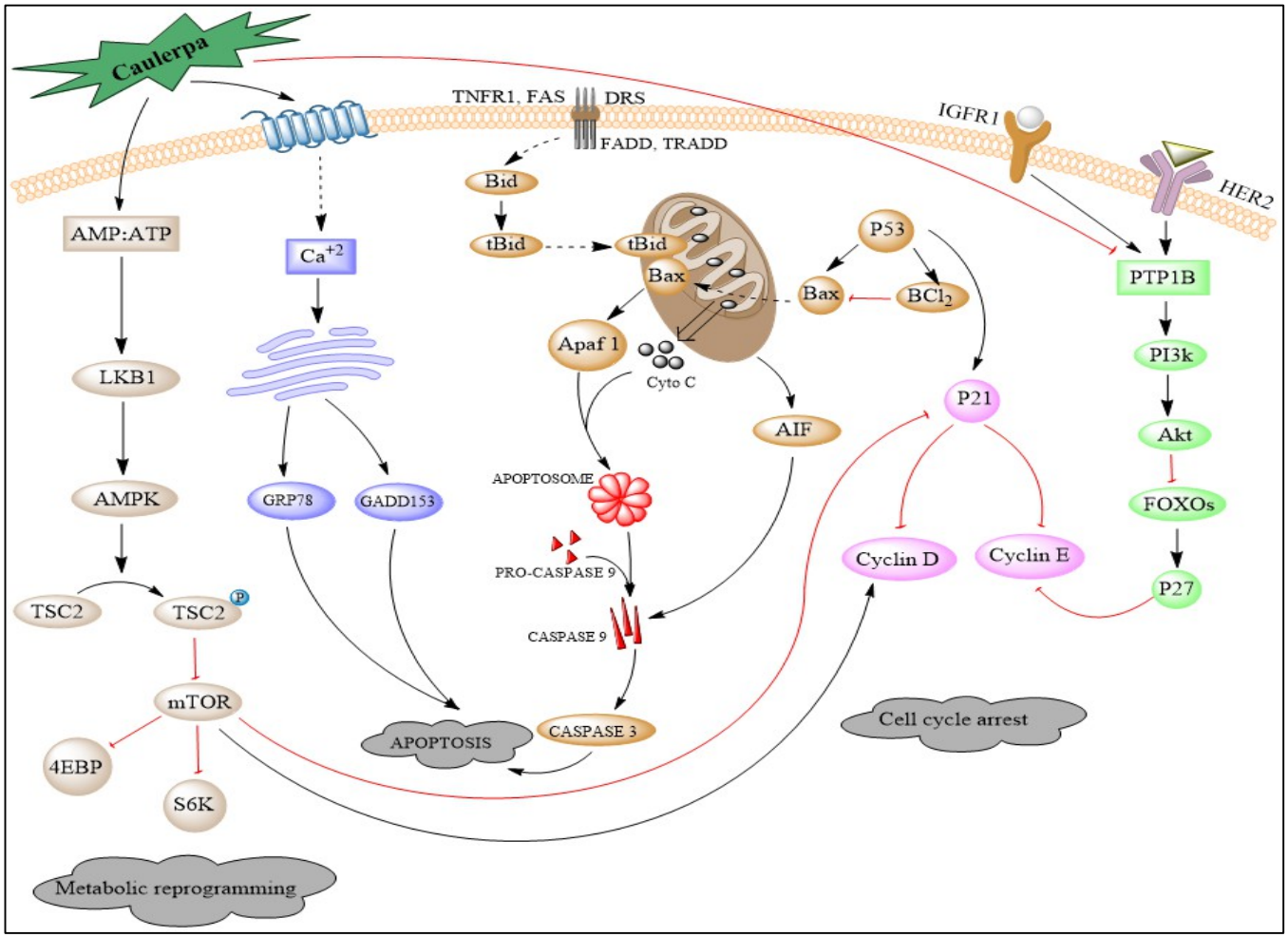

Figure 2.2 Proposed mechanism of action of *Caulerpa* in cancer signalling. Complex network of modulations induced by *Caulerpa* on AMPK (light brown), ER Stress (blue), mitochondrial stress (dark brown), PTP1B inhibition (green) and cell cycle arrest (purple) pathways are depicted, that subsequently result in metabolic reprogramming, apoptosis and cell-cycle arrest in cancer cells. Translocation is depicted by dashed arrows, and inhibition by red arrows (Mehra *et al.,* 2018b).

MATERIALS AND METHODS

I. Objective 1 Development of DNA barcodes for inter-specific and intraspecific level taxonomic identification of evaluated *Caulerpa* spp. and designing a database of Indian algae based on morphological and molecular data

3.1 Taxon Sampling

Algal specimen were collected from various sites of Indian coasts, as listed in **Table 3.1** and **Figure 3.1**. The selection of sampling sites was random and based on sample availability both in terms of geographical location and season. The samples were initially washed thoroughly with artificial sea water on-site, to remove sediments and brought to lab in zipped bags. A thorough cleaning was done again with artificial sea water followed by a rinse with distilled water. Each sample was divided in to two fractions, one fresh fraction was processed for molecular analyses and the other fraction was shade dried and stored in zipped bags until further use.

3.2 Morphological Characterization

Morphological analysis of the collected samples was done and macroscopic images were captured using Canon EOS 60D camera (Lens 18200 mm, F 3.5) (**Figure 3.2**). The following morphological features were recorded – thallus colour, thallus shape, stolon texture, branching pattern, ramuli shape, ramuli length, frond shape, and length.

3.3 Preparation of Herbarium Vouchers

Dried herbarium vouchers of each sample were prepared on acid-free herbarium sheets and voucher IDs were designated, as per the format of Central University of Punjab, Bhatinda. Annotated herbaria were prepared and submitted to University Herbarium, Central University of Punjab, Bathinda.

3.4 DNA Isolation

Total genomic DNA was extracted from 15 algal specimens by HiPurA^{TM} Algal Genomic DNA Extraction Kit (HiMedia Laboratories Pvt. Ltd., Mumbai) following manufacturer's protocol (Bast *et al.,* 2014a). DNA concentration and purity was tested using NanoDrop Spectrophotometer (Thermo Scientific NanoDrop 2000).

3.5 PCR Amplification and Amplicon Purification

PCR amplification of the target genomic region was done using *Caulerpa* (genus) specific primers for ITS1 (internal transcribed spacer region 1), *rbc*L (Ribulose-1,5-bisphosphate carboxylase/oxygenase large-chain gene), *tufA*, and 18S, which were generated using Primer3Plus and synthesized from Imperial Life Sciences (ILS), India (**Table 3.2**). For each 20µL PCR-reaction mixture, 2µL of 10X reaction buffer (Applied Biosystems, India), 4µL each of 10µM respective primer (Imperial Life Sciences), 2µL of 2.5mM dNTP mixture (Applied Biosystems), 0.5U of DreamTaq DNA polymerase (5U/µL) (Applied Biosystems) and sterile de-ionised water was added. PCR was carried out in programmable thermal cycler (Veriti™, Applied Biosystems) and reaction profile comprised an initial denaturation at 94˚C for 4 min, followed by 35 cycles of 94˚C for 0.5 min, 50˚- 58˚C for 2 min and 72˚C for 2 min, and a final extension of 72˚C for 10 min. Amplified products and a standard 100bp DNA marker were electrophoresed on 1.5% agarose gels for 30 min at 100V and visualized with ethidium bromide (EtBr). Product purity was tested using NanoDrop™ 2000 Spectrophotometer (Thermo Scientific). Amplified PCR products were purified using ExoSAP-IT® PCR Product Cleanup Reagent (Applied Biosystems) following manufacturer's protocol (Bast *et al.,* 2014b).

3.6 DNA Sequencing

The purified PCR products were subjected to bi-directional DNA sequencing using ABI 3730*xl* DNA Analyzer (Applied Biosystems). Sequencing was performed using BigDye™ terminator v3.1 Cycle Sequencing Kit (Applied Biosystems, India), as per manufacturer's protocol (Supplementary File protocol/Programme). The chain-termination products were purified by BigDye XTerminator ™ Purification Kit (Applied Biosystems). The plate was sealed with adhesive tape seal and vortexed for 30 min. The plate was loaded on the ABI3730*xl* DNA Analyzer and run using POP-7™ Polymer (Applied Biosystems) (Bast *et al.,* 2014b).

3.7 Barcode based identification and Multiple Sequence Alignment

The generated DNA sequence data was analyzed (Geneious), and only high-quality sequences (>50%) were chosen for further analyses. The chimeras were removed and contigs were generated using Geneious™ v6.1.5 which were further used for homology search by BLASTn (NCBI). Barcodes were identified based on both percent similarity score and morphology. Further, multiple sequence alignment of sequences generated in the present study and all the representative *Caulerpa*

sequences available in GenBank (**Table No. 3.3**), was carried out using MUSCLE algorithm of Geneious v6.1.5. The alignments were edited by manually and ends were trimmed to minimize the number of missing sites across taxa. was carried out with, using Mega v7 (Bast F, 2014).

3.8 Phylogenetic Analysis

The alignments were exported to MEGA v7 and best-fitting nucleotide substitution models were tested using ML ModelTest. The pairwise distances within sequences was calculated using p-distance model in MEGA v7. Phylogenetic analysis was conducted by Bayesian Inference (BI) using MrBayes plug-in v3 (Ronquist *et al.,* 2003) of Geneious v6.1.5 (Bast F, 2014).

3.9 Development of Database

A comprehensive database was designed with google site, in collaboration with other lab members. The database contains information pertaining to all Indian marine algae collected and identified by our laboratory. As part of this thesis, a dedicated section of genus *Caulerpa* with details of various species collected in the study, was generated. Further details are discussed in next chapter.

II. Objective 2 Comparative evaluation of *in-vitro* anti-cancer and anti-oxidant activities of *Caulerpa* spp.

3.10 Extract Preparation

Algal samples were thoroughly cleaned with distilled water to remove surface contaminants and excess salts. The samples were shade dried for 7-10 days and pulverized to powder using electric grinder. 10 gm of algal powder was macerated individually with 100 ml of different solvents viz. chloroform, ethyl acetate, methanol and water, up to 24 h. The extracted algal extract was filtered using a Whatman filter Paper Grade 1 (110 mm) to remove cell debris and later, centrifuged at 5000 rpm for 5 min. The residue was again extracted with the respective solvents and the whole procedure was repeated twice, until 72 h. The filtrate (extract) was collected in round bottom flask (RBF) and concentrated under reduced pressure on rotary evaporator at standard temperatures recommended for each solvent (Gupta *et al.,* 2016). The concentrated extract was re-dissolved in culture-grade dimethylsulfoxide (DMSO) for storage until further use.

3.11 Phycochemical Assays

Qualitative analyses were done to detect the presence of various phycochemical constituents of the algae including alkaloids, tannins, flavonoids, cardiac glycosides and anthraquinones by the methods described previously (Mehdinezhad *et al.,* 2016).

3.12 Cell Culture

NCI-H1299 (lung carcinoma), T-47D and MDA-MB-231 (Breast cancer) cells were purchased from National Centre for Cell Science (NCCS), Pune. T-47D were routinely cultured in RPMI 1640 (Roswell Park Memorial Institute) (Gibco by Life Technologies, USA) while MDA-MB-231 and NCI-H1299 were maintained in DMEM (Dulbecco's modified eagle medium), high glucose (Gibco by Life Technologies, USA) supplemented with 10% fetal bovine serum (FBS) (HiMedia Laboratories) at 37°C, 5% CO_2 and 95% relative humidity. Seed stocks were prepared in DMSO and stored at -80°C.

3.13 Anti-proliferative Assay

In vitro assessment of anti-proliferative activity of *Caulerpa* extracts (CEs) was carried out by MTT (3-[4,5-dimethylthiazol-2-yl]-2,5-diphenyltetrazolium bromide) assay (Xue *et al.,* 2012). NCI-H1299, T-47D, MDA-MB-231 and hPBMCs (human peripheral blood mononuclear cells) were seeded at a density of 10000 cells per well, respectively, in 96-flat well culture plates. The cell monolayers were allowed to grow in 10% FBS supplemented medium until 24 hr, after which the cells were subjected to serum starvation to achieve synchronized growth of cells. The complete medium was replenished after 12 hr and cells were treated with CEs at concentrations of 0.1, 0.25 and 0.5 µg/µL, in triplicates. After 48 hr, cells were washed with 1X phosphate buffer saline (PBS) and assayed with 0.5 mg/ml MTT prepared in PBS. The plates were re-incubated for 4 h in dark. Thereafter, the supernatant was discarded and formazan crystals were dissolved in 100 µL DMSO at constant shaking, for 30 min. The absorbance was recorded at 570 nm on microplate reader (BioTek™ Synergy™ H1).

3.14 Annexin V/FITC Affinity Assay

MDA-MB-231 cells were cultured on sterile cover-slips overlaid on 35 mm petri-dishes filled with DMEM medium, for 24 h. The cells were treated with sub-lethal doses of CMEs of TEN-158 and KNY-254 for 24 h and incubated at 37°C. After 24 h, cells on the coverslips were gently washed with 1x PBS and stained with FITC-Annexin V conjugate as per the manufacturer's protocol. The cells were incubated in dark for 30 min. The cover-slips were mounted over clean glass slides using Fluoromount aqueous mounting medium from Sigma. The slides were visualized on confocal Lase Scanning Microscope and images were captured at 60x (Mhashilkar *et al.,* 2001).

3.15 Cell Cycle Analysis

Cell cycle assay was performed on MDA-MB-231 cells by method described previously (Joshi *et al.,* 2017). MDA-MB-231 cells were grown in 96 well plates at a density of 10000 cells/ well. The cells were treated with 0.25 µg/µL CME for 48 h at 37°C, after which cells were washed with 1X PBS. Cells were harvested and subjected to chilled ethanol followed by incubation at -20°C for 4 h. After incubation, cells were treated with ribonuclease A (100 µg/ml) to ensure RNA degradation, if any. Then the cells were centrifuged and washed with 1X PBS. After washing, cells were stained with 50 µg/ml propidium iodide (PI) and incubated for 30 min, at room temperature in dark and then, analysed on flow cytometer (BD Accuri).

3.16 DHE Assay

Intracellular ROS levels were monitored by the changes in fluorescence obtained from oxidation of DHE (dihydroethidium) to ethidium (ETH), mainly by superoxide radical ($O^{\bullet}_2{}^-$). The assay was performed on T-47D and MDA-MB-231 cells, with 0.1, 0.25 and 0.5 µg/µL of CME treatments for 24 h. The cells were washed twice with 1X PBS and the fluorescence was measured using a microplate reader (BioTek™ Synergy™ H1), after staining with 10 µM DHE at 535/635 nm (Chauhan *et al.,* 2016).

3.17 Enzyme Assays

3.17.1 Glutathione Reductase (GR) Assay

Glutathione reductase (GR) or glutathione sulfhydryl reductase (GSR) catalyzes the reduction of glutathione (GSSG) to glutathione (GSH) in an NADPH dependent reaction. GSH acts as a crucial intracellular anti-oxidant by combating the hydroperoxide free radicals [$OH^{\bullet}$]. GR activity was assayed by monitoring oxidation

of NADPH to $NADP^+$ at 340 nm, in a reaction mixture constituting 50 µL assay buffer, 5 µL 20 mM GSSG, 5 µL 2mM NADPH, 5 µL cell lysate, 35 µL double distilled water and 0.05 or 0.1 µg/ml CME. The experiment was performed in triplicates and percent change in absorbance was calculated after normalizing the data with untreated control (Carlberg and Mannervik, 1985).

3.17.2 Superoxide dismutase (SOD) Assay

SOD activity was assayed by pyrogallol method, which relies on the principle of competition between pyrogallol auto-oxidation by $O_2^{\bullet -}$ and dismutation of $O_2^{\bullet -}$ by the enzyme. The protocol was adapted as described by Marklund and Marklund, 1974 with slight modifications (Marklund and Marklund, 1974). SOD activity was assayed by monitoring change in absorbance of pyragallol at 420 nm, in a reaction mixture constituting 50 µL 0.1 M Tris, 16 µL 6 mM EDTA, 34 µL 6 mM pyrogallol prepard in 0.1N HCl and 5 µL cell lysate and 0.05 or 0.1 µg/ml CME. The experiment was performed in triplicates and percent change in absorbance was calculated after normalizing the data with untreated control.

3.17.3 Catalase Assay

Catalase activity was measured using method described by Aebi, 1984, which records the disappearance of peroxide spectrophotometrically at 240 nm (Aebi, 1984). In a reaction mixture, 0.059 M H_2O_2 prepared in 0.05 M phosphate buffer (pH 7.0), enzyme extract and CME were taken and mixed well at room temperature followed by immediate absorbance measurement at 240 nm for 3 min.

3.18 JC-1 Assay

The changes in mitochondrial transmembrane potential (MMP) in MDA-MB-231 cells were determined using 5,5',6,6'-tetraethylbenzimidazolylcarbocyanine iodide (JC-1) probe with a microplate reader (Alex *et al.,* 2014). JC-1 generates red/orange fluorescent J-aggregates (650±15 nm) inside the mitochondria at hyperpolarized membrane potential while at depolarized membrane potential, it remains as a green fluorescent monomer with emission wavelength of 570±20 nm. MDA-MB-231 cells were grown in 96 well plates at a density of 10,000 cells/ well. The cells were treated with 0.10 and 0.25 µg/µL CME for 24 h at 37°C, after which cells were washed with 1X PBS. 20 µM JC1 was used to stain the cells for 30 min at 37°C. The fluorescence

was recorded at 485/535 and 550/600 nm and results were expressed in terms of ratio of JC-1 monomer/aggregate.

3.19 Scratch Wound Healing Assay

Metastatic property of the CME treated cells was monitored by scratch wound healing assay (Liang *et al.,* 2007). MDA-MB-231 cells were seeded in 24-well tissue culture plate in 10% FBS supplemented DMEM. The cells were allowed to reach 80-90% confluence until 24 hr. Cells were scratched gently along the horizontal axis of the plate using a sterile 10 µL microtip and each well was marked along the perpendicular axis to locate the read position after each interval. The detached cells were washed gently with fresh media twice. Wells were replenished with fresh medium containing sub-lethal doses of CME. Cells were grown for 48 h and images were captured at 0 and 48 h. The gap distance was quantitatively evaluated using imageJ software.

3.20 LC-MS Analysis

LC-MS was carried out on Water Alliance HPLC using an analytical Reverse Phase C-18 PUMP: SPD10AVP Phenomenex column (25 cm x 2.5 mm)) and an Atmopsheric-Pressure Chemical Ionization (APCI) source. The column was run in positive Electron Spray Ionization (ESI) mode with m/z of 50-1000. 10 µL of sample was injected and methanol: DMSO (50:50) was used as mobile phase. The column temperature was maintained at 250°C and flow rate was maintained at 2ml/min. The results were analyzed using ClassVP integrated software.

3.21 Column chromatography

The most potent bioactive extract *i.e.* KYN-254 was subjected to column chromatography over silica gel (60-120 mesh) using gradient elution with petroleum ether (PE) and ethyl acetate (EtOAc). 10 g of crude extract was loaded on silica gel (60-120) column (60 cm x 4cm) and eluted with PE: EtOAc, in increasing gradient of EtOAc viz. 90:10, 80:20, 70:30, 65:35.

3.22 Molecular Docking

Investigation of interaction patterns of *Caulerpa* constituents with the signaling proteins involved in cancer cell physiology, molecular docking was performed (Kaur *et al.,* 2018). 3-Dimensional co-crystal structures of proteins (**Table 3.5**) with

respective inhibitors, were retrieved from Protein Data Bank (PDB). The proteins were pre-processed, to remove adjunct moieties, correction of native protein structure, and correction of ionization, tautomeric states of amino acid residues and Gasteiger chargers (using PyMol visualizer) and protein preparation was done using protein preparation wizard of Maestro v11.5. Chemical structures of the ligands (biomolecules of *Caulerpa*) (**Table 3.6**) were drawn in ChemDraw Professional v and were optimized to get the energy minimized structures. The grid was prepared using receptor grid generation module. The location and dimensions of the grid box were acquired from the coordinates of the centroid of the already embedded inhibitors of the respective protein molecules, using Maestro visualizer. Each docking experiment was done by Lamarckian Genetic Algorithm (LGA) and lowest predicted binding free energy of the most probable interactions were calculated.

III. Objective 3 Analysis of putative correlation between anti-cancer activity and phylogeny of *Caulerpa*

The putative correlation of phylogeny and anti-cancer activity of various CMEs was studied by using IC_{50} values and pairwise genetic distance. For better analysis, the phylogram with best resolution was chosen and for calculating pairwise-genetic distance the species with best IC_{50} (least IC_{50}) was taken as standard. Statistical analysis for correlation was done by calculating Coefficient of Determination (R^2) using Microsoft excel. A scatter plot of IC_{50} as a function of pairwise genetic distance was created, with straight line equation and R^2 value.

Table 3.1 Details of samples and sampling sites

S. No.	Sample ID	Location	GPS coordinates	Collected by
1.	**MDP-13.13**	Mandapam, Tamil Nadu	9°16'16.8"N 79°08'03.5"E	Dr. Felix Bast
2.	**KAL-45**	Kalapathar, Andaman Islands	10°39'31.3"N 92°34'55.8"E	Dr. Felix Bast
3.	**OKH-29**	Okha, Gujarat	22°28'41.5"N 69°04'47.5"E	Richa Mehra
4.	**OKH-36**	Okha, Gujarat	22°28'41.5"N 69°04'47.5"E	Richa Mehra
5.	**DWA-95**	Dwarka, Gujarat	22°14'28.1"N 68°57'22.5"E	Richa Mehra
6.	**DWA-96**	Dwarka, Gujarat	22°14'28.1"N 68°57'22.5"E	Richa Mehra
7.	**VER-138**	Veraval, Gujarat	20°54'32.3"N 70°21'10.0"E	Richa Mehra
8.	**VER-153**	Veraval, Gujarat	20°54'32.3"N 70°21'10.0"E	Richa Mehra
9.	**TEN-158**	Tenneti, Vishakhapatnam, Andhra Pradesh	17°33'56.8"N 83°10'30.8"E	Richa Mehra
10.	**THO-173**	Thotlakonda, Vishakhapatnam, Andhra Pradesh	17°49'01.8"N 83°24'48.2"E	Dr. Felix Bast
11.	**KAK-193**	Kakinada, Andhra Pradesh	16°55'27.8"N 82°15'23.8"E	Dr. Felix Bast
12.	**KAK-196**	Kakinada, Andhra Pradesh	17°00'35.5"N 82°17'17.1"E	Dr. Felix Bast
13.	**PUD-197**	Pudimadaka, Andhra Pradesh	17°29'05.9"N 83°00'03.4"E	Dr. Felix Bast
14.	**KNY-254**	Kanyakumari, Tamil Nadu	8°04'42.3"N 77°33'04.9"E	Richa Mehra
15.	**KNY-255**	Kanyakumari, Tamil Nadu	8°04'42.3"N 77°33'04.9"E	Richa Mehra

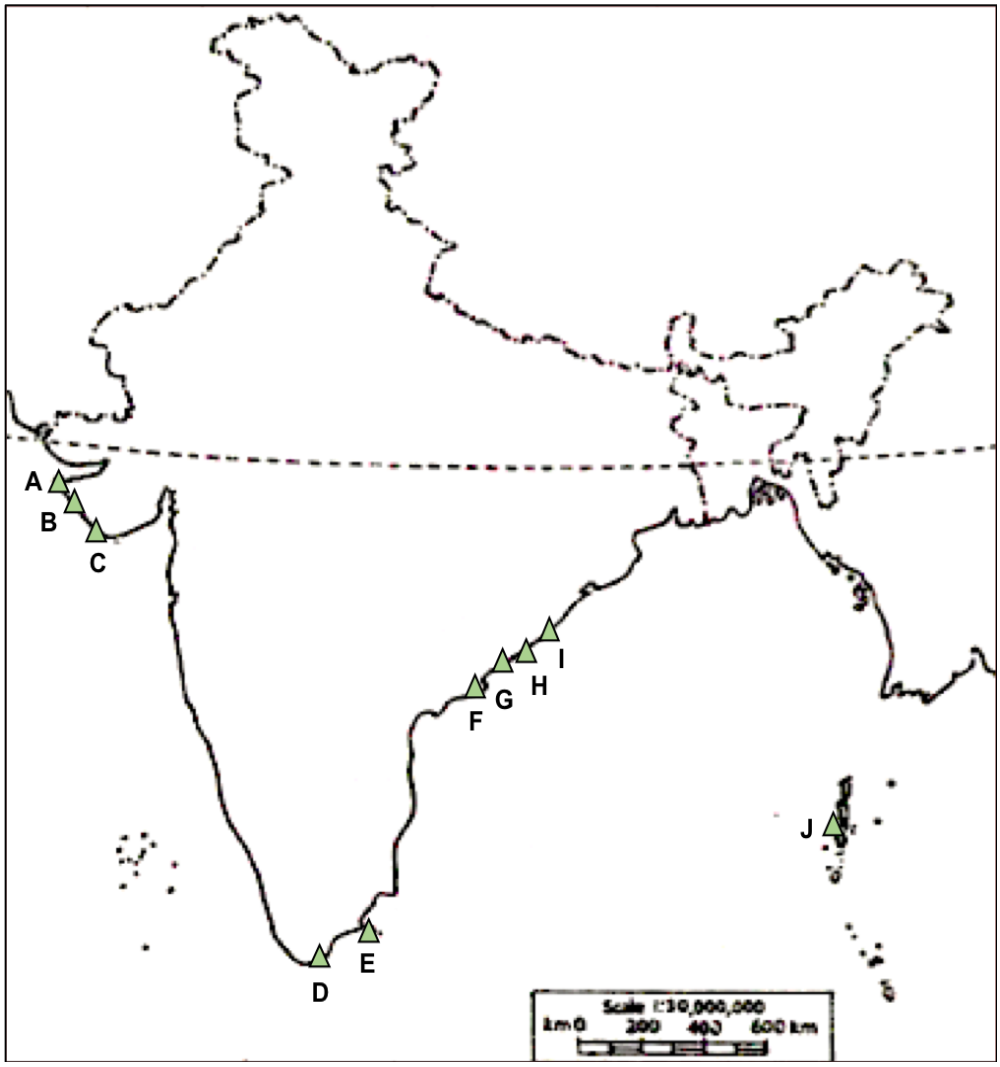

Figure 3.1 Outline map of India depicting sampling locations. The number coding inferred from Table Map downloaded from *surveyofindia.gov.in*

Table 3.2 Details of primers used in the study

Primer	Primer Sequence
18S F	CAACCTGGTTGATCCTGCCAGT
18S R	TGATCCTTCTGCAGGTTCACCTAC
ITS1 F	CCTCTGAACCTTCGGGAG
ITS1 R	TTCACTCGCCATTACT
*rbc*L F	GCTTATGCWAAAACATTYCAAGG
*rbc*L R	AATTTCTTTCCAAACTTCACAAGC
tufA F	TGAAACAGAAMAWCGTCATTATGC
tufA R	CCTTCNCCGAATMGCRAAWCGC

Table 3.3 Details of previously published sequences available in NCBI nucleotide database and their GenBank accession Numbers.

Species	Target Genomic Region	GenBank Accession No.
C. racemosa var. *lamourouxii*	ITS1	AY334303
C. ferugsonii	ITS1	KR478537
C. lentillifera	ITS1	JN034414
C. microphysa	ITS1	KR478536
C. verticillata	ITS1	JQ745716
C. verticillata	ITS1	JF932265
C. mexicana	ITS1	AJ007818
C. scalpelliformis	ITS1	KJ934750
C. scalpelliformis var. *denticulata*	ITS1	JF932275
C. scalpelliformis f. *dwarkensis*	ITS1	JF932264
C. racemosa f. *occidentalis*	ITS1	JF932274
C. racemosa var. *macrophysa*	ITS1	AY206421
C. racemosa var. *laetevirens*	ITS1	AY205290
C. racemosa f. *cylindracea*	ITS1	AY173119
C. cylindracea	ITS1	KC507519
C. racemosa	ITS1	AJ297639
C. corynephora	ITS1	KF840135
C. racemosa var. *corynephora*	ITS1	JQ745713
C. veravalensis	ITS1	JQ745716
C. cupressoides	ITS1	KF840133
C. serrulata	ITS1	JQ745711
C. sertularioides f. *longipes*	ITS1	JQ745715
C. ashmeadii	ITS1	DQ652534
C. prolifera	ITS1	KC507537
C. taxifolia	ITS1	JQ745717
C. taxifolia	ITS1	JQ745710
Halimeda macrophysa	ITS1	AF407251
Halimeda borneensis	18S	AF416387
C. verticillata	18S	JQ745691
C. verticillata	18S	JF932252
C. microphysa	18S	JF932256
C. lentillifera	18S	JN034412
C. taxifolia	18S	JF932257
C. veravalensis	18S	JQ745688
C. scalpelliformis f. *dwarkensis*	18S	JF932251
C. scalpelliformis var. denticulata	18S	JF932262
C. racemosa var. *turbinata*	18S	JN034413
C. racemosa f. *occidentalis*	18S	JF932261
C. macrodisca	18S	KY387611
C. mexicana	18S	JQ745692
C. sertularioides f. *longipes*	18S	JQ745687
C. sertularioides f. *brevipes*	18S	JF932262
Halimeda gracilis	*rbc*L	FJ624494
Ulva fasciata	*rbc*L	EU484418
Caulerpella ambigua	*rbc*L	KM186536
C. hedleyi	*rbc*L	KF649929
C. cliftonii	*rbc*L	FR848354
C. verticillata	*rbc*L	FR66354

C. filicoides	rbcL	FR848351
C. ferugsonii	*rbc*L	KF649942
C. cactoides	*rbc*L	FR848360
C. simpliciuscula	*rbc*L	FR848346
C. papillosa	*rbc*L	KF649952
C. vesiculifera	*rbc*L	KF649950
C. sedoides	*rbc*L	KM016918
C. opposita	*rbc*L	KF649949
C. okamurae	*rbc*L	AB038484
C. microphysa	*rbc*L	JF932282
C. lentillifera	*rbc*L	JN034416
C. paspaloides	*rbc*L	AY942171
C. longifolia	*rbc*L	FR668299
C. remotifolia	*rbc*L	FR848355
C. urvilleana	*rbc*L	KM186538
C. mexicana	*rbc*L	JQ745706
C. prolifera	*rbc*L	AY942173
C. sertularioides	*rbc*L	AB054014
C. taxifolia	*rbc*L	JQ745703
C. webbiana	*rbc*L	FR848353
C. cupressoides	*rbc*L	AB054008
C. parvifolia	*rbc*L	KF649963
C. chemnitzia	*rbc*L	KF256121
C. peltata	*rbc*L	JQ745704
C. macrodisca	*rbc*L	KF256127
C. filiformis	*rbc*L	FR848349
C. racemosa	*rbc*L	AJ512484
C. oligophyta	*rbc*L	KF256112
C. nummularia	*rbc*L	AB054010
C. subserrata	*rbc*L	AB054015
C. brachypus	*rbc*L	AB038483
C. cylindracea	*rbc*L	KF840142
C. scalpelliformis	*rbc*L	JQ745700
C. scalpelliformis var. *denticulata*	*rbc*L	JF932288
C. scalpelliformis f. *dwarkensis*	*rbc*L	JF932277
Halimeda opuntia	*tufA*	AM049967
Caulerpella ambigua	*tufA*	KM186522
C. obscura	*tufA*	FR848335
C. alternans	*tufA*	KF649862
C. muelleri	*tufA*	KF649863
C. flexilis	*tufA*	JN817643
C. trifaria	*tufA*	KF649861
C. brownii	*tufA*	FR848341
C. cliftonii	*tufA*	FR848340
C. filicoides	*tufA*	KM186529
C. simpliciuscula	*tufA*	FR848333
C. vesiculifera	*tufA*	KF649878
C. ferugsonii	*tufA*	JN817655
C. bartoniae	*tufA*	FJ810426
C. opposita	*tufA*	JN817648
C. okamurae	*tufA*	FN667650
C. cactoides	*tufA*	JN817650

C. agardhii	*tufA*	KF314140
C. hodgkinsoniae	*tufA*	KF649883
C. sedoides	*tufA*	FM956039
C. geminata	*tufA*	AJ417968
C. lanuginosa	*tufA*	DQ652496
C. paspaloides	*tufA*	AJ417965
C. longifolia	*tufA*	KF649914
C. constricta	*tufA*	KF314150
C. mexicana	*tufA*	KC153518
C. antoensis	*tufA*	KJ957105
C. parvifolia	*tufA*	FM956029
C. scalpelloformis	*tufA*	KF840150
C. urvilleana	*tufA*	JN645172
C. manorensis	*tufA*	FN667649
C. peltata	*tufA*	FM956060
C. nummularia	*tufA*	FM956059
C. selago	*tufA*	FM956061
C. chemnitzia	*tufA*	KJ956061
C. sertularioides	*tufA*	AJ417946
C. racemosa	*tufA*	JN645149
C. macrodisca	*tufA*	JN817666
C. racemosa f. *macrophysa*	*tufA*	KJ957085
C. racemosa f. *macrophysa*	*tufA*	KC153520
C. elongata	*tufA*	FM956049
C. prolifera	*tufA*	JX206460
C. floridana	*tufA*	KF921071
C. ashmeadii	*tufA*	DQ652362
C. distichophylla	*tufA*	AJ417940
C. taxifolia	*tufA*	KJ957127
C. cupressoides	*tufA*	AJ417929
C. serrulata	*tufA*	AJ417932
C. lessonii	*tufA*	FM956016
C. webbiana	*tufA*	KJ956016
C. fastigata	*tufA*	FM956031
C. subserrata	*tufA*	AJ417935
C. brachypus	*tufA*	KF314158
C. biserrulata	*tufA*	AFM956011
C. filiformis	*tufA*	AJ417964
C. corynephora	*tufA*	KF314158
C. racemosa	*tufA*	JN645167
C. racemosa	*tufA*	JN645164
C. racemosa	*tufA*	JN645157
C. racemosa	*tufA*	JN645163
C. racemosa	*tufA*	JN645150
C. racemosa f. *cylindracea*	*tufA*	FM956048
C. cylindracea	*tufA*	JN817677

Table 3.4 Protein Data Bank (PDB) IDs of protein molecules used for molecular docking

Protein	PDB ID
AMPK	4EAI
mTOR	4JSV
Akt2	1O6L
PI3K	5XGI
IGF-1R	5HZN
PERK	4X7H
BID	4QVE
Bax	4BD8
P53	4HJE
BCL2	4AQ3
APAF1	3JBT
PTP1B	2QBP

Table 3.5 Details of ligands used for molecular docking analysis

S. No.	Ligand	Mass	Structure
1.	Caulerpin	398.13	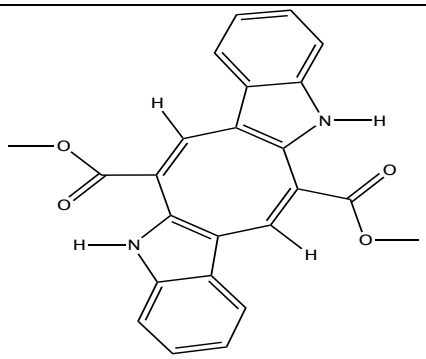
2.	Caulersin	342.10	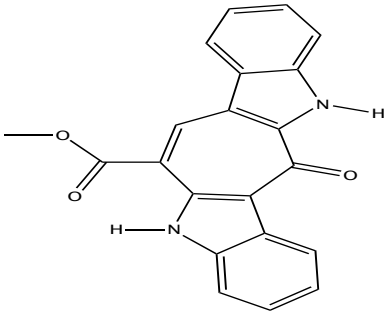 (b)
3.	Caulerpenyne	374.17	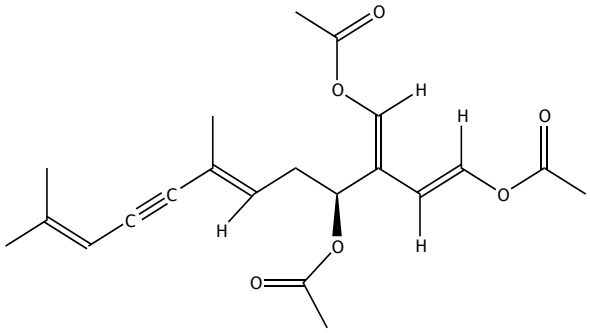
4.	Racemosin C	288.10	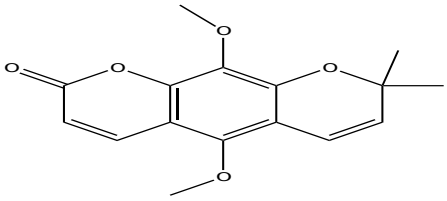
5.	CR1	404.26	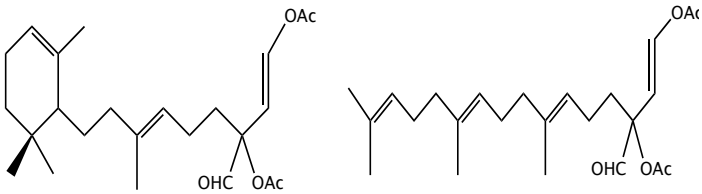

6.	CR2	342.10	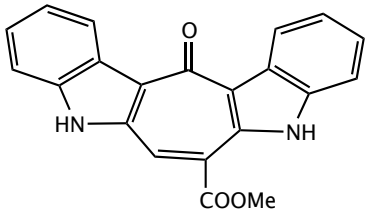
7.	CR3	296.31	
8.	CR4	268.15	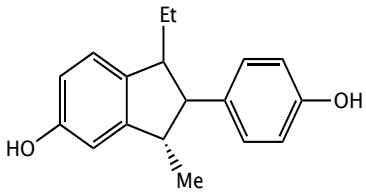
9.	CR5	338.32	
10.	CR6	360.23	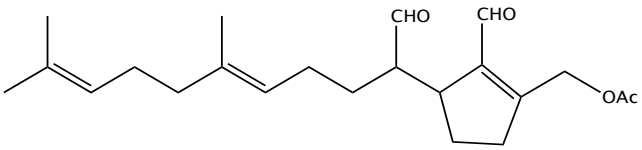

RESULTS

I. Objective 1 Development of DNA barcodes for inter-specific and intraspecific level taxonomic identification of evaluated *Caulerpa* spp. and designing a database of Indian algae based on morphological and molecular data.

4.1 Morphological Analysis

The morphological analysis of all the samples was done (**Figure 4.1**) and a brief account of macroscopic features is given below–

4.1.1 MDP-13.13 *C. scalpelliformis*

The thallus is yellowish green in color and has broad leaf-like appearance. The thallus is further divided in to stolon, leafy fronds and rhizoids. Stolons are pale, simple and slightly branched**.** The fronds or branches are flat-leaf like and glossy in appearance, growing up to 3-8 cm in length. Ramuli or branchlets are broad with entire margin and ovate ends.

4.1.2 KAL-45 *C. racemosa*

The thallus is yellowish green and has overall grape-like appearance. Stolon is slender, cylindrical, highly branched and entangled. Fronds bear globular ramuli growing in alternate arrangement and resemble bunch of grapes. Frond length varies from 1-5 cm. Ramuli are round in shape, crowded along central axis and range from 2-4 mm in diameter.

4.1.3 OKH-29 *C. scalpelliformis*

The thallus is olive green to dark green in color. It is divided into stolon, upright fronds and downright rhizoids. Stolon is slender, naked and branched. Fronds are flat, wider at the base, seldom branched, alternately arranged and grow at 1-2 cm intervals, up to a length of 3-8 cm. Ramuli are flattened leaf-like, glabrous and scalpelliformed

4.1.4 OKH-36 *C. verticillata*

The thallus is dark green in color, small and forms a fuzzy mat-like appearance on the substratum. Thallus is also delicate, stoloniferous and bears erect rhizoids. Fronds are divided into erect blades bearing ramuli, with aculeate tips and verticillate divisions. Frond length varies from 1-5 cm.

4.1.5 DWA-95 *C. sertularioides*

The thallus is olive green to dark green in color and bears comb-like upright fronds. Fronds are upright, with numerous cylindrical ramuli. The frond length varies from 4-9 cm. Ramuli are mucronate, pinnate, cylindrical and not flat, unlike *C. taxifolia*. Ramuli tips are tapered towards the end and terminate in sharp points. Ramuli length varies from 5-8 mm.

4.1.6 DWA- 96 *C. racemosa*

The thallus is dark green to yellowish green in color and has grape-like morphology. Erect fronds arise from a creeping slender stolon, which is highly branched and entangled. Fronds are hydrated and resemble bunch of grapes, with globular ramuli growing alternately. Frond length may vary from 1-4 cm. Ramuli are crowded along central axis, round in shape with 2-4 mm in diameter.

4.1.7 VER-138 *C. lentillifera*

The thallus is grass-green, and has berry or small grape-like appearance. Stolon is cylindrical, bearing erect fronds above and rhizoids below. Fronds are upright, spaced at 3-14 mm apart, each made up of cylindrical axis of 2.5-7 cm tall, beset with ramuli arranged radially and crowdedly. Ramuli are 2-4 mm long with short stalk and globular head of diameter 1.5 mm.

4.1.8 VER-153 *C. corynephora*

The thallus is yellowish green to dark green, heavily branched and entangled. Fronds bear several round and branched ramuli, that are crowded along the central axis giving a grape-like appearance. The length of frond varies from 1-6 cm and diameter of ramuli ranges from 2-4 mm.

4.1.9 TEN-158 *C. taxifolia*

Thallus is yellowish green in color, comprising erect fronds and numerous rhizoids. Stolon is slender, non-fleshy from which flattened, segmented fronds arise. The fronds grow up to a length of 3-7 cm and give a feathery or comb-like appearance to thallus. Midrib is slightly flattened, and appears oval in cross-section. Ramuli grow opposite to each other and slightly curve towards the tip, ranging in length from 4-8 mm.

4.1.10 THO-173 *C. taxifolia*

The thallus is yellowish green to dark green in color, bearing slender stolon, upright fronds and numerous rhizoids. Fronds appear feather-like with leafy blades, each having a flattened mid-rib that appears oval in cross-section. Fronds are sometimes branched, where a secondary branch grows from primary branch. Ramuli are arranged in opposite manner and slightly curved towards the tip, ranging in length from 3-8 mm.

4.1.11 KAK-193 *C. taxifolia*

The thallus is light green to grass green, heavily branched and entangled. Fronds bear several globular and branched ramuli, that are crowded along the central axis giving a grape-like appearance. The length of frond varies from 1-4 cm and diameter of ramuli ranges from 2-4 mm.

4.1.12 KAK-196 *C. taxifolia*

The thallus is light to dark green in color, with slender stolon. Fronds are non-fleshy, flattened, segmented with feather-like appearance. Stolon is slender, non-fleshy and midrib is slightly flattened, appears oval in cross-section. The ramuli grow in opposite arrangement and slightly curved towards the tip. Frond length varies from 2-6 cm and ramuli length varies from 3-7 mm.

4.1.13 PUD-197 *C. taxifolia*

The thallus is dark green to yellowish green in color and constitutes feather-like upright fronds. Stolon is slender, non-fleshy and midrib is slightly flattened, appears oval in cross-section. Fronds bear flattened ramuli growing in opposite arrangement, and slightly tapered at ends. Frond length varies 4-10 cm and ramuli length varies from 4-8 mm.

4.1.14 KNY-254 *C. racemosa*

Thallus is grass green in color and divided in slender stolon bearing upright elongated fronds, and downright rhizoids. Stolon are naked, bears short rhizoidal pillars having rhizoidal clusters. Fronds bear clavate ramuli radially and distichously distributed Fronds length varies from 3-10 cm and ramuli diameter varies from 2-4 mm.

4.1.15 KNY-255 *C. scalpelliformis*

The thallus is olive green to dark green, divided into stolon, upright leafy fronds and downright rhizoids. Stolon is branched and glossy in appearance. Fronds are seldom branched with secondary branch arising from primary branch, and grow at 1-2 cm intervals, up to a length of 3-8 cm. Ramuli are flattened leaf-like, glabrous and scalpelliformed.

4.2 Herbarium Records

Annotated herbarium records of all the samples were generated and submitted to herbaria maintained at Central University of Punjab. A Herbarium Accession Number was assigned to each sample as per the University's guidelines. The format is as follows– For a species named *Caulerpa racemosa* the herbarium voucher includes initials of genus name and species name, its year of collection and isolate number e.g. 'CUPVOUCHER-CR-2016-1'. Representative image of herbarium record is shown in **Figure 4.2** and list of all samples in **Table 4.1**.

4.3 Database of Indian Algae

A database of Indian algae, named *DbIndAlgae* was designed and can be accessed at http://bit.ly/db-ia. Morphological and molecular data generated in the study was uploaded on the site. As of now, site contains information regarding 15 *Caulerpa* samples that correspond to 7 different species and their geographical isolates. These species are grouped in a dedicated section and assigned an individual page. A webpage of *DbIndAlgae* is shown in **Figure 4.3**. Each webpage contains following features–

- **Unique User ID (UUID):** A UUID with subsequent numeral code, referring to geographical location of the sample and serial number referring serial of sample acquisition is assigned to each sample. For example, *C. scalpelliformis* collected from Okha, Gujarat is coded as OKH-29.
- **Sample Image:** Macroscopic images of all samples clicked in laboratory with scale-bar are uploaded on the designated web-pages.
- **Classification:** Taxonomic rank of each species is given.
- **Distribution:** Site of sample collection, with GPS coordinates is described.
- **Description:** Morphological features of each sample are described.
- **DNA Sequence Data:** GenBank accession number of DNA sequence data (if submitted/received) along with marker details are listed.
- **Key References:** Important literature of the species in question is listed.

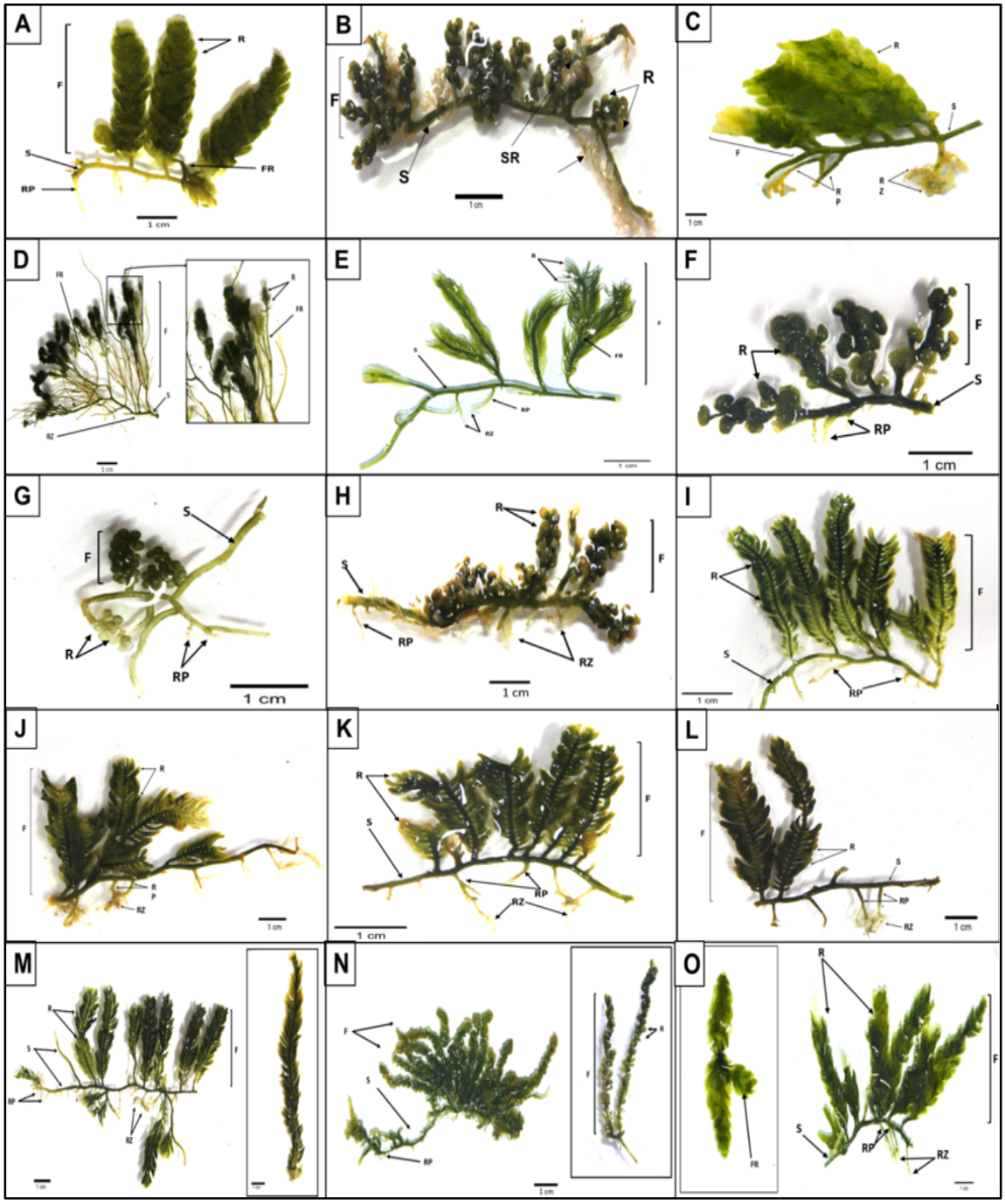

Figure 4.1 Macroscopic images of various *Caulerpa* samples. A) MDP-13.13; B) KAL-45; C) OKH-29; D) OKH-36; E) DWA-95; F) DWA-96; G) VER-138; H) VER-153; I) TEN-158; J); THO-173; K) KAK-193; L) KAK-196; M) PUD-197; N) KNY-254; O) KNY-255. R: Ramuli, F: Frond; S: Stolon; RZ: Rhizoids; RP: Rhizoidal Pillars; FR: Frond Ramification; SR: Stolon Ramification.

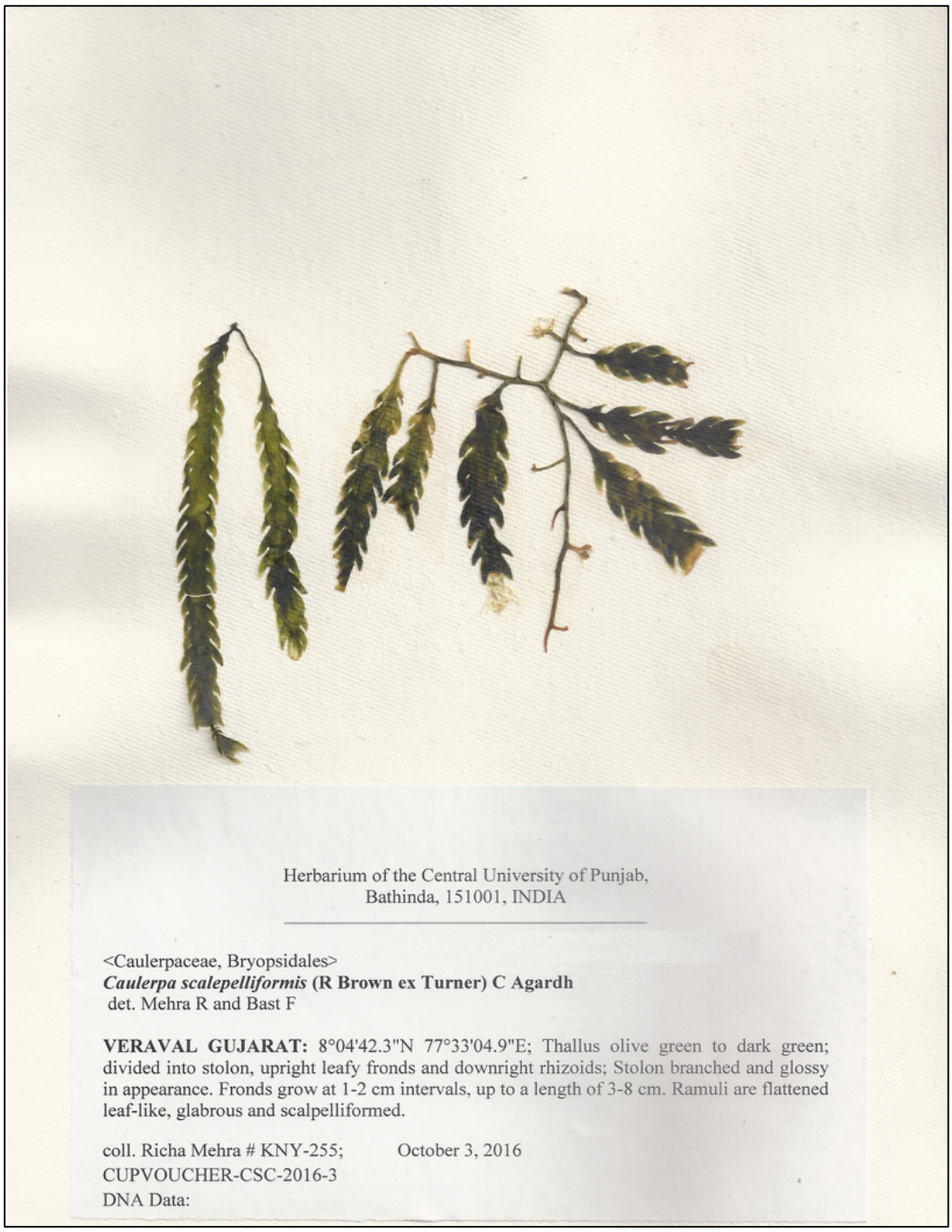

Figure 4.2 Representative image of herbarium record of KNY-255 *C. scalpelliformis*

Table 4.1 List of herbarium record of various *Caulerpa* samples

S. No.	Sample ID	Identification	Herbarium Voucher No.
1.	MDP-13.13	*C. scalpelliformis*	CUPVOUCHER-CS-2014-1
2.	KAL-45	*C. racemosa*	CUPVOUCHER-CR-2014-1
3.	OKH-29	*C. scalpelliformis*	CUPVOUCHER-CS-2015-2
4.	OKH-36	*C. verticulata*	CUPVOUCHER-CV-2015-1
5.	DWA-95	*C. sertularioides*	CUPVOUCHER-CSE-2015-1
6.	DWA-96	*C. racemosa* f. *macrophysa*	CUPVOUCHER-CR-2015-2
7.	VER-138	*C. lentillifera*	CUPVOUCHER-CL-2015-1
8.	VER-153	*C. corynephora*	CUPVOUCHER-CC-2015-1
9.	TEN-158	*C. taxifolia*	CUPVOUCHER-CT-2015-1
10.	THO-173	*C. taxifolia*	CUPVOUCHER-CT-2015-2
11.	KAK-193	*C. taxifolia*	CUPVOUCHER-CT-2015-3
12.	KAK-196	*C. taxifolia*	CUPVOUCHER-CT-2015-4
13.	PUD-197	*C. taxifolia*	CUPVOUCHER-CT-2015-5
14.	KNY-254	*C. racemosa*	CUPVOUCHER-CR-2016-4
15.	KNY-255	*C. scalpelliformis*	CUPVOUCHER-CS-2016-3

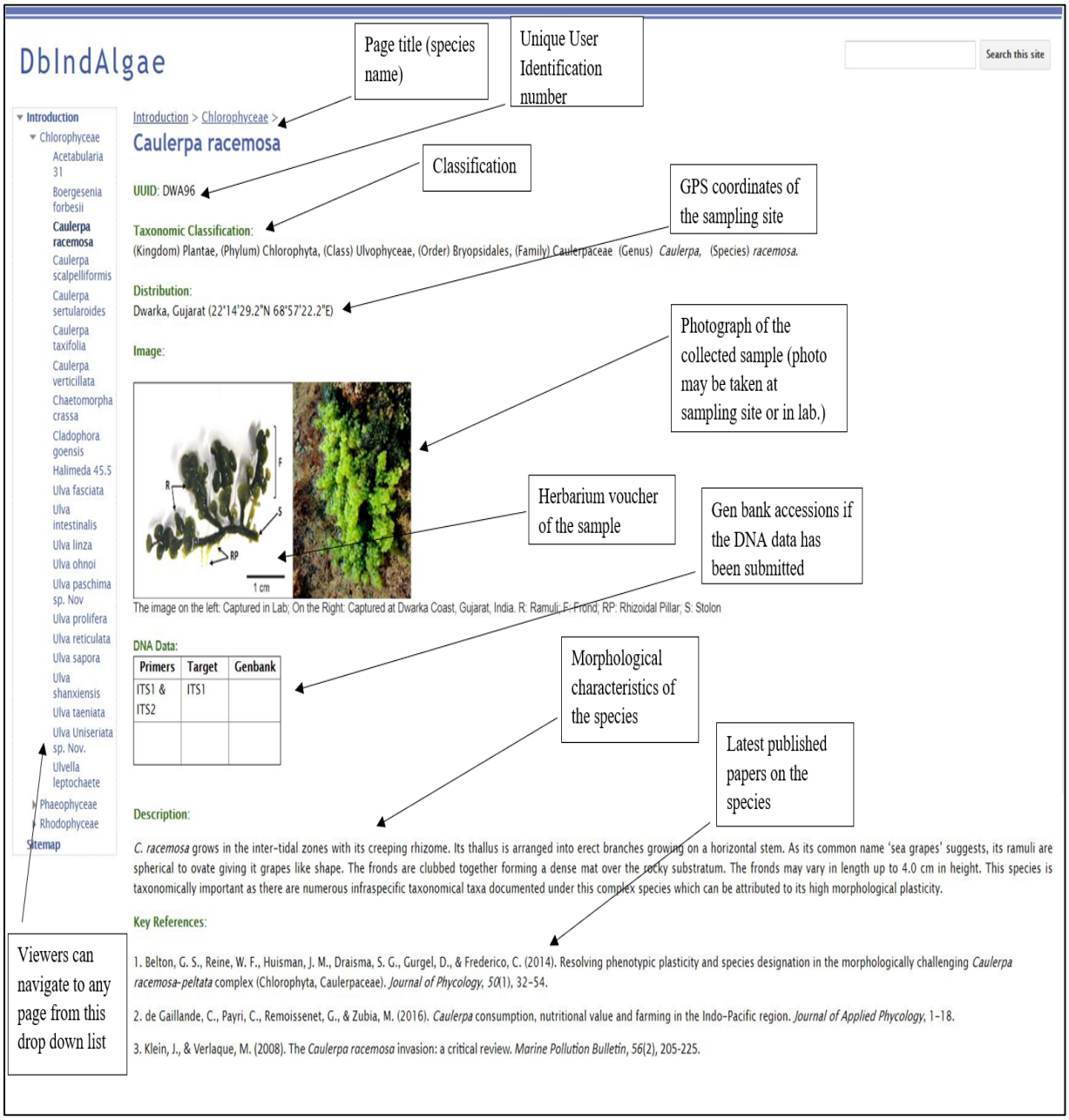

Figure 4.3. Representative image of database DbIndAlgae displaying its salient features.

4.4 DNA Barcoding

Morphological identification of all algal specimen was complemented with DNA barcoding and phylogeny assessment, in order to validate the species identification. A total of 41 DNA barcodes, with 15 from ITS, 8 from *tufA*, 9 each for 18S and 9 *rbc*L, were generated. The top BLASTn hits for all barcode sequences along with accession number, query cover, E value, and percent identity are summarized in **Table 4.2.**

4.4.1 Phylogeny with ITS

A total of 15 barcodes of *Caulerpa* species were generated with ITS and submitted to NCBI. Phylogenetic assessment of 15 ITS sequences from the current study and 27 published sequences from GenBank, was done. The tree was rooted with *Halimeda macrophysa* (AF407251) as outgroup and both Bayesian Inference (BI) and Maximum Likelihood (ML) phylograms were constructed. As all BI and ML phylograms were mostly congruent, only BI phylograms are discussed in the results and ML trees are added in supplementary files (**Appendix 1**). The MUSCLE alignment build for ITS1 region was 864 bp in length, with 205 (24%) conserved sites, 634 (74%) variable sites, 381 (44%) parsim-info sites and 246 (28%) singleton sites. The BI tree was generated using Hasegawa-Kishino-Yano model with Gamma distributed rate variation among sites (HKY+G). The total chain length was 1,100,000 and mean LnL value was -8220.97. The phylogram is shown in **Figure 4.4**. and resolved in to 6 lineages corresponding, Sedoideae, Charoideae, Fillicoideae, Thuyoideae, where Sedoideae and Fillicoideae formed paraphyletic clades. The posterior probability value (P value) varied from as low as 0.50 to a maximum of 0.96. The specimen OKH-36 identified as *C. verticillata* was nested with other *C. verticillata* sequences under section Charoideae; MDP 13.13, KNY-255, OKH-29 were identified as *C. scalpelliformis* and were grouped under section Fillicoideae; KAN-254, KAL-96, identified as *C. racemosa* and VER-153 identified as *C. corynehora* clustered under section Sedoideae; and TEN-158, KAK-193, KAK-196, PUD-197, TEN-158, THO-173 identified as *C. taxifolia* were clustered together in section Fillicoideae.

4.4.2 Phylogeny with 18S

A total of 9 barcodes of *Caulerpa* species were generated with 18S and submitted to NCBI. Phylogenetic assessment of 9 ITS sequences from the current study and 16 published sequences from GenBank, was done. The tree was rooted with *Halimeda borneensis* (AF416387) as outgroup and both BI and ML phylograms were constructed. The MUSCLE alignment build for 18S region was 1133 bp in length, with 923 (81%) conserved sites, 187 (17%) variable sites, 59 (5%) parsim-info sites and 124 (11%) singleton sites. The best fitting substitution model for BI tree was HKY+G model. The phylogram build using HKY+G model and phylogram was generated with total chain length of 1,100,000 and mean LnL value of -2854.27. The phylogram is shown in **Figure 4.5**. and resolved in to 4 different lineages corresponding, Sedoideae, Fillicoideae, and Charoideae, and section Sedoideae was again paraphyletic. The phylogram was supported with strong P values ranging from as low as 0.73 to 0.99. The specimen MDP 13.13, KNY-255 were identified as *C. scalpelliformis* and were grouped under section Fillicoideae; KAL-45 identified as *C. racemosa* clustered in section Sedoideae; OKH-29 identified as *C. scalpelliformis* was nested with other *C. scalpelliformis* sequences and PUD-197, TEN-158, KAK-193, KAK-196 identified as *C. taxifolia* were clustered together in section Fillicoideae.

4.4.3 Phylogeny with *rbc*L

A total of 9 barcodes of *Caulerpa* species were generated with rbcL and phylogenetic assessment of these 9 sequences and 45 published sequences from GenBank, was done. The tree was rooted with *Halimeda gracilis* (FJ6244944) and *Ulva fasciata* was taken as an additional outgroup. The MUSCLE alignment build for *rbc*L region was 1048 bp in length, with 615 (58%) conserved sites, 428 (40%) variable sites, 227 (22%) parsim-info sites and 196 (19%) singleton sites. The best fitting substitution model for BI tree was HKY+G model. The phylogram was generated with total chain length of 1,100,000 and mean LnL value of -6133.471. The phylogram is shown in **Figure 4.6**. and resolved in to 17 different lineages, with 12 corresponding to section Fillicoideae, Phyllantoideae, Vaucherioideae, Paspaloideae, Sedoideae, Charoideae, Cliftonii, Hedleyi, and Caulerpella while five clades were unidentified. The section Fillicoideae, Phyllantoideae, were paraphyletic with their descendants distributed in to different lineages. The phylogram was supported with P values ranging from 0.68 to 1. The specimen MDP

13.13, OKH-29, KNY-255 were identified as *C. scalpelliformis,* were grouped under section Fillicoideae; KAK-196, PUD-197, TEN-158, THO-173, identified as *C. taxifolia* were clustered together in section Fillicoideae; and VER-138 identified as *C. lentillifera* was clustered under section Sedoideae. Of the new or unidentified clades, clade 1 comprises *C. corynephora*, *C. veravalensis*, *C. serrulata*, *C. cylindracea* with posterior probability value of 0.76; clade 2 comprises *C. nummularia* with P value of 0.69; clade 3 was supported by P value of 0.86 and comprises *C. oligophyta* and *C. racemosa*; clade 4 was supported by P value of 0.98 and comprises *C. macrodisca* and *C. peltata*; Clade 5 supported by P value of 1, comprises C. cupressoides and C. webbiana.

4.4.4 Phylogeny with *tufA*

A total of 8 barcodes of *Caulerpa* species were generated with *tufA* and phylogenetic assessment of these 8 sequences along with 63 published sequences from GenBank, was done. The tree was rooted with *Halimeda opuntia* (AM049967. The MUSCLE alignment build for *tufA* region was 991 bp in length, with 516 (52%) conserved sites, 451 (45%) variable sites, 280 (28%) parsim-info sites and 167 (17%) singleton sites. The best fitting substitution model for BI tree was HKY+G model. The phylogram was generated with total chain length of 1,100,000 and mean LnL value of -7803.966. The phylogram is shown in **Figure 4.7**. and resolved in to 18 different lineages, with 15 corresponding to section Sedoideae, Vaucherioideae, Phyllantoideae, Brioideae, Thuyoideae, Fillicoideae, Paspaloideae, Lycopodioideae, Charoideae, Cliftonii, Araucarioideae, and Caulerpella. The section Fillicoideae, and Sedoideae were paraphyletic with their descendants distributed amongst different lineages. The phylogram was supported with P values greater than 0.5. The specimen KAK-196, KAK-193, PUD-197, TEN-158 identified as *C. taxifolia* were clustered together in section Fillicoideae; KNY-254 identified as *C. racemosa* was clustered under section Sedoideae; OKH-29, MDP 13.13, KNY-255 identified as *C. scalpelliformis,* were grouped under section Fillicoideae. Two new lineages were observed in this phylogram where lineage 1 comprises *C. chemnitzia, C. selago, C. nummularia, C. peltata, C. manorensis, C. urvilleana*, supported by P value of 0.88; and lineage 2 comprises *C. antoensis, C. mexicana, C. constricta* supported by P value of 0.93.

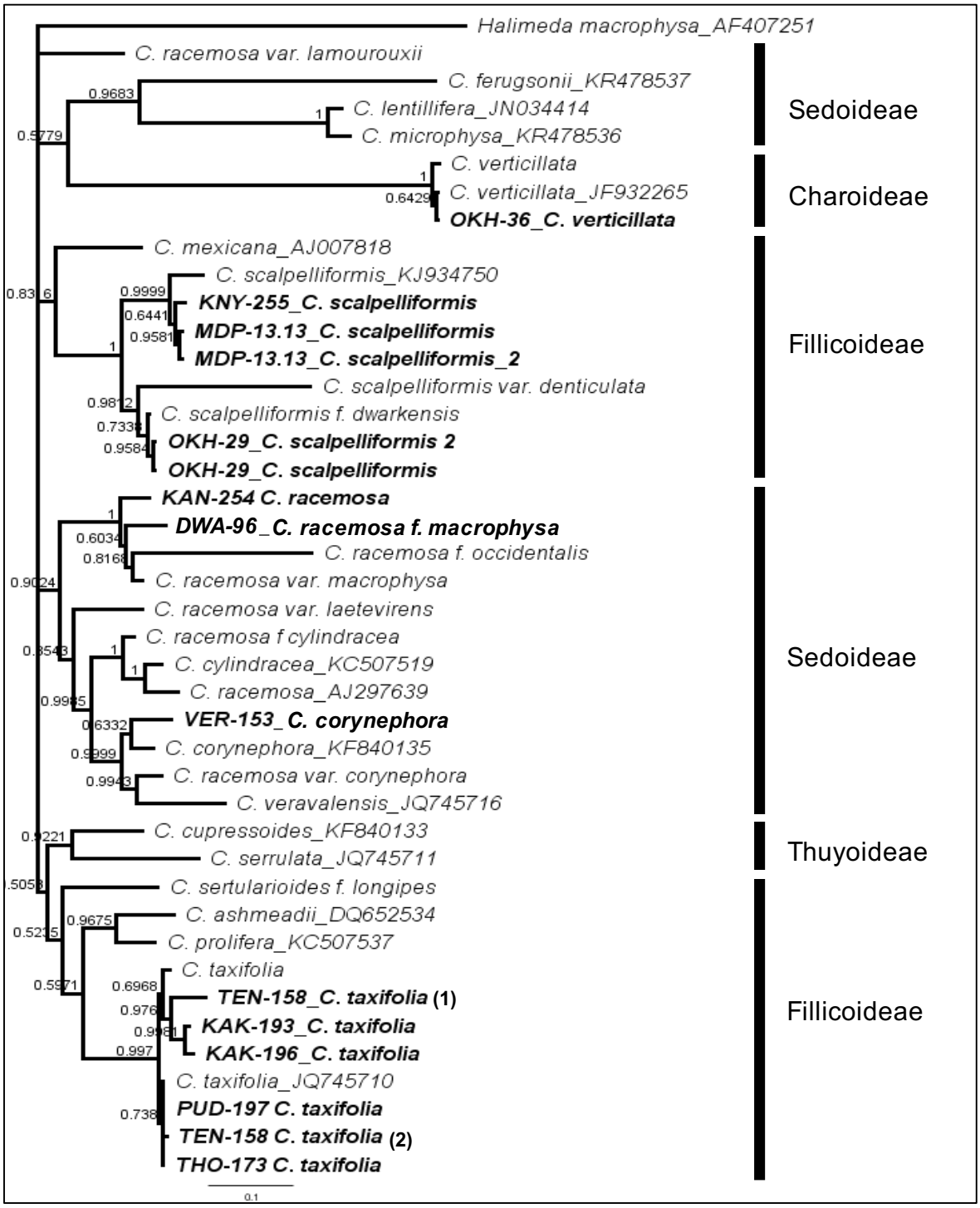

Figure 4.4 Bayesian Inference phylogram based on nuclear ITS data, rooted with *Halimeda macrophysa* (AF407251) as outgroup. ML model used was HKY+G. Bayesian posterior probabilities >0.5 are indicated above the branches. Total chain length = 1,100,000 and mean LnL = -8220.97. Scale bar at the bottom indicates number of nucleotide substitutions per site.

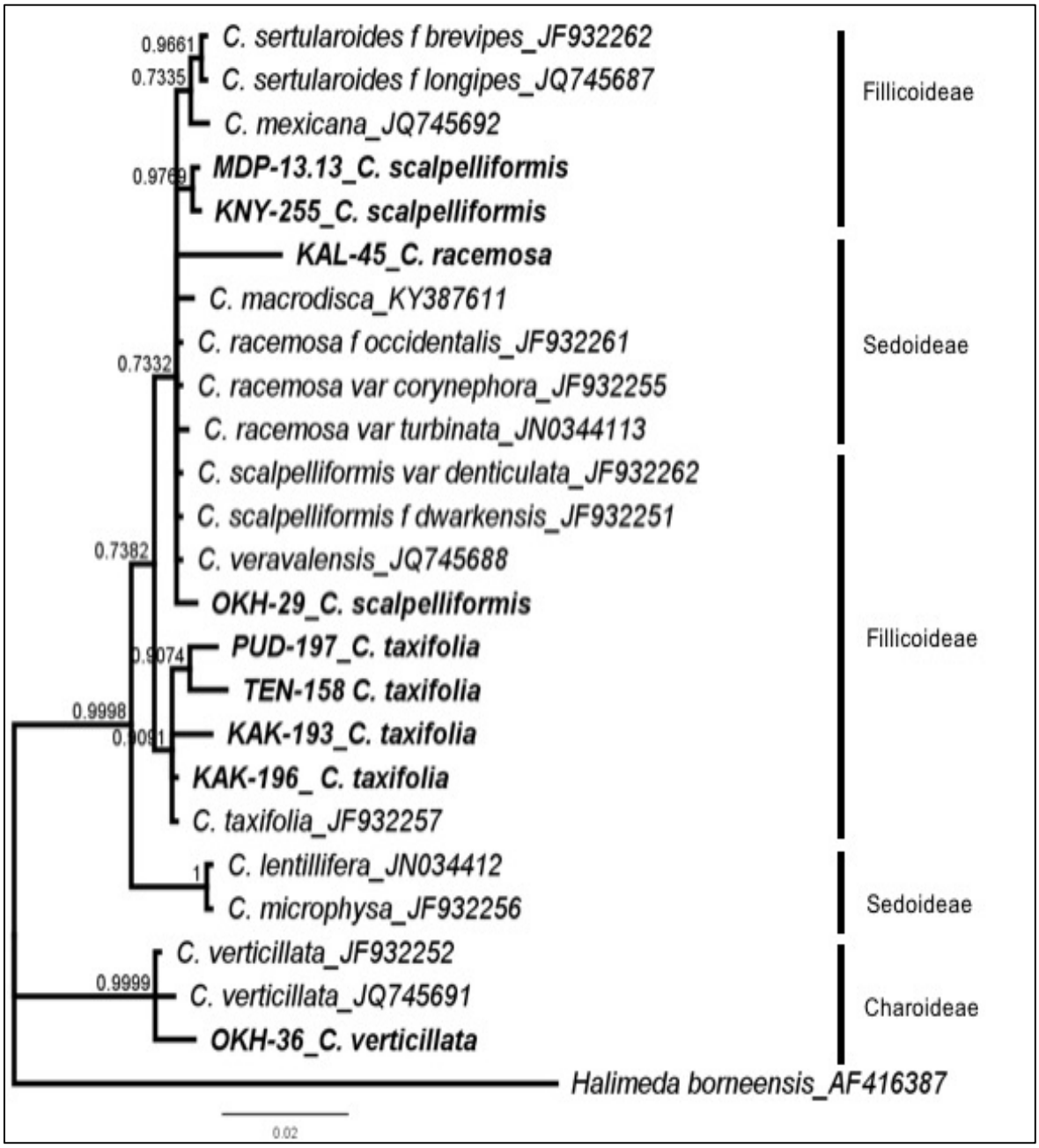

Figure 4.5 Bayesian Inference phylogram based on nuclear 18S data, rooted with *Halimeda borneensis* as outgroup. ML model used was HKY+G. Bayesian posterior probabilities >0.5 are indicated above the branches. Total chain length = 1,100,000 and mean LnL = -2854.27. Scale bar at the bottom indicates number of nucleotide substitutions per site.

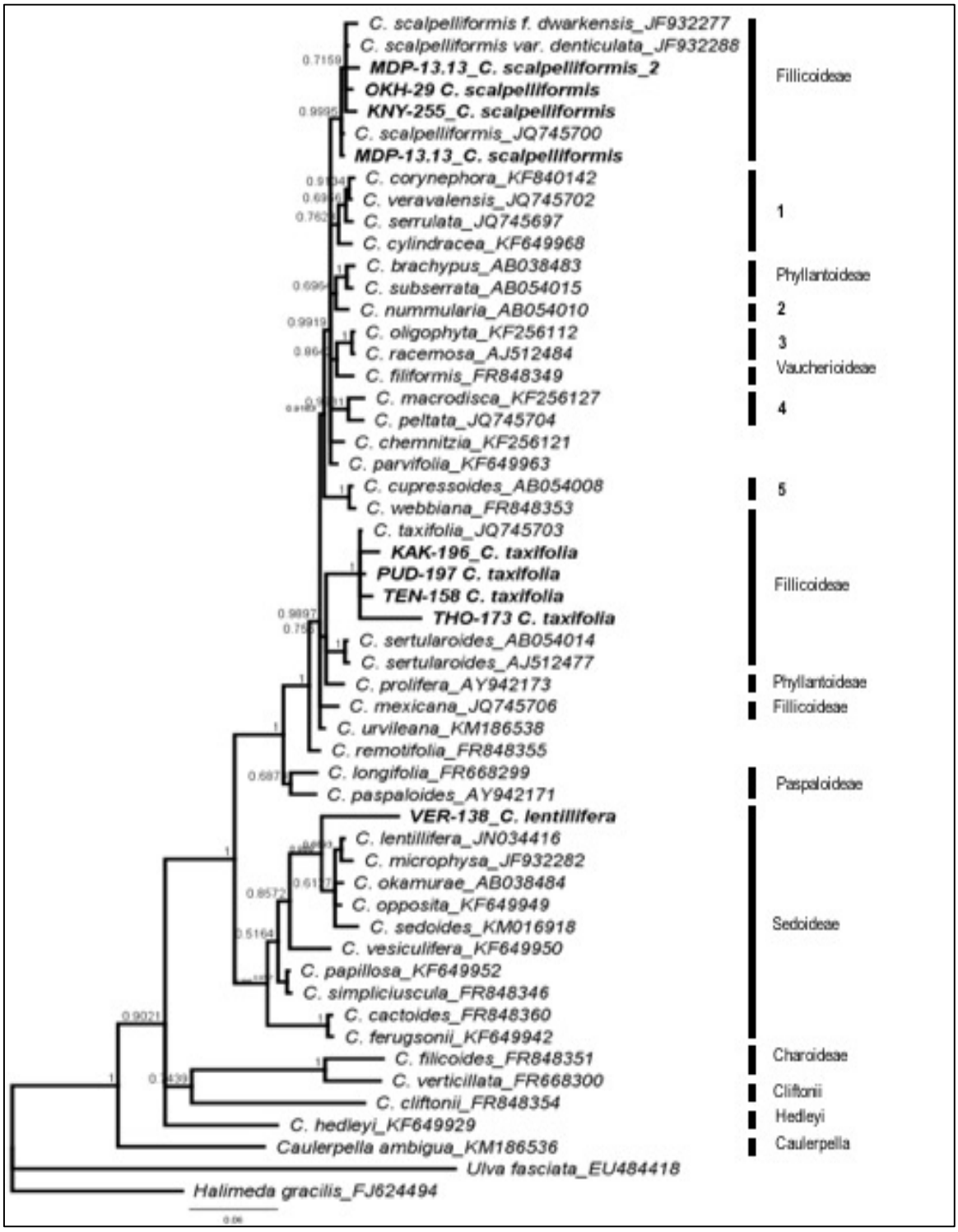

Figure 4.6 Bayesian Inference phylogram based on chloroplast *rbc*L data, rooted with *Halimeda gracilis* and *Ulva fasciata* as outgroup. The tree was generated using HKY+ G ML model. Bayesian posterior probabilities >0.5 are indicated above the branches. Total chain length = 1,100,000 and mean LnL = -6133.471. Scale bar at the bottom indicates number of nucleotide substitutions per site.

Figure 4.7 Bayesian Inference phylogram based on chloroplast *tufA* data, rooted with *Halimeda opuntia* as outgroup. The tree was generated using HKY+ G ML model. Bayesian posterior probabilities >0.5 are indicated above the branches. Total chain length = 1,100,000 and mean LnL = -7803.966. Scale bar at the bottom indicates number of nucleotide substitutions per site.

Table 4.2 Details of Top Blastn hits with query cover, E value and percent identity of sequences of various *Caulerpa* species generated in the study

S. No.	Sample ID	Molecular Marker	BLASTn hit (Accession Number)	Query cover	E value	% Identity
1.	DWA-96	ITS	*C. racemosa* f. *macrophysa* (JF932272)	93	0	98
2.	VER-153	ITS	*C. corynephora* (KF840135)	98	0	96
3.	TEN-158 (1)	ITS	*C. taxifolia* (JQ745710)	95	0	98
4.	KAK-196	ITS	*C. taxifolia* (JQ745710)	99	0	99
5.	KNY-254	ITS	*C. racemosa* (DQ652262)	98	0	96
6.	KNY-255	ITS	*C. taxifolia (JQ745717)*	100	0	99
7.	MDP-13.13 (1)	ITS	*C. scalpelliformis* (KF840132)	98	0	99
8.	MDP-13.13 (2)	ITS	*C. scalpelliformis* (KF840132)	99	0	100
9.	KNY-255	ITS	*C. scalpelliformis* (KF840132)	98	0	99
10.	OKH-29	ITS	*C. scalpelliformis* f. *dwarkensis* (JF932264)	100	0	99
11.	OKH-29	ITS	*C. scalpelliformis* f. *dwarkensis* (JF932264)	100	0	99
12.	OKH-36	ITS	*C. verticillata* (JF932265)	94	0	99
13.	PUD-197	ITS	*C. taxifolia* (JF932270)	100	0	99
14.	TEN-158 (2)	ITS	*C. taxifolia* (JF932270)	96	0	99
15.	THO-173	ITS	*C. taxifolia* (JQ745710)	100	0	99
16.	KAK-196	*rbc*L	*C. taxifolia* (AB054016)	100	0	97
17.	MDP-13.13	*rbc*L	*C. scalpelliformis* (KF840139)	100	1e-119	99
18.	MDP-13.13	*rbc*L	*C. scalpelliformis* (JQ745700)	100	0	99
19.	OKH-29	*rbc*L	*C. racemosa* cf. var. *macra* (FR848358)	99	0	98
20.	KNY-255	*rbc*L	*C. scalpelliformis* (JQ745700)	99	0	99
21.	PUD-197	*rbc*L	*C. taxifolia* (AB054016)	99	0	99
22.	TEN-158	*rbc*L	*C. taxifolia* (AB054016)	99	0	99
23.	THO-173	*rbc*L	*C. taxifolia* (JQ745703)	96	0	98

24.	VER-138	*rbc*L	*C. lentillifera* (JN034416)	97	5e-159	98
25.	KNY-255	t*ufA*	*C. scalpelliformis* (KF840150)	95	0	98
26.	KAK-196	t*ufA*	*C. taxifolia* (KJ957132)	95	0	98
27.	KAK-193	t*ufA*	*C. taxifolia* (KJ957127)	93	0	98
28.	KNY-254	t*ufA*	*C. racemosa* (KJ957088)	94	0	98
29.	OKH-29	t*ufA*	*C. scalpelliformis* (KF840150)	98	0	99
30.	MDP-13.13	t*ufA*	*C. scalpelliformis* (KF840150)	88	0	99
31.	PUD-197	t*ufA*	*C taxifolia* (KJ957127)	98	0	100
32.	TEN-158	t*ufA*	*C taxifolia* (KJ957127)	100	0	100
33.	MDP-13.13	18S	*C. scalpelliformis* (KF840143)	100	0	99
34.	KAL-45	18S	*C. racemosa* (JF932255)	98	0	99
35.	KAK-193	18S	*C. taxifolia* (JQ745689)	98	0	99
36.	PUD-197	18S	*C. taxifolia* (JQ745689)	100	0	99
37.	KAK-196	18S	*C. taxifolia* (JQ745689)	99	0	99
38.	OKH-29	18S	*C. scalpelliformis* f. *dwarkensis* (JF932251)	100	0	99
39.	OKH-36	18S	*C. verticillata* (JQ745691)	99	0	99
40.	TEN-158	18S	*C. taxifolia* (JQ745689)	99	0	99
41.	KNY-255	18S	*C. scalpelliformis* (KF840143)	100	0	99

II. Objective 2 Comparative evaluation of *in-vitro* anti-cancer and anti-oxidant activities of *Caulerpa* spp.

4.5 Extract Preparation

The extracts were prepared using different solvents viz. chloroform, chloroform, ethyl acetate, methanol and water. For preliminary screening 1 g of dried powder of each sample was saturated with 5 ml of solvent and left overnight, with subsequent extraction. The yield of each sample varied from 8.1 ± 0.2% to 9.89 ± 0.1% of dry weight. It is also noteworthy that yield of dry samples was also around 10-14%, suggesting a total low yield of crude extracts from *Caulerpa* species.

4.6 Phycochemical Assays Reveal Presence of Bioactive Moieties

The phycochemicals determined from all samples are presented in **Table 4.3**. All the species showed variable amounts of alkaloids, terpenoids, steroids, tannins, saponins, flavonoids, and phenols while anthraquinones and glycosides were absent in all the species. Both the isolates of *C. taxifolia i.e.* KAK-196 and TEN-158 indicated absence of tannins unlike other species, whereas steroids were absent in TEN-158 and couldn't be determined in KAK-196. Likewise, three isolates of *C. racemosa i.e.* DWA-96, VER-153, and KNY-254 depicted almost similar types of metabolites with probable variations in their quantities. *C. sertularioides*, MDP-13.13 exhibited alkaloids, terpenoids, steroids, tannins, saponins, flavonoids and phenols. *C. verticillata* OKH-36, contained alkaloids, terpenoids, steroids, and saponins while presence of flavonoids is uncertain, *C. scalpelliformis* KNY-255, showed presence of alkaloids, terpenoids, steroids, tannins, and saponins.

4.7 CMEs Possess Anti-Proliferative Activity

Primary screening of various CMEs was conducted on MDA-MB-231 and H1299 cells, which revealed that methanolic extracts have better efficacy than other solvent extracts tested. Henceforth, further evaluation was done using methanolic extracts of *Caulerpa* (CMEs). Effect of various CMEs on cell viability of three different cancer cells (MDA-MB-231, T-47D and H1299) was studied, at different doses. The results reveal significant ($p<0.5$; $p<0.01$; and $p<0.001$) cytotoxicity of CMEs in all three types of cancer cells, with overall maximum potency against MDA-MB-231 cells, after 48 h treatment. The best IC_{50} was observed for *C. racemosa* isolate KNY-254, followed by TEN-158 in MDA-MB-231 cells. The IC_{50} values of all the samples are

depicted in **Table 4.4**. On the contrary, no significant cytotoxicity was observed by any of the CMEs on hPBMCs, suggesting their selective cytotoxicity towards cancer cells (**Figure 4.9**). Variations amongst different geographical isolates were also observed suggesting different types and/or quantities of bioactive metabolites. In addition, time-dependent response of CMEs was investigated at three time periods viz. 24 h, 48 h and 72 h at same doses, which depicted an initial time-dependent cytotoxicity from 24 h to 48h, after which no significant increase was observed (**Figure 4.10**). Therefore, 48 h time period is inferred optimal for treatment of CMEs in MDA-MB-231 cells.

4.8 Annexin V/FITC Affinity Assay Indicates Apoptotic Cell Death by KNY-254 and TEN-158

Assessment of apoptosis induction was analyzed by staining MDA-MB-231 cells by Annexin V/FITC. The effect of methanolic extracts of *C. racemosa* KNY-254 and *C. taxifolia* TEN-158 was seen under Confocal Laser Scanning Microscope-CLSM IX-83, FV1200 (Olympus, Japan). These two species were selected based on their best overall observed bioactive potential. Annexin V is utilized as a protein probe to detect the presence of apoptotic cells displaying phosphatidylserine (PS) on outer leaflet of plasma membrane and FITC is a fluorescent probe conjugated to Annexin V. The results show that the treated set of cells exhibit induction of apoptosis as suggested by more green fluorescence detected w.r.t. untreated control cells. **Figure 4.11** depicts the contrasting imaging observed in untreated v/s treated cells, depicting early sign of apoptosis.

4.9 CMEs Cause Cell Cycle Arrest in MDA-MB-231 cells

The effect of CMEs on cell cycle progression of MDA-MB-231 cells was analyzed by flow cytometry (BD Accuri 6). The results revealed perturbations in cell cycle progression in comparison to untreated control cells. The control cells displayed normal cell cycle progression with 60.16% cell population in G1 phase, 14.47% in S phase and 25.67% in G2 phase. On the contrary, in treated cells a net increase in cells at G1 (4-24%) and S (12-29%) phase; with concomitant decrease in G2 phase was observed, except *C. verticillata* OKH-36 where only G1 phase arrest was observed (**Figure 4.12**).

4.10 Intracellular Oxidative Stress by CMEs Treatment

The level of intracellular ROS in cancer cells, as examined by DHE, depicts a significant ($p<0.05$; $p<0.001$) increase after treatment with CMEs (**Figure 4.13**). ROS production in MDA-MB-231 cells was augmented up to 2-4 folds w.r.t. untreated control cells, post 24 h treatment with CMEs. The maximum augmentation was observed by *C. racemosa* KNY-254 followed by, *C. taxifolia* TEN-158 and *C. racemosa* DWA-96 at 25 µg/µL. The results suggest all CMEs are capable to induce ROS production in MDA-MB-231 cells, in a dose-dependent manner.

4.11 CMEs Modulate Anti-Oxidant Enzyme Machinery

In order to examine the effect of CMEs on the anti-oxidant enzyme machinery of cells, relative enzyme activity of SOD, catalase and GR was investigated. A 0.20-0.43 fold increase in SOD; 0.22-0.62 fold decrease in catalase and 0.70-0.85 fold decrease in GR activity w.r.t. untreated control cells, was recorded in MDA-MB-231 cells (**Figure 4.14).** The maximum change in activity was depicted by *C. racemosa* isolate KNY-254 and DWA-96, followed by *C. taxifolia* isolate TEN-158.

4.12 MMP disruption by CMEs Treatment

JC-1 is a cationic dye which measures the MMP by accumulation in the energized mitochondria. It exists in two forms, one is monomeric form that emits green fluorescence, and second is aggregate form that emits red fluorescence. A decrease in aggregate to monomer ratio indicates a depolarized mitochondrial membrane while reverse indicates a hyperpolarized mitochondrial membrane. CMEs had a pronounced effect on MMP with gradual increase in aggregate/monomer ratio in a concentration dependent manner, as depicted in MDA-MB-231 cells (**Figure 4.15**). An increase ranging from 1.3 – 2.4 folds was observed, at 0.1, 0.25 and 0.5 µg/µL concentrations of CMEs, with highest increase displayed by *C. racemosa* isolate KNY-254, followed by *C. taxifolia* isolate KAK-196. The results suggest a dose-dependent increase in MMP of MDA-MB-231 cells, in response to CMEs.

4.13 Scratch Wound Assay Reveals Inhibition of Cell Migration

Scratch wound assay is an *in vitro* model system to investigate invasion of cancer cells where a manual wound is introduced using sterile microtips, and the ability of cells to restore the wound is analyzed with and without drug treatment. The CMEs were investigated for their effect on invasion of MDA-MB-231 cells, up to 48 h at

sub-IC_{50} doses. MDA-MB-231 cells were allowed to attain 90% confluency and scratched transversely to create an artificial wound using a sterile 20 µL microtip. Wells were washed with 1X PBS and images of were captured at 0 h. Later, the cells were incubated with CMEs and allowed to restore the wound. Cells were observed after 48 h and the results revealed that CMEs suppressed the migration of MDA-MB-231 cells w.r.t. untreated control cells. After 48 h cells were stained with 0.1% crystal violet for 30 min and images were captured. The extent of inhibition was calculated in terms of percentage using ImageJ software. The control cells were able to restore the growth completely in the wounded zone after 48 h, while various CMEs suppressed the migration of cells from 55 to 71% (**Figure 4.16, 4.17**). The maximum inhibition was observed by *C. verticillata* OKH-36 followed by *C. racemosa* DWA-96 and KNY-254.

4.14 Chemical Constituents Characterized by LC-MS

The methanolic extract of *C. racemosa* KNY-254 was subjected to column chromatography on C_{18} classical normal phase silica column, Novapak (3.9 X 150 mm). The chromatogram revealed several compounds some of which are previously published and others are unreported, to the best of my knowledge. The chromatograph is shown in **Figure 4.18**. Probable structures were assigned to individual peaks based on systematic search for molecules matching extracted ion mass chromatograms, available in previously published literature. A total of six molecules namely CR1, CR2, CR3, CR4, CR5, and CR6 (**Figure 4.19**), were identified from previous literature while other six molecules were unreported and believed to be novel (**Figure 4.20**). The retention time and mass of identified compounds are listed in **Table 4.5**.

4.15 Column Chromatography

A total of 380 fractions of 10 ml each were collected and fractions were thoroughly analyzed for single spots using pre-coated aluminum TLC plates (Merck). We were able to collect three set of fractions, seemingly purified and single spots. These fractions were individually pooled to obtain 3 concentrated stock compounds viz. PC1, PC2, and PC3. The molecular weight of samples was 6.0 mg, 7.0 mg and 20.0 mg, respectively. The samples were sent for H^1 NMR and C^{13} NMR analysis to Indian Institute of Science and Education Research (IISER), Mohali. However, the

initial results revealed that the purified stocks are still mixture of two or more compounds, which could not be resolved further.

4.16 Molecular Docking Reveals Cross-talk Between *Caulerpa* constituents and Cancer Signaling Proteins

Theoretical investigation of binding patterns of various compounds obtained from *Caulerpa* and the possible target proteins involved in cancer signaling was done using molecular docking. The protein-inhibitor complexes were chosen in order to compare the level of interactions with already existing standard inhibitors. The Glide score (Gscore) of protein-ligand interaction comprising various *Caulerpa* constituents is shown in **Table 4.6.** and 2D interaction diagrams are depicted in **Figure 4.21**. The Gscore is an approximate measure of ligand binding free energy, thus, lowest the Gscore, better the interaction. As evident from the Gscore results, the best interaction with Bcl2 was shown by CR3; in case of AMPK & mTOR Kinase, Racemosin C exhibited the best G score (-4.722 and -7.455, respectively); in case of BID, PI3K, PTP1B, CR4 exhibited the best Gscore (-1.869, -8.958, -3.863, respectively); while in case of PERK, IGF-1R and Akt2, Caulersin exhibited the best Gscore -6.015, -7.302, -5.862, respectively), of all the tested compounds. Overall, the docking results reveal that *Caulerpa* constituents are involved in cancer signaling pathways and display moderate interactions, that needs further validation.

III. Objective 3 Analysis of putative correlation between anti-cancer activity and phylogeny of *Caulerpa*

The putative correlation between phylogenetic status of various *Caulerpa* species and their anti-cancer potential was investigated using Pearson's correlation method. For the analysis, the phylogram with *tufA* previously inferred as the most informative and better resolved phylogram was chosen. The species having best IC_{50} value *i.e. C. racemosa* KNY-254 was considered as a reference and the pairwise genetic distance of all the species in question was calculated with the reference species. The analysis revealed a weakly positive correlation between the two parameters, with R^2 value of 0.44 (**Figure 4.22**). Notably, a debilitated correlation could be seen amongst the species where increasing genetic distance results in increasing IC_{50} value with the exception of *C. taxifolia* TEN-158. However, no firm conclusion could be drawn at this stage mainly owing to a smaller number of samples and considerable genetic distance amongst the geographical isolates.

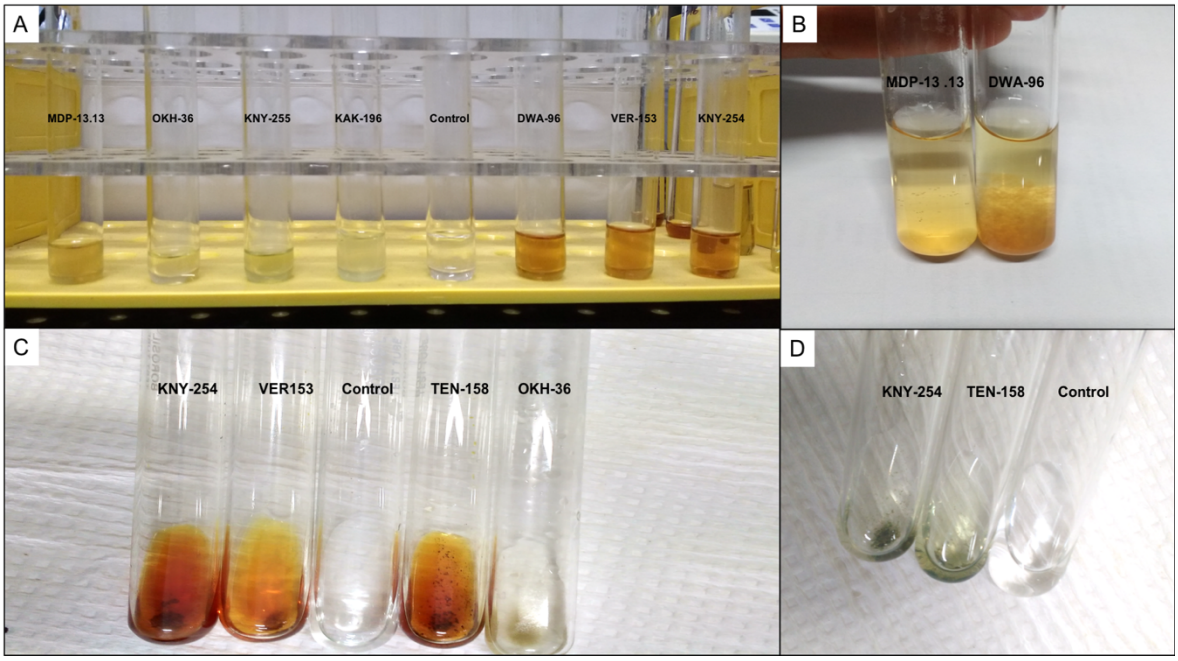

Figure 4.8 Phycochemical screening in various *Caulerpa* extracts: A), B) Test for Flavonoids: Yellowish-brown color indicating positive reaction; C) Test for Alkaloids: Reddish precipitates indicating positive reaction; D) Test for Tannins: Greenish precipitates indicating positive reaction

Table 4.3 Phycochemical analysis of various *Caulerpa* samples

Metabolite	MDP-13	OKH-36	DWA-96	VER-153	KNY-254	KAK-196	TEN-158	KNY-255
Alkaloids	+	+	+	+	++	+	+	+
Terpenoids	+	+	+	+	++	++	++	+
Steroids	+	+	+	+	+	+/-	-	+
Tannins	+	-	+	++	++	-	-	+
Saponins	+	+	+	+	+	+	+	++
Flavonoids	+	+/-	++	++	++	+	+	+/-
Anthraquinones	-	-	-	-	-	-	-	-
Glycosides	-	-	-	-	-	-	-	-
Phenol	+	-	+	+	+	++	++	-

++ indicates strong positive; + indicates fairly positive, - indicates absence and +/- indicates weakly positive or uncertainty

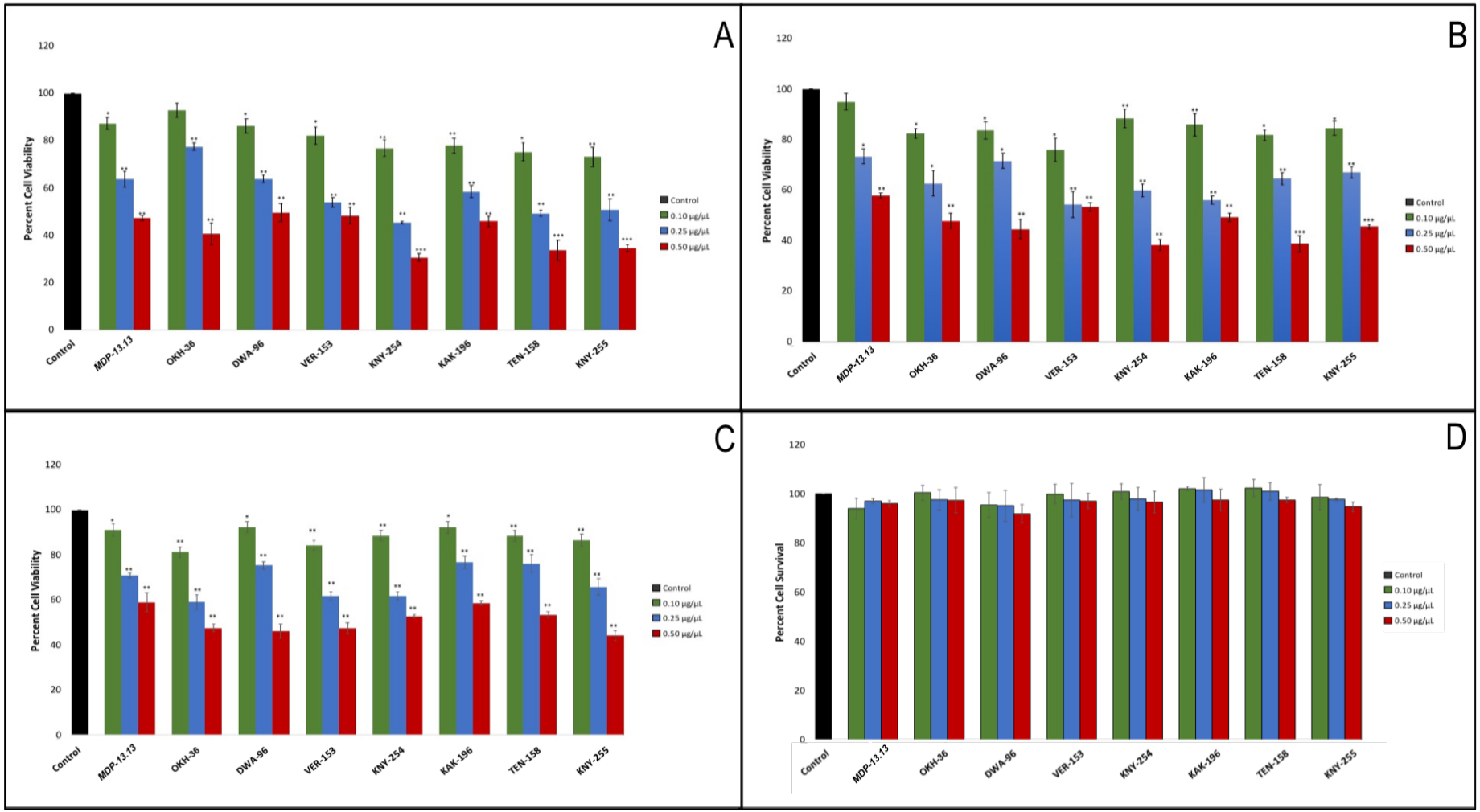

Figure 4.9 Cell proliferation as assayed after 48 h, using MTT, on different cancer cells at concentrations viz. 0.10, 0.25 and 0.50 μg/μL of CMEs. A) MDA-MB-231, B) T-47D, C) H1299, D) hPBCs . (*p<0.05; **p<0.01; and ***p<0.001)

Table 4.4 Half maximal inhibitory concentrations (IC_{50}) of various CMEs as calculated on MDA-MB-231, T47-D and H1299. Concentrations are expressed in μg/μL with SD.

Sample ID	MDA-MB-231	T47-D	H1299
MDP-13.13	0.451 ± 0.014	-	-
OKH-36	0.436 ± 0.024	0.461 ± 0.040	0.447 ± 0.016
DWA-96	0.430 ± 0.020	0.449 ± 0.031	0.468 ± 0.024
VER-153	0.359 ± 0.173	-	0.459 ± 0.031
TEN-158	0.246 ± 0.009	0.390 ± 0.020	0.481 ± 0.007
KAK-196	0.387 ± 0.078	0.432 ± 0.023	-
KNY-254	**0.226 ± 0.004**	**0.364 ± 0.008**	**0.383 ± 0.028**
KNY-255	0.272 ± 0.043	0.446 ± 0.013	0.432 ± 0.008

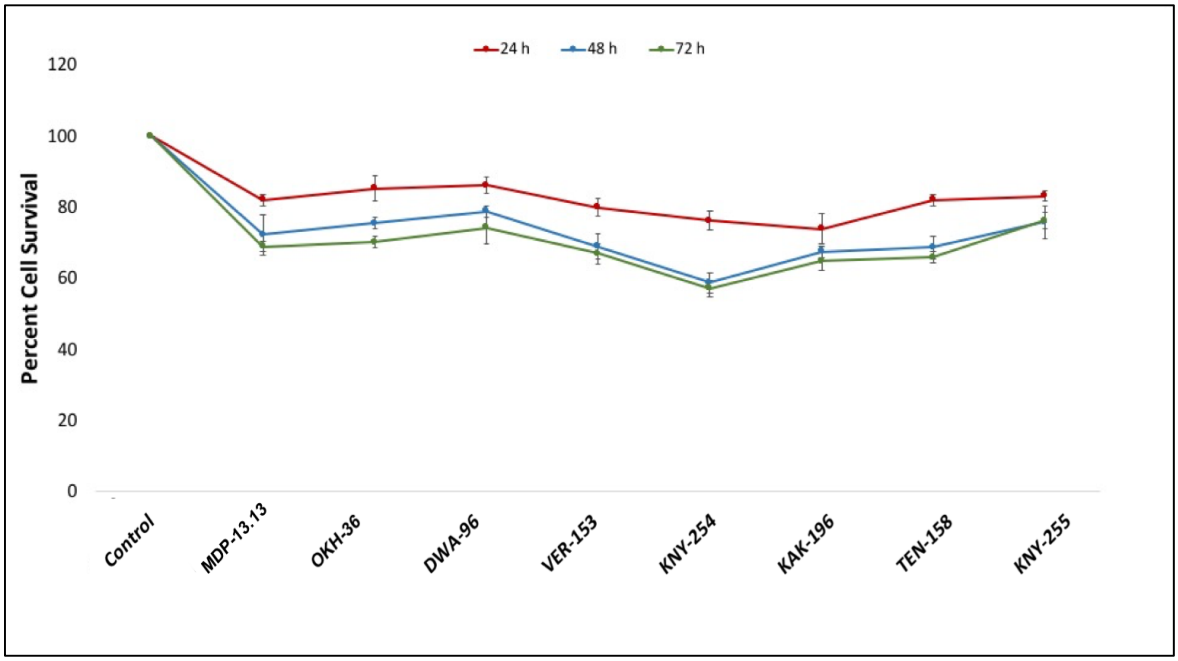

Figure 4.10 Cell proliferation assayed in time-dependent manner using MTT, after 24h, 48h and 72h on MDA-MB-231 with sub-lethal doses of CMEs

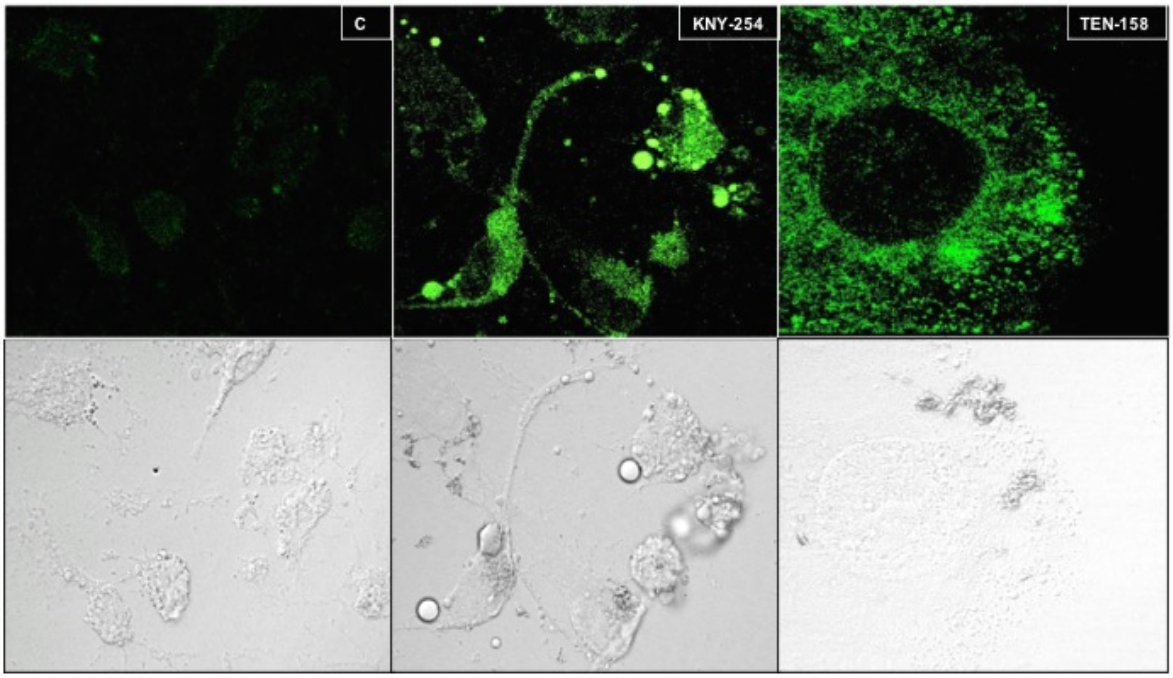

Figure 4.11 Apoptosis analysis assessed by Annexin V/FITC staining, as visualized by confocal laser scanning microscope (CLSM), in MDA-MB-231 cells, after treatment with IC_{50} concentrations of KNY-254 and TEN-158. Top row shows cells emitting fluorescence and bottom row shows cells visualized under Differential Interference Contrast (DIC) mode.

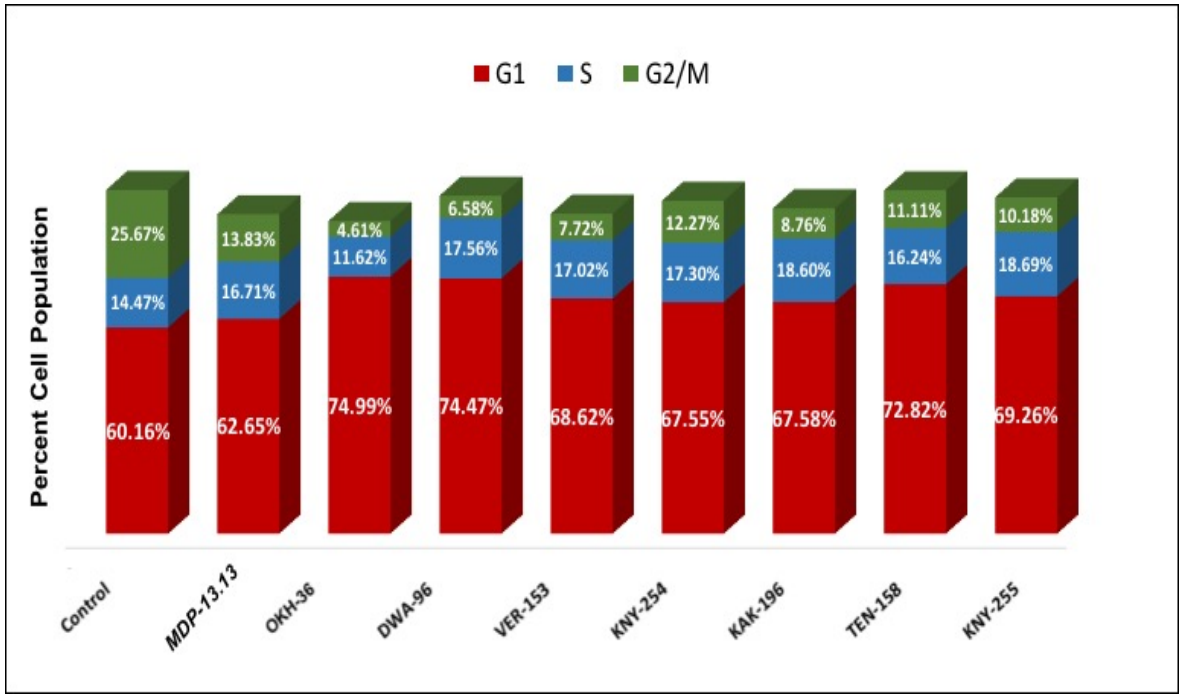

Figure 4.12 Cell cycle analysis by PI staining, as assessed by flow cytometry, in MDA-MB-231 cells, after treatment with sub-lethal concentrations of CMEs for 48 h.

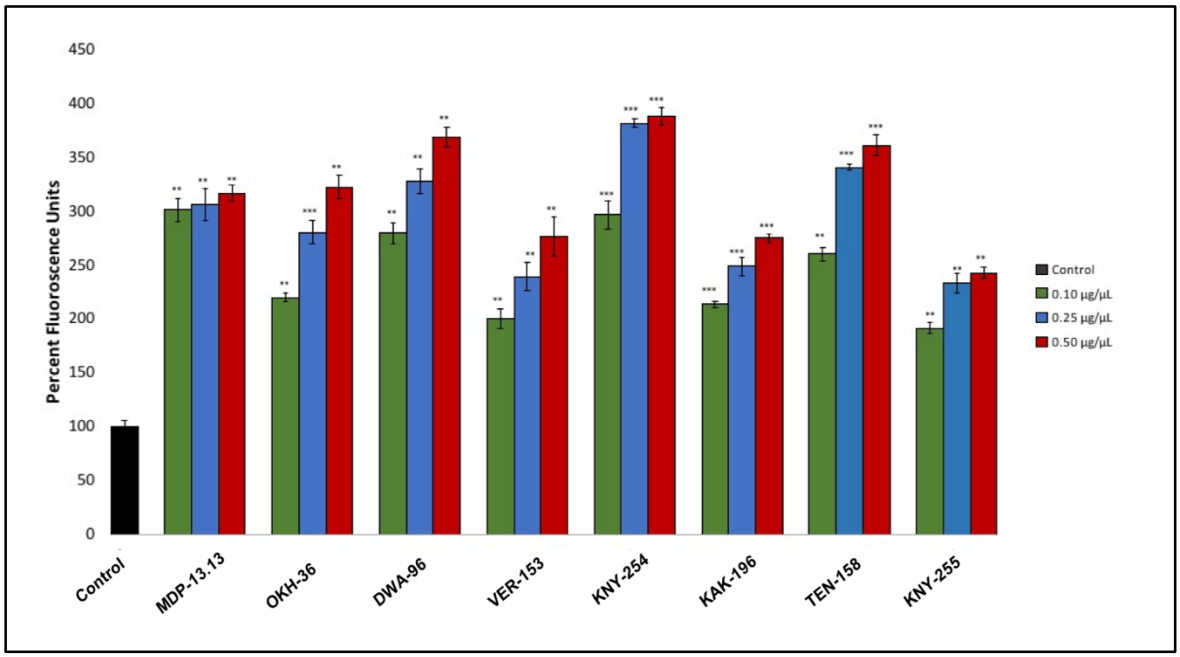

Figure 4.13 Intracellular ROS production assayed by DHE after 24h, on MDA-MB-231 cells, with 0.10, 0.25 and 0.50 μg/μL of CMEs. (*p<0.05; **p<0.01; and ***p<0.001)

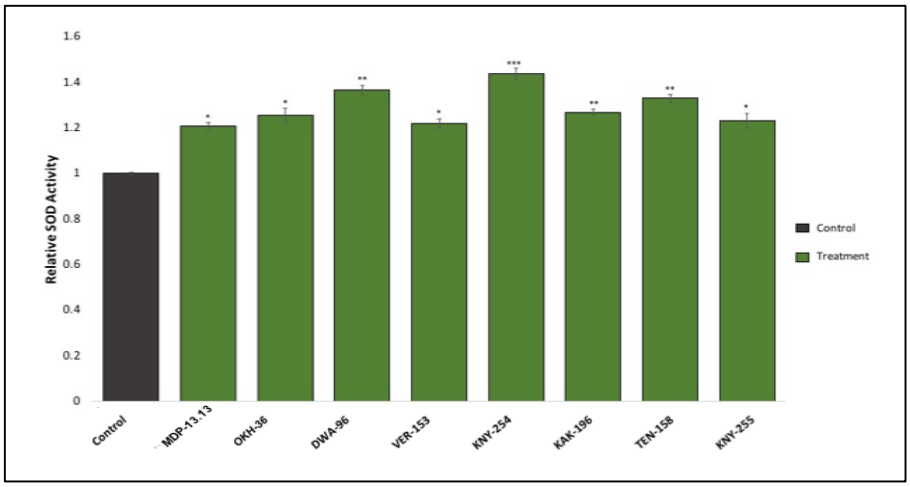

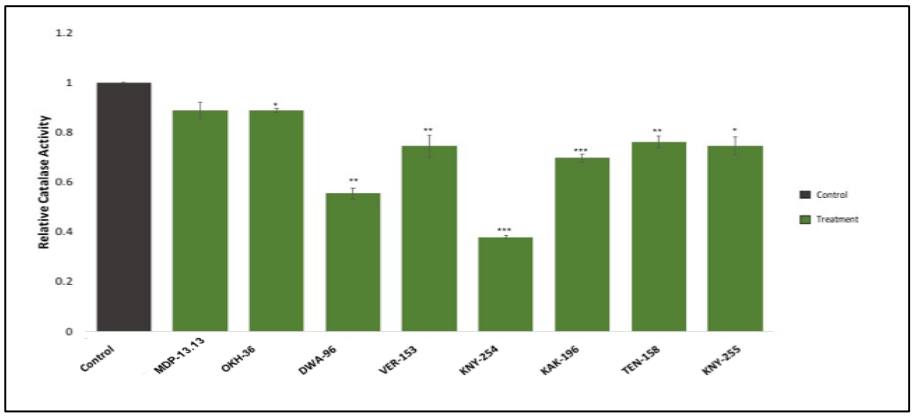

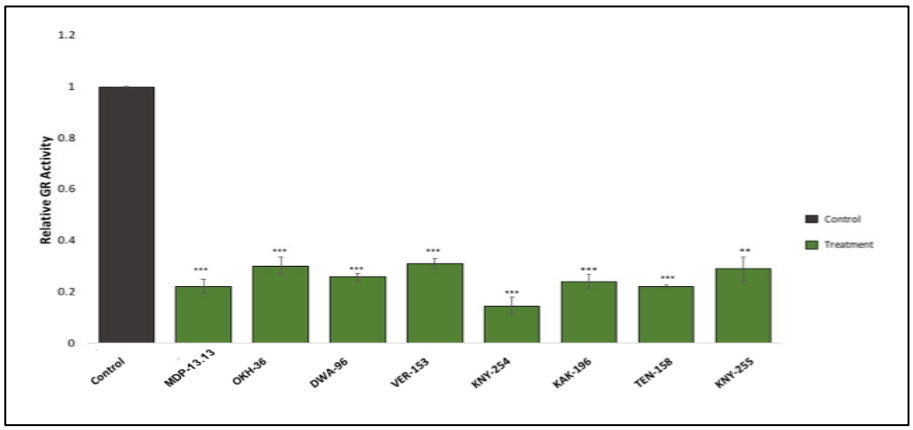

Figure 4.14 SOD, Catalase, and GR activity analysis in MDA-MB-231 cells after treatment with sub-lethal concentrations of CMEs. A) Superoxide dismutase; B) Catalase; and C) Glutathione reductase. (*p<0.05; **p<0.01; and ***p<0.001)

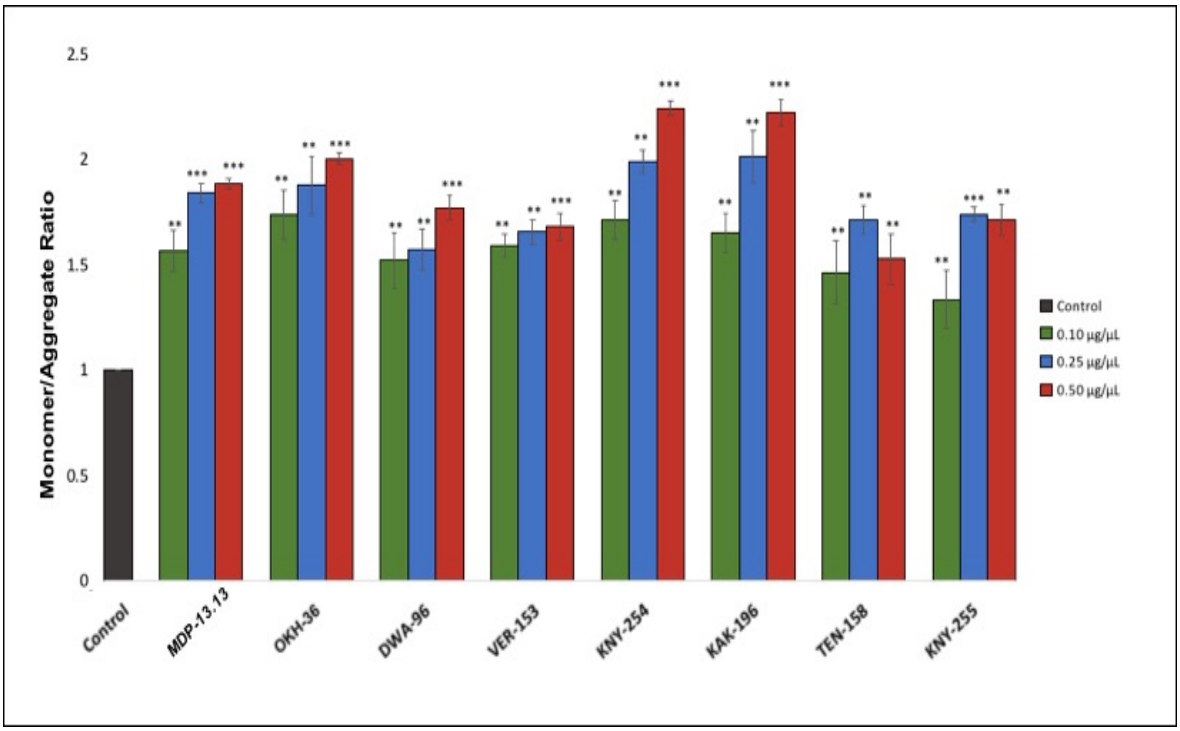

Figure 4.15 Mitochondrial membrane potential assessed spectrophotometrically, by JC-1, in MDA-MB-231 cells, after treatment with 0.10, 0.25 and 0.50 μg/μL of CMEs. (*p<0.05; **p<0.01; and ***p<0.001)

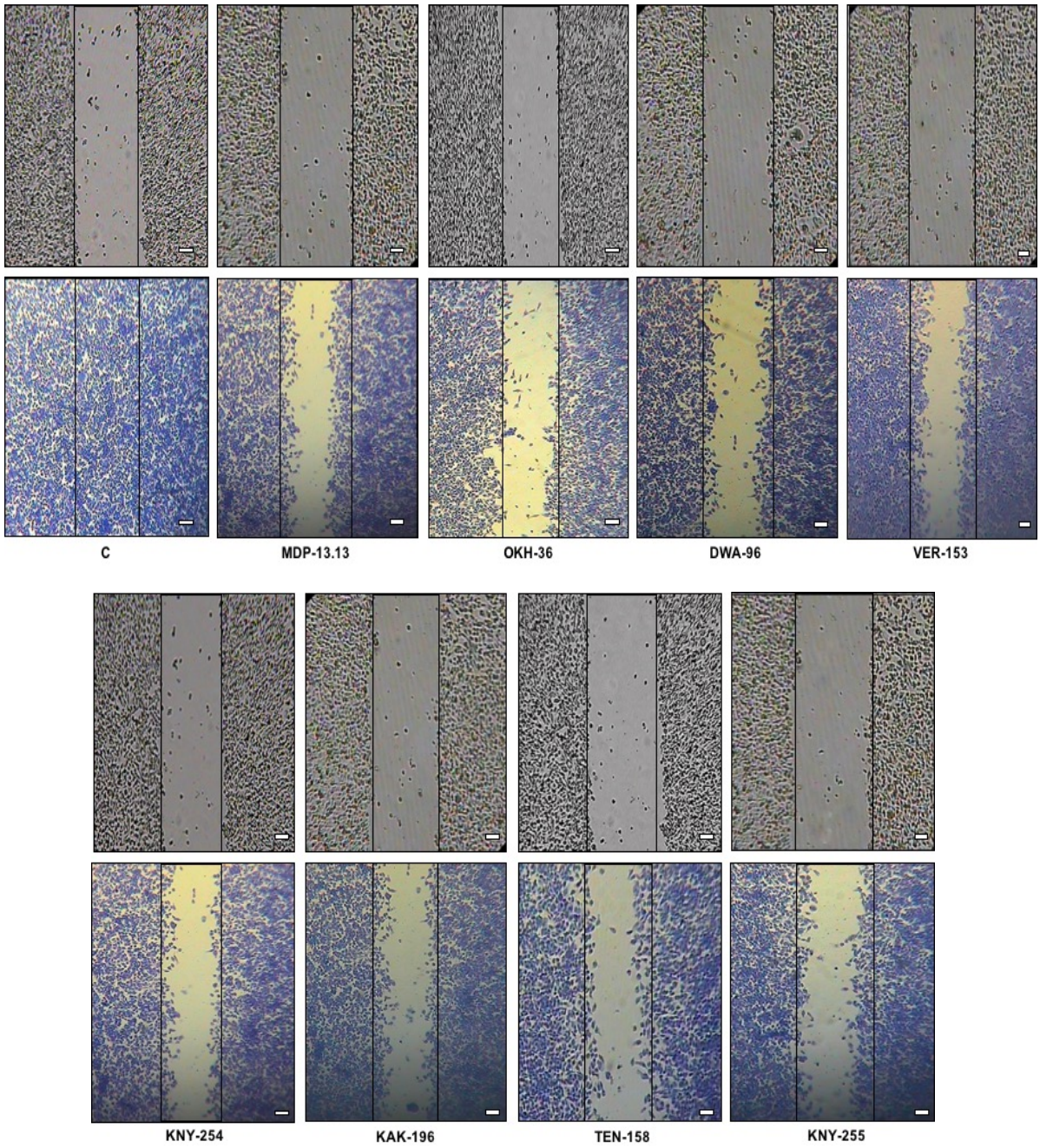

Figure 4.16 Anti-invasion activity assessment of various CMEs at sub-lethal doses, up to 48h, by scratch wound assay, in MDA-MB-231 cells. Scale bar at the bottom equals100 μm.

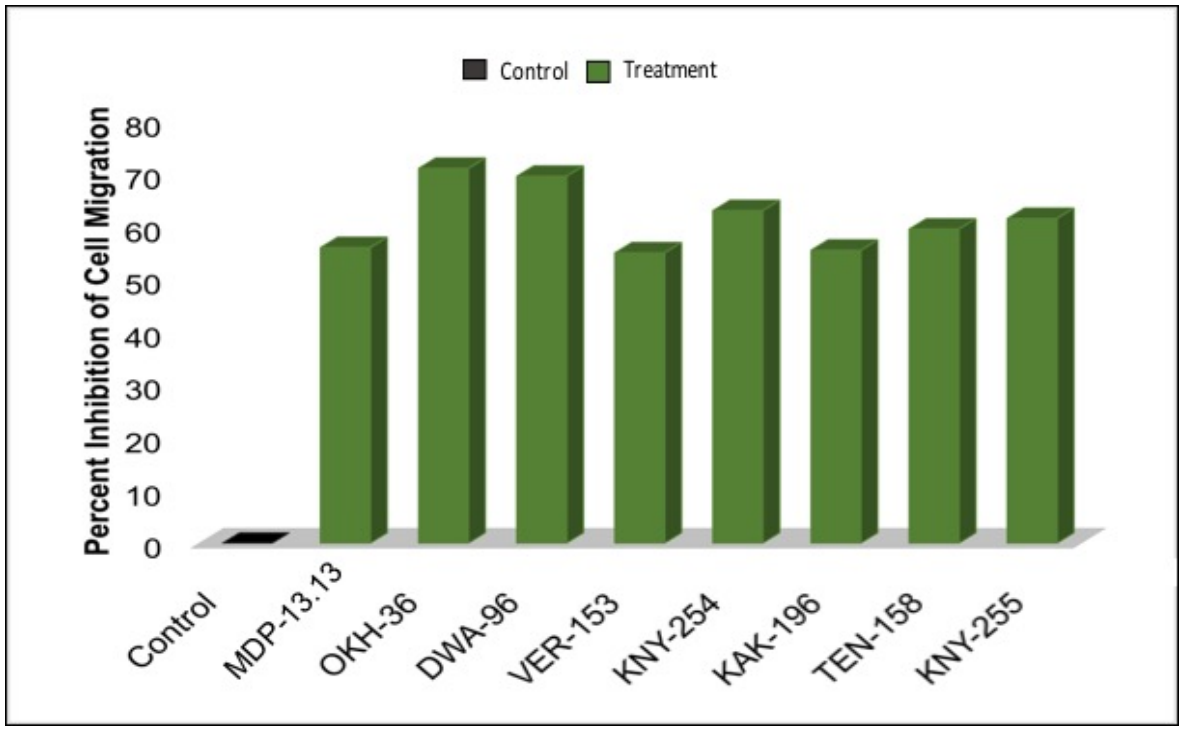

Figure 4.17 Graphical depiction of percent inhibition of cell migration in MDA-MB-231 cells by various CMEs at sub-lethal doses, up to 48h, by scratch wound assay.

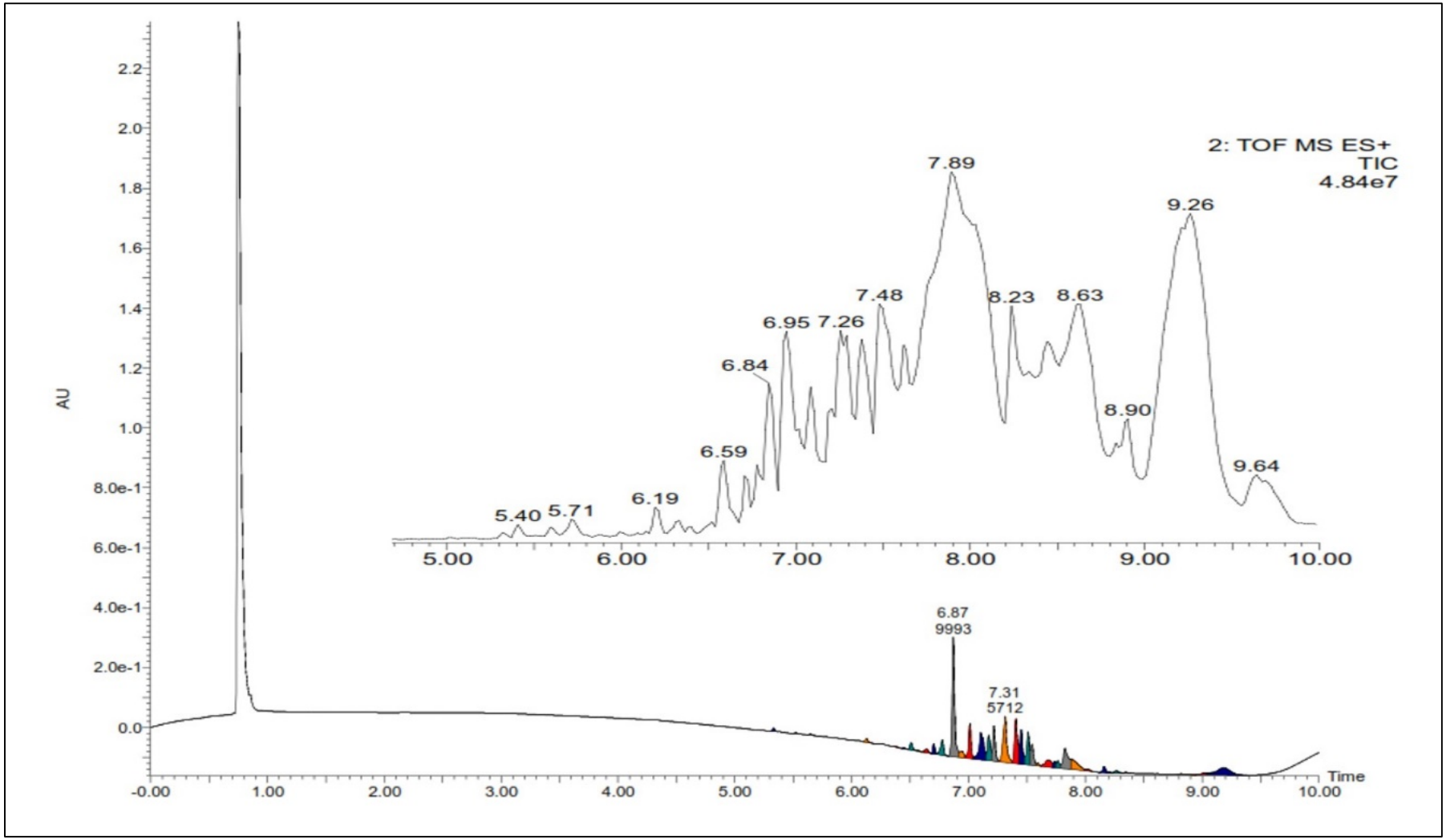

Figure 4.18 LC-MS chromatogram of methanolic extract of *C. racemosa* KNY-254

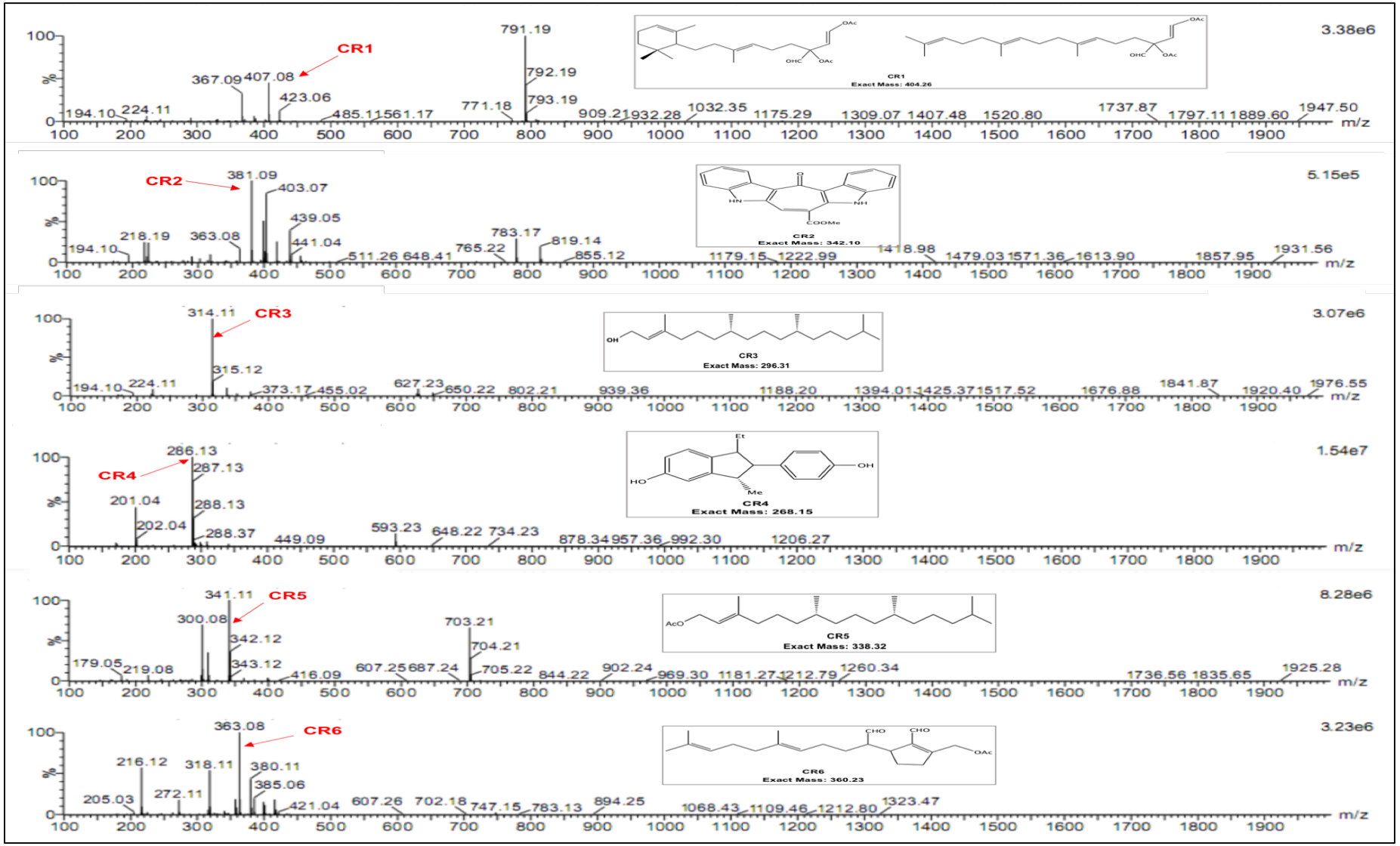
CR1
CR1
Exact Mass: 404.26
3.38e6
CR2
CR2
Exact Mass: 342.10
5.15e5
CR3
CR3
Exact Mass: 296.31
3.07e6
CR4
CR4
Exact Mass: 268.15
1.54e7
CR5
CR5
Exact Mass: 338.32
8.28e6
CR6
CR6
Exact Mass: 360.23
3.23e6
m/z

Figure 4.19 LC-MS fragmentation data of the identified probable constituents present in *C. racemosa* KNY-254

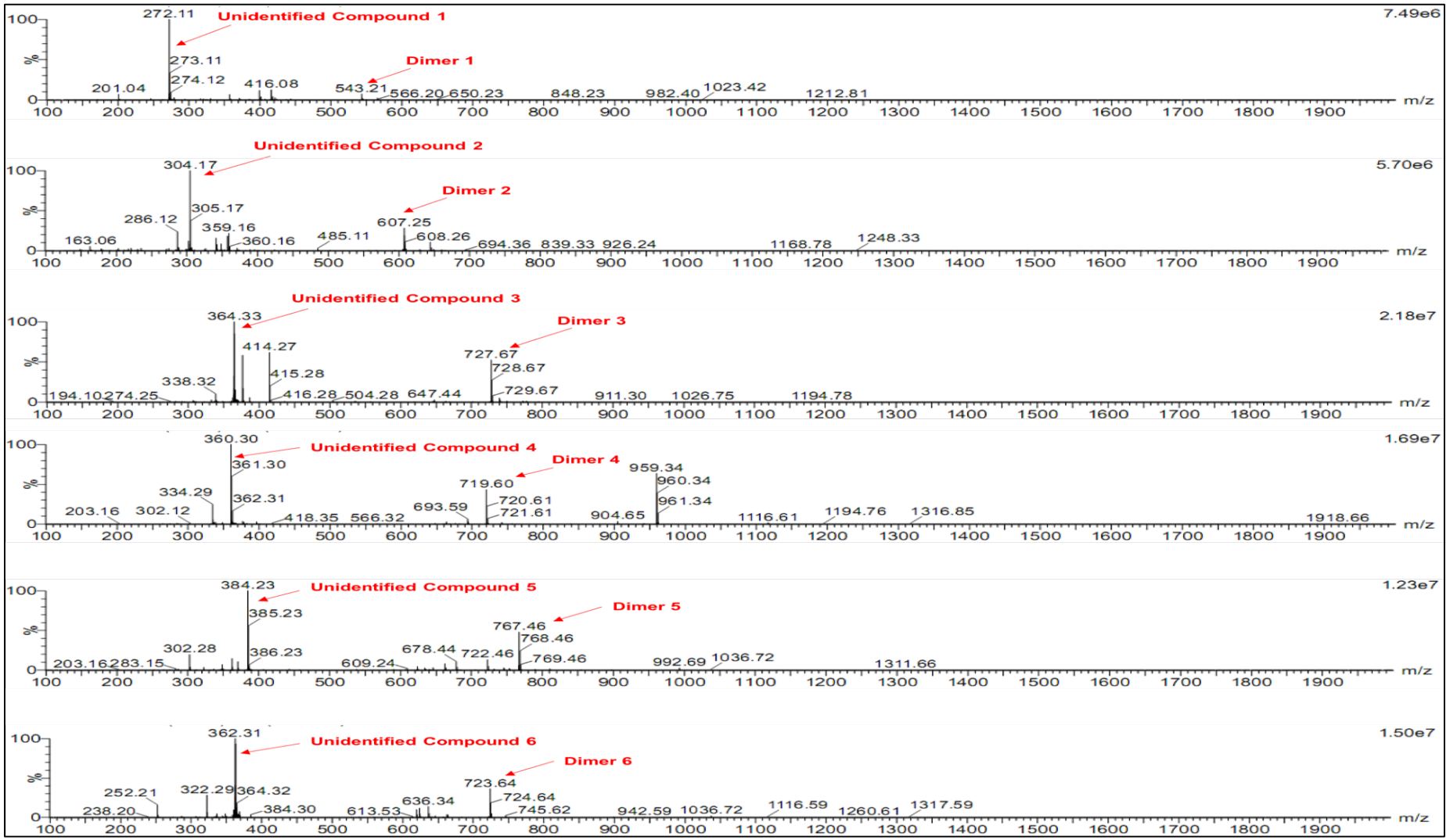

Figure 4.20 LC-MS fragmentation data of the unidentified probable constituents present in *C. racemosa* KNY-254

Table 4.5 Details of identified probable constituents determined from LC-MS fragmentation data of *C. racemosa* KNY-254

S. No.	Code	Retention Time	Exact mass	Observed Mass
1.	CR1	6.192	404.26	$[M+Li]^+$
2.	CR2	5.592	342.10	$[M+K]^+$
3.	CR3	5.403	296.31	$[M+NH_4]^+$
4.	CR4	6.947	268.12	$[M+NH_4]^+$
5.	CR5	6.844	338.32	$[M+Li]^+$
6.	CR6	6.707	360.23	$[M+Li]^+$

Table 4.6 Glide Score for interactions of various *Caulerpa* constituents with respective protein molecules

Ligands	Proteins								
	Bcl2	**AMPK**	**mTOR kinase**	**BID**	**PERK**	**IGF-1R**	**PI3K**	**PTP1B**	**Akt2**
Racemosin C	-5.236	**-4.722**	**-7.455**	0.209	-5.336	-5.382	-7.832	-3.183	-3.710
Caulerpin	-5.214	-3.680	-7.433	-	-4.820	-1.001	-	-3.670	-3.880
Caulersin	-4.331	-3.463	-5.291	-1.482	**-6.015**	**-7.302**	-7.306	-3.316	**-5.826**
Caulerpenyne	-2.887	-2.240	-3.329	-	-1.882	-	-3.516	-2.531	-2.127
CR1 (Isomer 1)	-2.760	-1.355	-2.972	-	-4.461	-2.606	-4.866	-2.671	-2.530
CR1 (Isomer 2)	-2.859	-3.201	-4.546	-	-5.057	-5.360	-2.842	-2.938	-2.074
CR2	-4.389	-3.589	-7.406	-	-5.902	-5.668	-5.763	-3.635	-4.231
CR3	**-5.277**	-2.120	-3.501	-	-2.965	-3.788	-1.820	-2.486	-2.338
CR4	-5.173	-4.535	-7.397	**-1.869**	-5.205	-5.001	**-8.958**	**-3.863**	-5.024
CR5	-3.166	1.710	-3.958	-	-2.286	-3.648	-5.198	-1.917	-1.402
CR6	-4.129	-4.511	-4.610	-	-4.236	-3.528	-3.090	-2.991	-3.580
Standard	-12.836	-19.453	-15.382	-6.149	-14.753	-12.624	-16.782	-11.634	-19.060

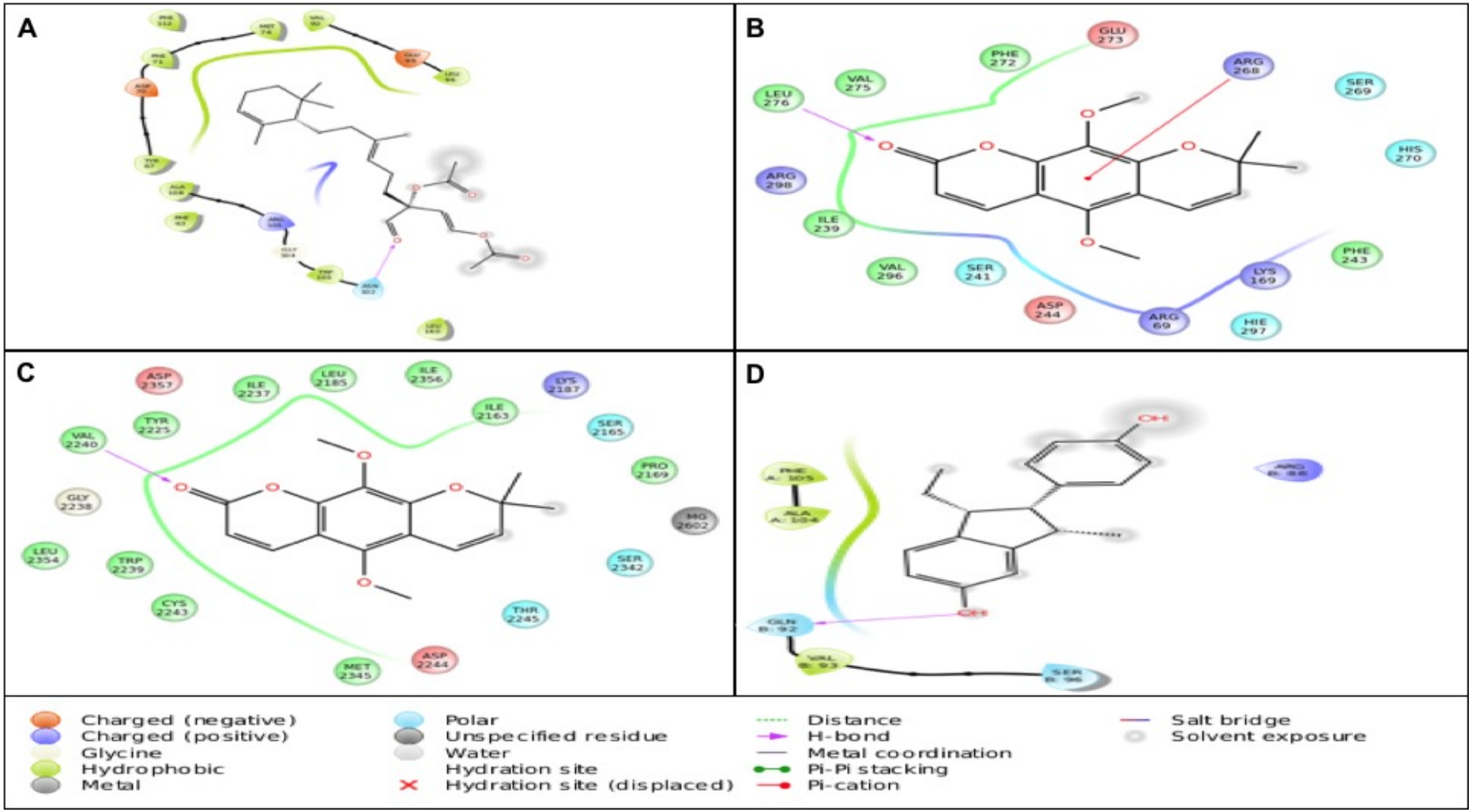

Figure 4.21 Molecular interactions of various *Caulerpa* constituents with proteins targets depicted as 2D interaction diagram. Color coding of moieties and type of interactions are described at the bottom of the Figure. The best protein-ligand complex for each protein is shown. A) Bcl2-CR3; B) AMPK-Racemosin C; C) mTOR Kinase-Racemosin C; D) BID-CR4.

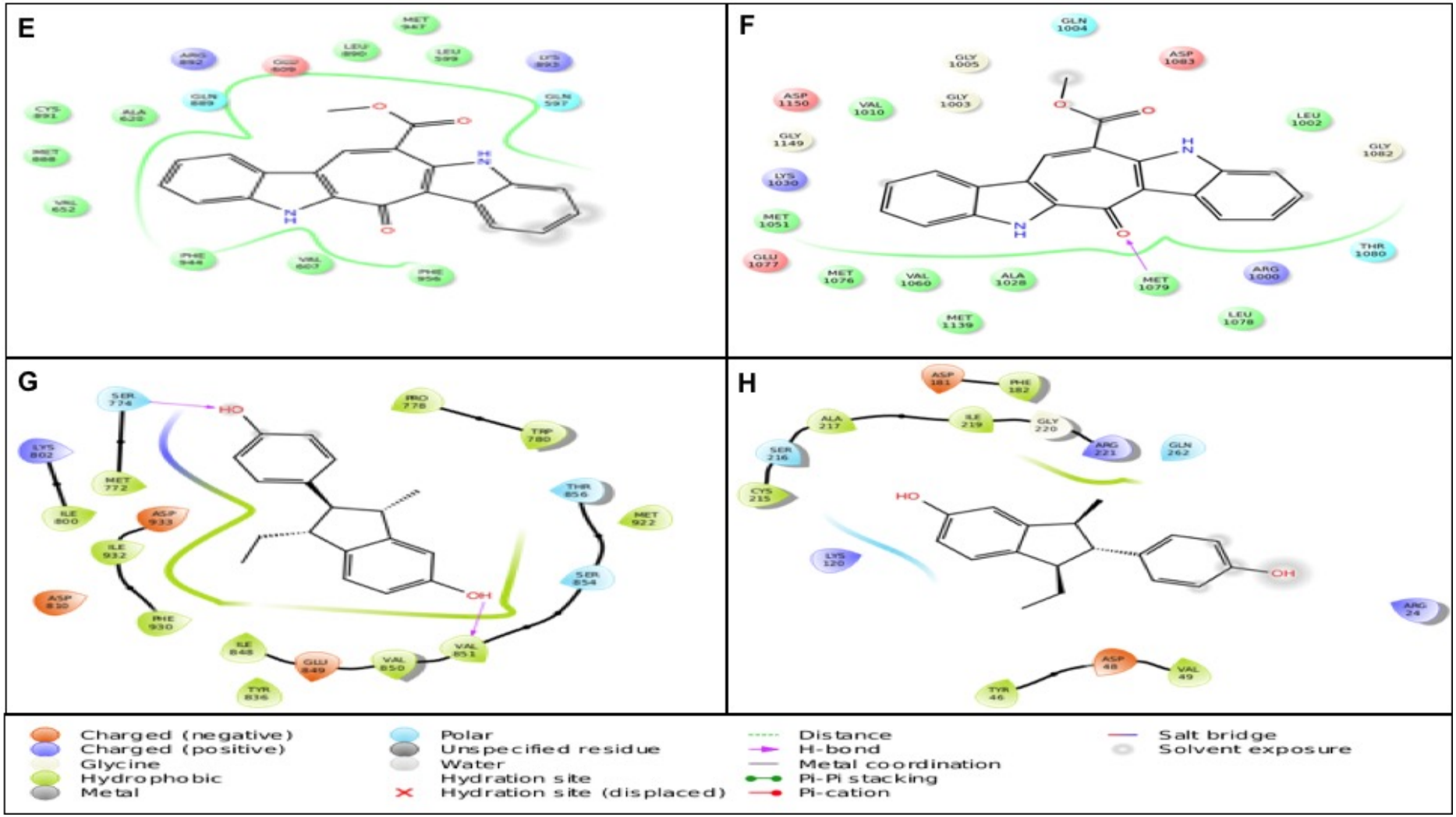

Figure 4.21 Molecular interactions of various *Caulerpa* constituents with proteins targets depicted as 2D interaction diagram. Color coding of moieties and type of interactions are described at the bottom of the Figure. The best protein-ligand complex for each protein is shown. E) PERK-Caulersin; F) IGF-1R-Caulersin; G) PI3K-CR4; H) PTP1B-CR4.

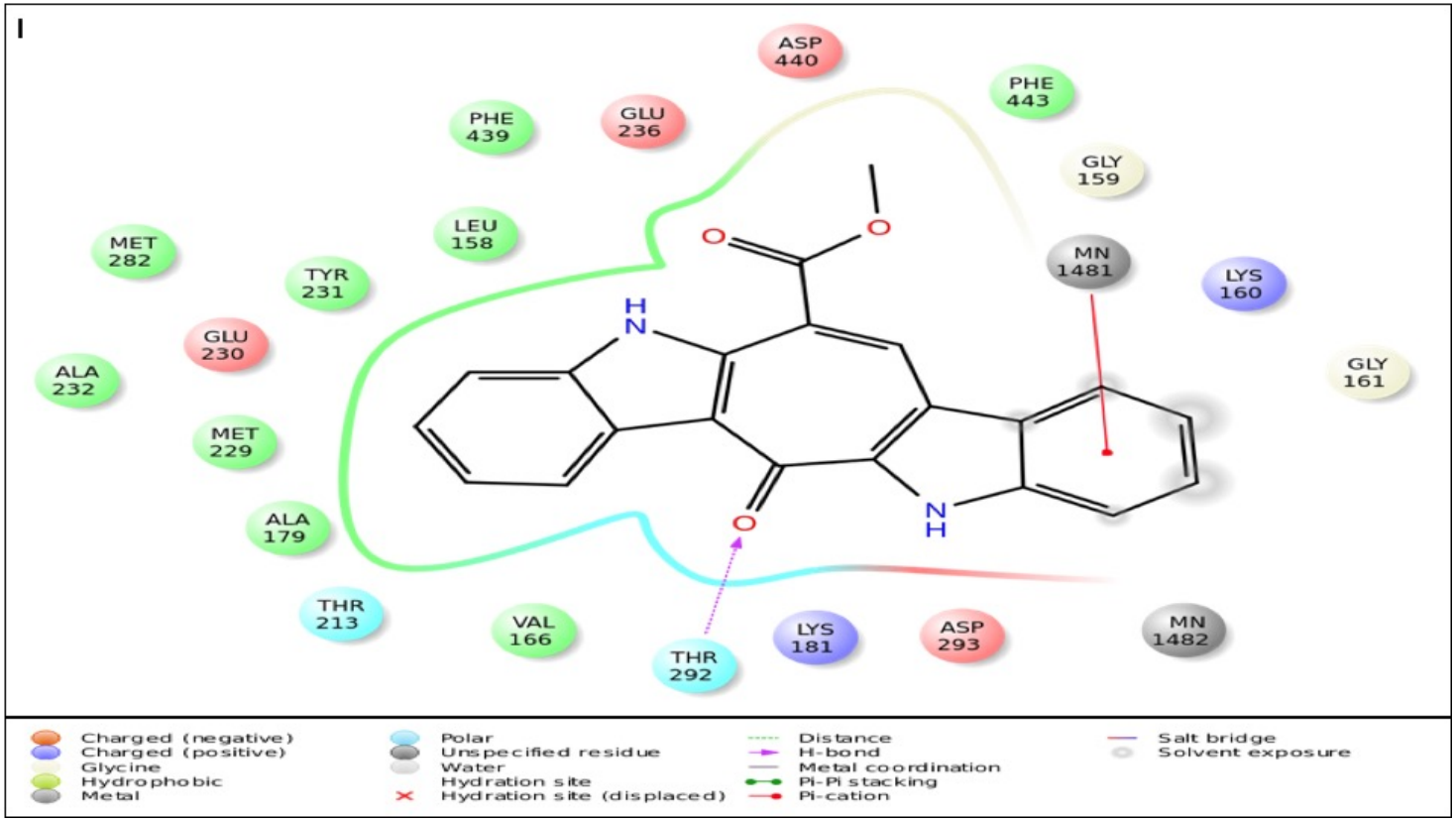

Figure 4.21 Molecular interactions of various *Caulerpa* constituents with proteins targets depicted as 2D interaction diagram. Color coding of moieties and type of interactions are described at the bottom of the Figure. The best protein-ligand complex for each protein is shown. I) Akt2-Caulersin

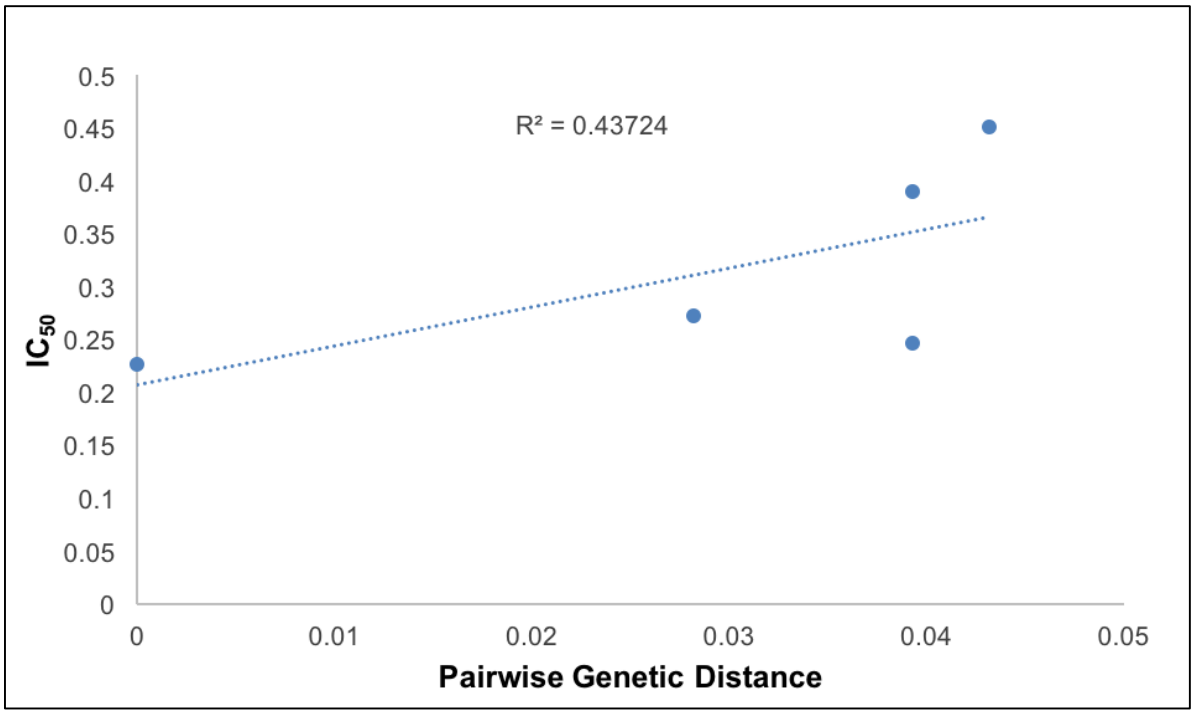

Figure 4.22 Pairwise genetic distance as a function of pairwise difference in IC_{50} as observed in MDA-MB-231 cells. *C. racemosa* KNY-254 with least IC_{50} *i.e.* 0.23 ± 0.0004 was used as reference to calculate the pairwise genetic distance as well as pairwise difference in IC_{50} with rest of the samples.

DISCUSSION

This study was aimed for barcoding based identification of various *Caulerpa* species; reassessment of phylogeny of genus *Caulerpa*, investigation and comparison of anti-cancer and anti-oxidant activities of *Caulerpa* species; analysis of putative correlation between phylogeny and anti-cancer activity; and to gain insights into chemical constituents of the most potent species. The genus *Caulerpa* J V Lamouroux (1809) falls under family Caulerpaceae and order Bryopsidales and has currently 97 currently accepted species and many more unverified taxonomic entries (Guiry and Guiry, 2018). The type species of the genus is *C. prolifera* (Forsskål) and type location is Alexandria, Egypt. As per the earliest monograph available, the genus is divided into twelve sections viz. *Vaucherioideae, Charoidke, Bryoideoe, Zosteroideoe, Phyllantoideoe, Filicoideoe, Hippuroideoe, Lycopodioideoe, Thuyoideoe, Araucarioideoe, Paspaloideae,* and *Sedoideo* (Bosse 1898), whereas the recently proposed classification scheme, inferred from *tufA* and *rbc*L, divides it into six subgenus viz. *Charoideae, Cliftonii, Caulerpella, Hedleyi, Araucarioideae,* and *Caulerpa* (Draisma *et al.,* 2014). In the current study, a total of 41 barcodes were generated, belonging to 7 different species viz. *C. scalpelliformis*, *C. racemosa*, *C. verticulata*, *C sertularioides*, *C. lentillifera*, *C. corynephora*, *C. taxifolia* and their geographical isolates. The phylogenetic assessment of *Caulerpa* was done using four molecular markers, viz. ITS, 18S, *rbc*L and *tufA*. Notably, the nucleotide coverage of ITS, 18S and *rbc*L was relatively lower than *tufA*. There were around 535 available nucleotide sequences of ITS but most of them belonged to a small number of species, 402 belonging to 18S, 220 belonging to *rbc*L and 1115 sequences of *tufA* region. Consequently, the BI phylograms generated with ITS and 18S could be resolved into 6 and 5 lineages belonging to previously known sections. The BI phylogram of *rbc*L generated from a total of 54 DNA sequences was divided into 17 different lineages, with 12 lineages corresponding to previously known sections and five unidentified clades. Likewise, the BI phylogram with 71 sequences of *tufA* was resolved into 18 different lineages, with 15 corresponding to previously known sections and 2 new lineages. Overall, the section Fillioideae and Sedoideae were found paraphyletic. Based on the results generated in the study, *tufA* is found as the most suitable barcode for the genus. The two new lineages have no earlier record and are supported by strong bootstrap values and the phylogenetic status of the concerned species is not clearly defined previously.

The most robust tree of all the four markers tested was *tufA* and is discussed in detail in this chapter. The efficacy of tufA, 18S and ITS was also proposed by Kazi *et al*., 2013. (Kazi *et al.,* 2013). The species falling under Section Sedoideae were distributed amongst three different clades, making it a paraphyletic clade. The species comprised *C. racemosa, C. cylindracea, C. elongata, C. macrodisca, C. geminata, C. sedoides, C. hodgkinsoniae, C. agardhi, C. cactoides, C. okamurae, C. opposita, C. bartoniae, C. ferugsonii, C. vesiculifera,* and *C. simpliciuscula.* Fama *et al.,* 2002 resolved section Sedoideae in to *C. racemosa* var*. lamourouxii, C. racemosa* var*. turbinata, C. racemosa* var. *occidentalis, C. racemosa* var. *macrophysa, C. racemosa* var*. peltata, C. racemosa, C. geminata, C. microphysa,* and *C. cactoides.* which is in harmony with the present study, but many species considered in the current study were not included in their study. Calvert *et al*., 1976 also grouped species *C. racemosa, C. microphysa, C. simpliciuscula, C. papillosa, C. cactoides, and C. geminate* under section Sedoideae, further validating our claim (Calvert *et al.,* 1976). In a similar study conducted by Draisma *et al.*, a well estimated time-calibrated tree was generated where the species *C. sedoides, C. catoides, C. opposita, C. bartoniea, C. ferugsonii, C. vesiculifera* and *C. simpliciuscula* were also grouped under section Sedoideae, however the account of rest of the species of the section was again missing from their study. Conversely, the species *C. elongata* was placed under section Araucarioideae in this study, while the present study placed it under Sedoideae with >0.95 posterior probability value (Draisma *et al.,* 2014).

The Section Vaucherioideae contained a single species *C. filiformis* which is congruent with the study conducted by Fama *et al.,* 2002. While Draisma *et al.,* 2014 placed *C. filiformis* into major section *Caulerpa*, under subgenus *Caulerpa* and Calvert *et al.,* 1976, placed *C. fastigata* under Vaucheroideae and *C. filiformis* under section Zosterioideae based on chloroplast ultrastructure but is not found harmonious with molecular phylogeny. *C. brachpus* and *C. subserrata* are unanimously grouped under Section Phyllantoideae (Calvert *et al.,* 1976, Fama *et al.,* 2002, Belton *et al.,* 2014). The section Fillicoideae, Brioideae, Thuyoideae, Papaloideae, lycopodioideae, Charoideae, Cliftonii were also non-conflicting and well supported by strong posterior probability values and validated from previous reports available (Fama *et al.,* 2002, Draisma *et al.,* 2014, Belton *et al.,* 2014).

However, the section Fillicoideae was found to be paraphyletic and needs further investigation along with section Sedoideae.

The two new lineages were found in the study, labelled as lineage 1 and lineage 2. The lineage 1 includes *C. chemnitzia, C. selago, C. nummularia, C. peltata, C. manorensis, C. urvilleana*, supported by P value of 0.88; and lineage 2 comprises *C. antoensis, C. mexicana, C. constricta* supported by P value of 0.93. Previously, *C. selago* is categorized under section Filicoideae by Fama *et al.,* 2002; while *C. manorensis* and *C. urvilleana* are placed under section *Caulerpa*, subgenus *Caulerpa* by Draisma *et al.,* 2014, however, the results place them in a well-resolved and supported clade. *C. nummularia* is also placed in a separate unidentified clade by Belton *et al.,* 2014 which supports our claim for the said species (Fama *et al.,* 2002; Draisma *et al.,* 2014). It is hereby proposed to reinstate *C. chemnitzia, C. selago, C. nummularia, C. peltata, C. manorensis, C. urvilleana* under one single lineage. Likewise, there is no previously available phylogenetic assignment of *C. antoensis* and *C. constricta*, which formed a separate clade with *C. mexicana*, previously categorized under section Filicoideae (Fama *et al.,* 2002). The lineage 2 can be found next to section Filicoideae and is indicative of recent diversification from the section forming an altogether different clade with strong posterior probability value 0.93. It is proposed to reinstate *C. mexicana* with *C. antoensis*, *C. constricta*. However, for further validations, there is an urgent need of extensive generation of molecular data and more comprehensive phylogenetic assessment at global level.

Caulerpa species are known to possess several bioactive compounds previously accounted for anti-microbial, insecticidal, anti-trypanosomal, anti-depressants, anti-inflammatory, anti-oxidant and anti-tumour activity (Kochanowska-Karamyan and Hamann 2010; Otoguro *et al.,* 2011; Paduch *et al.,* 2007; Roleira *et al.,* 2015). A sesquiterpenoid, CYN, is the major metabolite obtained from this species. Although it is also reported in other species of the genus, but maximum yield is obtained from *C. taxifolia*. CYN exhibits anti-microbial, neurotoxic, phytotoxic, anti-mitotic and anti-proliferative activity (Barbier *et al.,* 2001; Tejada *et al.,* 2016). Variations in the CYN content are observed w.r.t. season and level of competition (Dumay *et al.,* 2001). Besides, alkaloids like caulerpin, caulersin and racemosin C, with potent anti-cancer activities are reported from other

Caulerpa species, but not from *C. taxifolia, C. verticillata* and *C. sertularioides* (Yang *et al.,* 2015). In the present study, the evaluation of anti-cancer activity of various *Caulerpa* species was done and phycochemicals detected from *Caulerpa* species are in congruence with the literature with slight variations (Viswanathan *et al.,* 2013; Rusli *et al.,* 2016). These results suggest presence of potent bioactive compounds.

Cytotoxicity of various *Caulerpa* species is reported in literature, wherein growth inhibition was reported in myelomonocytic leukemia cells (WEHI-3) and human promyelocytic leukemia cells (HL-60) by *C. microphysa* (Lin *et al.,* 2012). In addition, cell viability of murine macrophage cells, RAW 264.7, was negligibly effected by *Caulerpa* extract suggesting its selective cytotoxicity against cancer cells. Likewise, CYN, obtained from *C. taxifolia* inhibited neuroblastoma cells, SK-N-SH cells and a gradual increase in cell death (Barbier *et al.,* 2001). A polysaccharide, ß-1,3-xylan, isolated from *C. lentillifera*, also inhibited cell viability in human breast cancer cells, MCF-7, in a dose-dependent manner, and demonstrated other apoptotic signals (Maeda *et al*., 2012). Cell cycle arrest and cytotoxicity by some *Caulerpa* species is previously reported where G_2/M phase arrest in colorectal cancer cells was observed by CYN obtained from *C. taxifolia* (Fischel *et al.,* 1995). In addition, interference in DNA replication and cell cycle arrest at a metaphase like stage in sea urchin embryos by CYN is also suggestive of its bioactive potential (Pesando *et al.,* 1996). Another study reports induction of G_0/G_1 phase arrest and formation of apoptotic bodies in a dose-dependent manner in HL60 cells (promyelocytic leukaemia) by methanolic extract of *C. racemosa*. The efficacy of Sri Lankan *C. racemosa* was reported to be maximum than *Chaetomorpha crassai*, *Sargassum crassifolium*, *Gracilaria acerosa*, *Chondrophycus ceylanicus*, and *Gracilaria corticata*, suggesting its pharmacological worth (Lakmal *et al.,* 2014). Likewise, *C. microphysa* extract blocked cell cycle at G_0/G_1 phase by downregulating the expression of cyclin D-E, CDK2, CDK6 and upregulation p21, p27, p53 and subsequently causes apoptosis in WEHI cells (Chou *et al.,* 2014). In the current study, varied range of cytotoxicity of CMEs was observed against breast (MDA-MB-231, T-47D cells) and lung cancer (H1299 cells), with insignificant effect on hPBMCs, suggesting, selective hindrance of cellular metabolism in cancer cells. Additionally, a net increase in cells at G1 and S phase; with concomitant decrease in G2 phase in all CMEs was observed, further validating our claims of anti-cancer activity of *Caulerpa* species.

Metastasis is crucially involved in aggravating the tumor progression and considered as an important target for cancer therapy. Previously, solvent extracts of *C. mexicana* and *C. sertularioides* portrayed significant inhibition of leukocyte migration to peritoneal cavity in mice models, stimulated with carrageenan (Brito da Matta *et al.,* 2011). In another study, caulerpin is reported to induce HIF-1 activation, suppression of VEGF and weak inhibition of migration in MDA-MB-231 cells. Caulerpin was also reported to disrupt mitochondrial respiration at complex I of electron transport chain (ETC) (Liu *et al.,* 2009). The apoptotic potential of *C. racemosa* var. *cylindracea* currently regarded synonymous to *C. cylindracea* extract, and purified CYN was also reported in neuroblastoma, SHSY5Y and Kelly cells, wherein the DNA dye, Hoechst 33342 was used to evaluate the live, dead and apoptotic cells (Cavas *et al.,* 2006). Likewise, β-1,3-Xylan obtained from *C. lentillifera* was reported to induce apoptosis in MCF-7 cells by chromatin condensation and degradation of poly ADP-ribose polymerase (Maeda *et al.,* 2012). The significant inhibition of cell invasion and presence of early apoptotic signals in MDA-MB-231 cells is reported *by* CMEs in the current study, suggesting apoptotic cell death and inhibition of tumor metastasis.

Cancer cells usually have an enhanced basal ROS level and maintain homeostasis for their survival. Any change with an increase or decrease, beyond restoration, may lead to disruption of redox balance and eventually to cell death, which is also a useful factor contributing towards anti-cancer therapy (Farooqi *et al.,* 2015; Noh *et al.,* 2015). Previously oxidative damage by pepsin-digested *C. microphysa* extract was shown by Chou *et al.,* (2014), wherein a 1-2.75 folds increase in ROS induction by 300 µg/mL extract in WEHI-3 cells, after 48 h treatment, is reported (Chou *et al.,* 2014). ROS induction was also reported by caulerpin, in SW480 and LOVO cells, which was associated with disrupted mitochondrial oxidative metabolism, that further leads to apoptosis (Yu *et al.*, 2016). Although *Caulerpa* species are known to exhibit good anti-oxidant enzyme machinery and high nutrition value (Cavas and Yurdakoc, 2005b; Kumar *et al.,* 2011), but there are scanty reports of modulations of anti-oxidant enzyme machinery of human cancer cells by *Caulerpa* metabolites. Astaxanthinmono and diesters obtained from green alga, *Haematococcus pluvialis,* exhibited similar effect in rat models for skin cancer, with increase in SOD, catalase and GSH levels (Rao *et al.,* 2013). Likewise, aqueous and ethanolic extracts of *C. racemosa* increased

SOD activity and other anti-oxidant enzyme activity in thalassemia rat models with iron overload, suggesting their anti-oxidant and iron chelating potential (Adham *et al.,* 2017). A marine red alga, *Gracilaria tenuistipitata* extract induces oxidative stress via elevated ROS and lowered GSH levels in oral cancer cells, Ca9-22 (Yeh *et al.,* 2012). The decrease in GSH levels may either be credited to decreased activity or downregulation of glutathione reductase (Trachootham *et al.,* 2009). Reduction of GSH which acts as an anti-oxidant in the system, enhances cell's susceptibility to intracellular ROS and leads to mitochondrial membrane modulations and DNA damage, resulting in apoptosis (Matthews *et al.,* 2006). The present study highlights that CMEs lead to an increase in ROS levels of breast cancer cells, and perturbs total enzymatic activity of SOD, catalase and GR of breast cancer cells, which is possibly another contributing factor in cancer cell death.

Mitochondrial health is critically associated with many physiological processes like ATP synthesis, ROS generation, Ca^{2+} sequestration, cargo transport and membrane dynamics (Sabharwal and Schumacker, 2014)). MMP is strictly regulated by proton gradients, ATP consumption, Ca^{2+} stores and mitochondrial respiration. Disruption of MMP is an imperative target of apoptotic signaling. Bioactive molecules that either depolarize or hyperpolarize the mitochondrial membrane, exhibit specific anti-cancer activity e.g. FCCP and nigericin. FCCP is a potent uncoupler and transport protons across the inner mitochondrial membrane and dissipates the proton motive force (PMF), causing mitochondrial depolarization; whereas nigericin is an K^+/H^+ ionophore and acidifies the mitochondrial matrix causing an increase in pH and thereby, membrane hyperpolarization (Teodoro *et al.,* 2018). Growing body of evidences suggest that a sensitization of cancer cells by hyperpolarization of mitochondrial membrane is a pre-requisite for apoptosis (Ghosh *et al.,* 2016). Infrequent reports of hyperpolarization of MMP are reported recently, in comparison to plethora of reports claiming depolarization of MMP (Perry *et al.,* 2011). Although, mitochondrial hyperpolarization is increasingly being accepted as an early sign of apoptosis and was also depicted in the Fas-H_2O_2–induced apoptosis in Jurkat leukemia T cells (Banki *et al.,* 1999). Similarly, systemic lupus erythematosus (SLE) T–cells undergo an abnormal apoptosis associated with hyperpolarization of MMP, extrusion of H^+ ions, elevated ROS, and diminished GSH (Gergely *et al.,* 2002). Increase in mitochondria potential and extrusion of H^+ ions are considered as a probable cause of elevated ROS which further induces

apoptosis in cancer cells (Tymoczko *et al.,* 2011)). Mitochondrial hyperpolarization was observed in intestinal cancer cells, Caco-2 wherein oxidized low-density lipoproteins induced mitochondria mediated apoptosis (Giovannini *et al.,* 2002). Likewise, major bioactive pigment of turmeric, curcumin, also induced transient mitochondrial hyperpolarization followed by release of cytochrome c and membrane potential disruption, associated with mtDNA damage that eventually leads to apoptosis in human hepatoma G2 cells (HepG2) (Cao *et al.,* 2007). During apoptosis, mitochondrial membrane undergoes hyperpolarization, in the priming phase followed by release of cytochrome c and potential disruption in the effector phase (Scarlett *et al.,* 2000). There are no previous reports of mitochondrial hyperpolarization by *Caulerpa* species, however, mitochondrial depolarization is reported by caulerpin in LOVO and SW80 cells, (colorectal cancer) (Yu *et al.,* 2016). In this study, all CMEs caused significant ($p<0.50$; $p<0.01$) increase in MMP and are believed to be associated with elevated ROS levels and cytotoxicity.

Marine bioactive compounds are structurally unique and are relatively underexplored. Previously, a total of 27 compounds have been isolated from *C. brownii* from Tasmanian coast, six of them are reportedly novel while one was isolated for the first time as natural product (Handley and Blackman, 2005). Yang *et al.,* 2015 have reported 18 chemical constituents from *C. racemosa*, 5 of which are unprecedented moieties including 3 diterpenoids, an α-tocopheroid, and a 28-oxostigmastane steroid. The two diterpenoid epimers, racemobutenolids A and B are unique lactones bearing β-methyl-γ-substituted butenolide moiety while the other diterpenoid, 4′,5′-dehydrodiodictyonema A, and the tocopheroid, α-tocoxylenoxy are first natural compound having hematinic acid ester and 3,5-dimethylphenoxy moiety, respectively. In addition, 9 of the isolated compounds displayed varied degrees of PTP1B inhibitory activities (Yang *et al.,* 2015). Besides, inter-species variations, seasonal variations, topological variations are reported from various species of *Caulerpa* (Meyer *et al.,* 1992; Robledo *et al.,* 2005). In order to gain further insights about the possible interacting protein targets involved in signaling pathways of cancer cells, molecular docking of identified *Caulerpa* constituents and known metabolites was performed. The results revealed weak to moderate interactions with almost all of the protein targets viz. Bcl2, AMPK, mTOR, BID, PERK, IGF-1R, PI3K, PTP1B and Akt2. These proteins are involved in metabolic reprogramming, cell cycle arrest and apoptosis via mitochondrial and/or

ER stress pathway, thereby killing cancer cells (Mehra *et al.,* 2018b; Mehra *et al.,* 2018d). In this study, probing of chemical constituents was attempted by LC-MS analysis followed by silica column based purification and possible known constituents (CR1-CR6) and six unidentified compounds were observed. The identified compound CR2 is an isomer of caulersin which is previously known for PTP1B inhibitory activity (Yang *et al.,* 2014). CR-4 is a synthetic compound and not reported naturally yet, as per my limited knowledge, while other compounds have been reported either from *C. brownii* or *C. racemosa* (Handley and Blackman, 2005; Yang *et al.,* 2015). It is believed that anti-cancer activity of *C. racemosa,* in the present study is partially or/and completely because of caulersin, as there are several studies associating PTP1B inhibitory activity with anti-cancer activity (Yang *et al.,* 2014).

Phylogeny is an underutilized yet powerful predictor of physiological traits of biological system. Amongst limited reports available, phylogeny has been proven as a useful tool for predicting webbing behavior of *Clitaetra* spiders, alkaloid content in *Cinchona* bark, protein family and functions (Wickstead and Gull, 2006; Kuntner and Agnarsson, 2009; Maldonado *et al.,* 2017). Researchers have now started to actively look for strong evolutionary tools to search pharmacologically important drugs, which is expected to bring revolutionary changes in the approach of medicinal research (Halse-Gramkow *et al.,* 2016; Guzman and Molina, 2018). There are a few reports of activity-genetic relatedness amongst bacteria, plants and marine sponges as discussed previously in chapter 2 (Kamke *et al.,* 2010; Evans-Illidge *et al.,* 2013) but no such investigation has been carried out in algae. In the present study, moderately positive correlation between phylogeny and anti-cancer activity of *Caulerpa* species was observed which is an important cue for the efficacy of this approach. However, due to relatively smaller number of samples and considerable genetic distance amongst the isolates, a strong correlation couldn't be inferred at this stage. Although this study is done at pilot-scale and implies moderate correlation between anti-cancer activity and phylogeny, it is strongly suggested to generate extensive molecular data for *Caulerpa* and other important marine algae, which can be utilized for such prediction based approaches to unravel the hidden treasures of giant oceans.

SUMMARY

This study deals deal with morphological as well as molecular identification of various *Caulerpa* species based on DNA barcode concerning inter-species and intra-species level taxonomic identification. A total of 15 algal specimen were analyzed that were identified as 7 different species viz. *C. racemosa*, *C scalpelliformis*, *C. sertularioides*, *C. verticillata*, *C. taxifolia*, *C. lentillifera*, *C. corynephora* and their geographical isolates. A total of 41 DNA barcodes were generated with 4 molecular markers (ITS, 18S, *rbc*L and *tufA*) and their phylogenetic assessment was done with aforementioned markers.

Based on BI and ML phylogenetic assessment *tufA* was found to be the most suitable marker for the genus *Caulerpa,* resolving the species into 17 different lineages, with 15 corresponding to already known section and 2 new lineages comprising, *C. chemnitzia, C. selago, C. nummularia, C. peltata, C. manorensis, C. urvilleana*, and *C. antoensis, C. mexicana, C. constricta*, respectively, supported by strong posterior probability and bootstrap values. The reinstatement of these species in the respective new lineages is hereby proposed. Additionally, a database named *DbIndAlgae* of Indian algae was generated and all the morphological as well as molecular data generated in this study is uploaded on the database. The next target was to evaluate *in-vitro* anti-cancer and anti-oxidant activities of *Caulerpa* spp. The results revealed the presence of variable amounts of bioactive compounds like alkaloids, terpenoids, steroids, tannins, saponins, flavonoids, and phenols amongst all CMEs. The selective cytotoxicity of CMEs was observed in breast (MDA-MB-231, T-47D cells) and lung cancer (H1299 cells) with insignificant effect on hPBMCs. Early apoptotic signals and anti-invasion activity was also confirmed in MDA-MB-231 cells, by Annexin V and scratch wound assay. Additionally, cell cycle arrest was confirmed in MDA-MB-231 cells at G1/S phase by CMEs using flow cytometry based PI analysis. Moreover, induction of intracellular ROS was highlighted by DHE assay in association with modulations of SOD, catalase and GR activity. Likewise, perturbed mitochondrial membrane potential was reported in response to CME treatment, as observed using confocal microscope. These results indicate apoptotic cell death of cancer cells by mitochondrial pathway. These results reveal significant anti-cancer activity of all CMEs tested on MDA-MB-231, T-47D, and H1299 cells with most potent effect observed by *C. racemosa,* KNY-254 on MDA-MB-231 cells. Subsequently, analysis of possible constituents of KNY-254 by

LC-MS was done, which revealed the presence of previously reported bioactive metabolite, caulerpin, and five reported and six unreported compounds. Molecular docking of these possible *Caulerpa* constituents displayed moderate interactions of most of the constituents with Bcl2, AMPK, mTOR kinase, BID, PERK, IGF-1R, PI3K, and PTP1B; with best interaction between PI3K and CR4. Lastly, in an attempt to analyze putative correlation between phylogeny and anti-cancer activity, a moderately positive correlation amongst the two was observed suggesting that phylogeny might provide cues for anti-cancer activity, subject to further validations.